Variable-Density Flow Processes in Porous Media On Small, Medium and Regional Scales

DISSERTATION

zur Erlangung des akademischen Grades

Doctor rerum naturalium
(Dr. rer. nat.)

vorgelegt

der Fakultät Umweltwissenschaften
der Technischen Universität Dresden

von

Dipl.-Hydrol. Marc Walther
Geb. am 07. November 1982 in Dohna

Erklärung des Promovenden

Die Übereinstimmung dieses Exemplars mit dem Original der Dissertation zum
Thema:

"Variable-Density Flow Processes in Porous Media
On Small, Medium and Regional Scales"

wird hiermit bestätigt.

Ort, Datum

Unterschrift
(Vorname Name)

This is for my wife and children.

Use what talents you possess;
the woods would be very silent if no birds sang there
except those that sang best.

Henry van Dyke

Abstract

Nowadays society strongly depends on its available resources and the long term stability of the surrounding ecosystem. Numerical modelling has become a general standard for evaluating past, current or future system states for a large number of applications supporting decision makers in proper management. In order to ensure the correct representation of the investigated processes and results of a simulation, verification examples (benchmarks), that are based on observation data or analytical solutions, are utilized to evaluate the numerical modelling tool.

In many parts of the world, groundwater is an important resource for freshwater. While it is not only limited in quantity, subsurface water bodies are often in danger of contamination from various natural or anthropogenic sources. Especially in arid regions, marine saltwater intrusion poses a major threat to groundwater aquifers which mostly are the exclusive source of freshwater in these dry climates. In contrast to common numerical groundwater modelling, density-driven flow and mass transport have to be considered as vital processes in the system and in scenario simulations for fresh-saltwater interactions.

In the beginning of this thesis, the capabilities of the modelling tool OPENGEO-SYS are verified with selected benchmarks to represent the relevant non-linear process coupling. Afterwards, variable-density application and process studies on different scales are presented. Application studies comprehend regional groundwater modelling of a coastal aquifer system extensively used for agricultural irrigation, as well as hydro-geological model development and parametrization. In two process studies, firstly, a novel method to model gelation of a solute in porous media is developed and verified on small scale laboratory observation data, and secondly, investigations of thermohaline double-diffusive Rayleigh regimes on medium scale are carried out.

With the growing world population and, thus, increasing pressure on non-renewable resources, intelligent management strategies intensify demand for potent simulation tools and development of novel methods. In that way, this thesis highlights not only OPENGEOSYS' potential of density-dependent process modelling, but the comprehensive importance of variable-density flow and transport processes connecting, both, avant-garde scientific research, and real-world application challenges.

Zusammenfassung

Heutzutage hängen Gesellschaften stark von den ihr zur Verfügung stehenden Ressourcen und der Langzeitstabilität der sie umgebenden Ökosysteme ab. Die numerische Modellierung hat sich als ein anerkannter Standard für die Bewertung vergangener, gegenwärtiger und zukünftiger Systemzustände bei Entscheidungsträgern etabliert. Um die korrekte Darstellung der untersuchten Prozesse und Ergebnisse einer Simulation zu gewährleisten, werden Verifikationsbeispiele (Benchmarks) genutzt, die auf Beobachtungsdaten oder analytische Lösungen basieren.

In vielen Teilen der Welt ist Grundwasser eine wichtige Ressource für Süßwasser. Zu der quantitativen Beschränkung unterirdischer Wasserressourcen kommt oft die Gefahr der Kontamination aus verschiedenen natürlichen oder anthropogenen Quellen. Besonders in ariden Regionen sind Grundwasserleiter, welche dort zumeist die einzige Süßwasserquelle darstellen, von mariner Salzwasserintrusion bedroht. Im Gegensatz zur herkömmlichen numerischen Grundwassermodellierung muss in diesen Systemen bei der numerischen Modellierung die dichteabhängige Strömung als wichtiger Prozess beachtet werden.

Zu Beginn dieser Arbeit wird unter Zuhilfenahme ausgewählter Benchmarks die Fähigkeit des Modellierungs-Tools OpenGeoSys verifiziert, die relevante Prozesskopplung abzubilden. Danach werden sowohl Anwendungs- als auch Prozessstudien auf verschiedenen Skalen vorgestellt. Bei ersteren wird ein für landwirtschaftliche Bewässerung genutztes, küstennahes Aquifersystem untersucht, und die zugehörige Erstellung des hydrogeologischen Modells aufgezeigt. In zwei anschließenden Prozessstudien, wird eine innovative Methode zur numerischen Modellierung der Gelierung eines gelösten Stoffes in porösen Medien entwickelt und mit Hilfe von Labordaten verifiziert. Anschließend werden theoretische Untersuchungen zu thermohalinen doppeldiffusiven Rayleigh-Systemen auf mittlerer Skala durchgeführt.

Mit zunehmender Weltbevölkerung und somit wachsendem Druck auf nicht-erneuerbare Ressourcen verlangen intelligente Managementstrategien leistungsfähige Simulationswerkzeuge sowie die kontinuierliche Entwicklung neuartiger Methoden. Auf diese Weise unterstreicht die vorliegende Arbeit nicht nur das Potenzial von OpenGeoSys zur dichteabhängigen Prozessmodellierung, sondern die umfassende Bedeutung dichteabhängiger Strömungs- und Transportprozesse in moderner Forschung und anwendungsbezogenen Herausforderungen.

Contents

Nomenclature

Roman Symbols

$\mathbf{e}$ Unit vector $(-)$

$\mathbf{q}$ Darcy vector (LT^{-1})

$\mathrm{E}_1(z)$ Exponential integral $(-)$

Le Lewis number $(-)$

Ra Rayleigh number $(-)$

$\mathrm{Ra}_\S$ Haline Rayleigh number $(-)$

Ra_Θ Thermal Rayleigh number $(-)$

A Area (L^2)

a Viscosity-concentration coefficient $(-)$

c Concentration $(-)$

c_0 Reference concentration $(-)$

c_{rel} Concentration ratio $(-)$

C_p^{f} Fluid isobaric heat capacity $(\mathrm{ML}^2\mathrm{T}^{-2}\theta^{-1})$

C_p^{S} Solid isobaric heat capacity $(\mathrm{ML}^2\mathrm{T}^{-2}\theta^{-1})$

D Hydrodynamic dispersion coeff. $(\mathrm{L}^2\mathrm{T}^{-1})$

d Factor of viscosity increase $(-)$

d' Saturated aquifer thickness (L)

D_m Molecular diffusion coeff. $(\mathrm{L}^2\mathrm{T}^{-1})$

e Factor of viscosity increase retainment $(-)$

f Factor of total viscosity change $(-)$

g	Gravitational acceleration (LT^{-2})
H	Height (L)
h	Hydraulic head (L)
h_{in}	Inflow hydraulic head (L)
h_{out}	Outflow hydraulic head (L)
j	Flux $(ML^{-2}T^{-1})$
K_f	Hydraulic conductivity (LT^{-1})
L	Length (L)
p	Pressure $(ML^{-1}T^{-2})$
p_{res}	Residual reduction pressure $(ML^{-1}T^{-2})$
Q	Discharge (LT^{-3})
q	Source term (T^{-1})
r	Radius (L)
S	Storage coeff. (L^{-1})
s	Drawdown (L)
S'	Saturation ratio $(-)$
S_s	Specific storage coeff. $(-)$
S_y	Specific yield (L^{-1})
T	Transmissivity (L^2T^{-1})
t	Time (T)
T'	Period (T)
t_{gel}	Time until gelation(T)
t_{inj}	Injection time span(T)
v	Velocity (LT^{-1})
$W(u)$	THEIS' well function $(-)$
x	Horizontal spatial variable (L)
z	Elevation (L)

Greek Symbols

α Overall horizontal wave number $(-)$

α^{f} Fluid thermal diffusivity $(\mathrm{L}^2\mathrm{T}^{-1})$

α^{s} Solid thermal diffusivity $(\mathrm{L}^2\mathrm{T}^{-1})$

α_l Longitudinal dispersivity (L)

α_t Transversal dispersivity (L)

β Maximum viscosity increase $(-)$

β_s Gelation speed $(-)$

δ_{ij} KRONECKER delta $(-)$

γ EULER-MASCHERONI constant $(-)$

γ_Θ Thermal expansion coeff. (θ^{-1})

γ_{c} Haline expansion coeff. $(-)$

κ Intrinsic permeability (L^2)

λ Decay coeff. (T^{-1})

λ^{f} Fluid thermal conductivity $(\mathrm{MLT}^{-3}\theta^{-1})$

λ^{s} Solid thermal conductivity $(\mathrm{MLT}^{-3}\theta^{-1})$

λ^c Half life of concentration (T^{-1})

μ Dynamic viscosity $(\mathrm{ML}^{-1}\mathrm{T}^{-1})$

μ_0 Reference dynamic viscosity $(\mathrm{ML}^{-1}\mathrm{T}^{-1})$

ω Oscillation frequency $(-)$

Φ Remediation potential $(-)$

Ψ Arbitrary system variable $(-)$

ψ Gelation retainment (L)

ρ Density (ML^{-3})

ρ^{f} Fluid density (ML^{-3})

ρ_0^{f} Reference fluid density (ML^{-3})

ρ^{s} Solid density (ML^{-3})

σ Heat capacity ratio $(-)$

Θ Temperature (θ)

Θ_0 Reference temperature (θ)

φ Porosity $(-)$

ξ Viscosity change coeff. $(-)$

ξ_Θ Thermal viscosity change coeff. (θ^{-1})

ξ_c Haline viscosity change coeff. $(-)$

ζ_{res} Residual reduction factor $(-)$

Acronyms

APPM   Assessment-, Prognoses-, Planning- and Management (tool)

BC   Boundary condition

GWL   Groundwater level

IDW   Inverse Distance Weighting (Interpolation)

IWAS   International WaterResearchAlliance Saxony

IWRM   Integrated Water Resources Management

MRMWR   Ministry of Regional Municipalities and Water Resources, Muscat, Oman

OGS   OpenGeoSys

PEST   Parameter estimation tool

PV   ParaView

List of Figures

List of Tables

Part I

Background and Fundamentals

Chapter 1

Introduction

1.1 Motivation

It is estimated that only 2.5 % of all water on earth is available as fresh water. The major part, approximately 95 % of the latter, is stored as deep groundwater or in glaciers and, thus, not always easily accessible (Oki and Kanae, 2006). However, especially in (semi-)arid regions, water supply strongly depends on often non-renewable, fossile groundwater resources (Bear, 1979). As water demand steadily increases due to growing population and economy, both quantitative and qualitative limitations emerge additionally. Firstly, as a result of excessive groundwater abstraction ("groundwater mining"), water tables decrease, exacerbating access to already limited fresh water. Secondly, for example contaminations with hazardous chemicals from industrial waste, pollution with harmful bacteria due to the absence of treatment facilities, or increased salinity from saltwater upconing or marine intrusion pose additional threats.

In order to ensure long-term stability of the valuable resource's availability, apparent groundwater issues have to be addressed and aquifer systems have to be managed properly (Krueger and Teutsch, 2013). Utilizing numerical models for the representation of underground flow and transport processes is nowadays common practice. Due to the ease of availability and the rapid development of information technology, scenario simulations can be carried out to assess fate of complex aquifer systems interacting with various partitions of the water cycle. Some state variables, e.g. temperature, for groundwater flow and transport simulations can generally be assumed to be constant. However, when fluid density or viscosity change, e.g. through the influence of dissolved solids, variable temperature, or even chemical reactions, groundwater flow cannot be handled independently from mass transport. Such coupled systems often pose advanced challenges on, both, process parametrization and numerical methods.

This thesis combines several process and application studies of subsurface flow and transport in porous media, and parametrization of associated processes. The

challenges affiliate variable-density, saturated groundwater flow processes on different scales. The scientific open-source tool OPENGEOSYS (Kolditz et al., 2012a) was enhanced by implementing key features of a gelation process, as well as utilized to perform various numerical simulations. Density-dependent modelling investigations were carried out to i) evaluate the current and future state of a heterogeneous groundwater system, ii) understand and validate vital processes of a viscosity changing solute for future usage in combination with remediation techniques, and iii) predict fate and demarcate states of double-diffusive regimes.

1.2 Structure of the Thesis

The document consists of three parts. Part I provides a general introduction and background on the topic, and presents the governing equations for density-dependent flow, solute and heat transport. A collection of benchmarks validates several aspects of the used numerical modelling tool. Part II contains small, medium and regional scale haline or thermohaline applications. As the main part of this thesis, Part II combines and amplifies the work of the scientific contributions published in literature. Namely, these are i) an extension for an inverse distance weighting interpolation, ii) investigations on transient saltwater intrusion in a coastal aquifer, and iii) gelation due to rapid viscosity change. Additionally, investigations on thermohaline convection in a double-diffusive RAYLEIGH regime are presented. Part III summarizes the work, points out general conclusions as well as major contributions, and finally, provides an outlook for future research activities.

Relevant peer-reviewed, first-author literature is attached to the thesis and accentuated by the use of the signature "[P#]: Author (Year)", with # as the equivalent number from the attached list in section "Publications", page Lib-13, and the respective citation, e.g. [P1]: Walther et al. (2012a). For secondary, additionally relevant literature the signature "[A#]: Author (Year)" is used (page Lib-13 ff.).

1.3 Variable-Density Flow in Literature

This work will consider setups with laminar flow including single-phase, single- or multi-component transport in porous media. Density-dependent flow, driven by mass or heat transport, or a combination of both, can also be found in many applications for multiphase and/or multicomponent setups in porous and/or fractured media (e.g. Böttcher (2013); Graf and Therrien (2005)) but is not part of this work.

Numerical modelling of groundwater flow is usually considered with numerous simplifications, as environmental boundary conditions provide relatively stable regimes. Including non-linear process coupling, usually raises requirements on numerical solvers and computational burden, which is why applications of variable-density processes show relatively young publication dates. Also, due to already mentioned increased computing capabilities, and escalating water demands in (semi-)arid regions, density-

driven flow found intense popularity in groundwater related studies in the recent decades.

Next to, and mostly based on analytical methods (e.g. the Ghyben-Herzberg relationship, or the Glover solution (Glover, 1959)) sharp-interface approaches provided first techniques to handle variable-density fluid behaviour (Bear, 1972, 1999). Well-known early combinations of experimental investigations and numerical methods are presented in Henry (1960), or Elder (1965); Elder (1967), laying foundations also for model benchmarking. Representation of a mixing interface zone by solving partial differential equations (PDE) was introduced in Frind (1982a), Voss (1984), or Diersch (1988). Recent remarkable publications, including different applications of variable-density flow, are Oldenburg and Pruess (1995), Kolditz et al. (1998), Diersch and Kolditz (2002), Park (2004), or Goswami and Clement (2007).

The list of citations is intentionally kept short at this section, definitely more literature could be listed on a multitude of different aspects of density-driven flow. More application-specific literature is presented in the individual chapters of the thesis providing a broader spectrum of the available publications.

Chapter 2

Theory and Methods

2.1 Governing Equations

2.1.1 Continuity Equation

To describe flow in porous media, one generally applies the continuity equation on the concept of the representative elementary volume (REV, see Bear (1972), Kolditz (2002)). The former can be formulated as a general balance equation of the form

$$\frac{\partial X}{\partial t} + \nabla \cdot \mathbf{j} = q_j \tag{2.1}$$

where X is volume density of flux $\mathbf{j}$, t is time, and q_j is sources or sinks. The left-hand side first term accounts for the accumulation over time (i.e. storage), the second quantifies fluxes through the REV (i.e. advection), and the right-hand side refers to production or reduction (i.e. sources/sinks).

2.1.2 Groundwater Flow Equation

From the general approach of (2.1), one can define the basic flow equation to describe movement of fluids in porous media as

$$\frac{\partial (S' \varphi \rho^{\mathrm{f}})}{\partial t} + \nabla \cdot (\varphi \rho^{\mathrm{f}} \mathbf{v}) = \rho^{\mathrm{f}} Q_\rho \tag{2.2}$$

S' is saturation ratio, φ is porosity, ρ^{f} is fluid density, $\mathbf{v}$ is fluid velocity vector, and $\rho^{\mathrm{f}} Q_\rho$ is source/sink term of fluid mass. The Darcy term can be formulated as

$$\mathbf{q} = \varphi \mathbf{v} = -\frac{\boldsymbol{\kappa} \rho_0^{\mathrm{f}} g}{\mu} \left(\nabla h + \left(\frac{\rho^{\mathrm{f}} - \rho_0^{\mathrm{f}}}{\rho_0^{\mathrm{f}}} \right) \mathbf{e} \right) \tag{2.3}$$

where $\mathbf{q}$ is the Darcy vector, $\boldsymbol{\kappa}$ is saturated intrinsic permeability tensor, ρ_0^{f} is reference fluid density, g gravity constant, μ is dynamic viscosity, h is equivalent freshwater head, and $\mathbf{e}$ is the unit vector in gravitational direction.

The relation between saturated intrinsic permeability tensor $\boldsymbol{\kappa}$ and saturated equivalent freshwater conductivity tensor $\mathbf{K_f}$, which is often used in groundwater applications, is given by

$$\boldsymbol{\kappa} = \frac{\mu}{\rho_0^{\mathrm{f}} g} \mathbf{K_f} \tag{2.4}$$

It may be convenient to define (2.2) and (2.3) in terms of hydraulic head h which can be derived from BERNOULLI's principle of hydraulic potential as $h = \frac{p}{\rho_0^{\mathrm{f}} g} + z$ where p is water pressure, and z is elevation.

To account for unconfined flow conditions in groundwater flow applications, an approach by Sugio and Desai (1987) is utilized, that, above the water table, reduces permeability κ as a function of pressure ($p < 0$), while the domain stays fully saturated (see [P2]: Walther et al. (2012b)).

2.1.3 Advection-Dispersion Equation

When dealing with miscible fluids of the same phase, and when individual concentrations do not interact between each other (e.g. through chemical or biological processes), transport process for solute i can be described within one single phase as

$$\frac{\partial(\varphi c_i)}{\partial t} + \nabla \cdot (c_i \varphi \mathbf{v}) - \nabla \cdot (\varphi \mathbf{D} \cdot \nabla c_i) = q_{c_i} \tag{2.5}$$

where c_i is concentration of solute i, $\mathbf{D}$ is tensor of hydrodynamic dispersion, and q_{c_i} represents sinks/sources of solute i. Following Bear (1979), $\mathbf{D}$ can be defined as the combination of molecular diffusion and mechanical dispersion by

$$\mathbf{D} = \tau D_m \delta_{ij} + \alpha_l \left| \mathbf{v} \right| \delta_{ij} + (\alpha_l - \alpha_t) \frac{v_i v_j}{|\mathbf{v}|} \tag{2.6}$$

where τ is tortuosity, D_m is molecular diffusion coefficient, δ_{ij} is KRONECKER delta, and $\alpha_{l/t}$ is dispersivity (longitudinal/transversal).

2.1.4 Heat Transport Equation

In some applications, heat transport processes may be considered in combination with fluid flow and mass transport. To describe heat transport within porous media under incompressible conditions, both, solid and fluid phases need to be considered. Heat radiation flux is usually insignificantly small compared to other heat transport processes. Without deformation or change of the porous medium structure, only heat conduction is relevant in the solid phase. For the fluid phase, heat convection needs to be considered additionally.

$$(\rho C_p)^{\mathrm{eff}} \frac{\partial \Theta}{\partial t} + (\rho C_p)^{\mathrm{f}} (\varphi \mathbf{v} \nabla \Theta) - \lambda^{\mathrm{eff}} \Delta \Theta = q_\Theta \tag{2.7}$$

with Θ as temperature, C_p^i as isobaric heat capacity, (superscripts for effective eff, fluid f, or solid s), λ^i as thermal conductivity, and q_Θ as thermal sources/sinks.

Commonly, local thermal equilibrium in fluid and solid phases is considered. The over both phases averaged, effective parameters for heat capacity are written as

$$(\rho C_p)^{\text{eff}} = (1 - \varphi)\,(\rho C_p)^{\text{s}} + \varphi\,(\rho C_p)^{\text{f}} \tag{2.8}$$

and similarly, for heat conductivity

$$\lambda^{\text{eff}} = (1 - \varphi)\,\lambda^{\text{s}} + \varphi\lambda^{\text{f}} \tag{2.9}$$

Several alternatives to acquire the aforementioned effective parameters are furthermore presented in Farouki (1981).

2.2 Fluid Properties for Flow and Transport Processes

2.2.1 Density

Besides applications investigating fate of non-aqueous-phase liquids, density-dependent flow and transport processes in groundwater usually occur under moderate conditions, i.e. in a single-phase continuum, without phase changes, comprehending relatively narrow fluctuations of process variables (e.g. temperature change in groundwater), and thus with only small (i.e. mostly neglectable) variations of state parameters (e.g. heat capacity). Yet, for applications dealing with thermohaline phenomena, fluid density is essentially sensitive on concentration and/or temperature. Therefore, the individual processes of the following studies are iteratively coupled by fluid density, neglecting the compressibility of the fluid associated to the change of pressure, through

$$\rho^{\text{f}} = \rho_0^{\text{f}}\,(1 + \gamma_{c_i}\,(c_i - c_{i,0}) + \gamma_\Theta\,(\Theta - \Theta_0)) \tag{2.10}$$

where subscript 0 accounts for reference values, and $\gamma_{c_i/\Theta}$ are coefficients of expansion resulting from the change of concentration or temperature, respectively, at constant pressure. Here, the expansion coefficients are used with the conventions $\gamma_{c_i} \geq 0$ and $\gamma_\Theta \leq 0$ to signify increasing density for increasing concentrations, and decreasing density for increasing temperature. Although more complex, non-linear relationships exist, this linear one is reported to be sufficient for marine water concentration (Park, 2004).

In principle, one would need to consider derivatives of density over time and space in equations (2.2) and (2.5). In the following, the Oberbeck-Boussinesq approximation was applied (Boussinesq, 1904), which is sufficient for small density gradients over time and space (Kolditz et al., 1998; Beinhorn et al., 2005; Langevin and Guo, 2006; Babu et al., 2012).

2.2.2 Viscosity

Similarly to density dependency, fluid viscosity usually can be treated as a constant value due to relatively steady surrounding conditions, i.e. small fluctuations

of temperature, pressure, or solute concentration result in insignificant variations of viscosity. For conditions of variable viscosity, it is possible to provide an equation of state for viscosity which may depend on temperature or solute concentration, similarly to equation (2.10).

$$\mu = \mu_0 \left(1 + \xi_{c_i} \left(c_i - c_{i,0}\right) + \xi_\Theta \left(\Theta - \Theta_0\right)\right) \tag{2.11}$$

where subscript 0 accounts for reference values, and $\xi_{c_i/\Theta}$ are coefficients of viscosity change resulting from the change of concentration or temperature, respectively, at constant pressure.

In general, variation of concentration (for marine saltwater) will result in a significantly larger change of density, than of viscosity, while the opposite is the case for variation of temperature (Ozbek et al., 1977; Kestin et al., 1981; Francke and Thorade, 2010). Therefore, $\xi_{c_i/\Theta} = 0$ for saltwater related applications, i.e. sections 3, p. I-15, and 5, p. II-9. For specific modelling tasks, determination of fluid viscosity can become very complex due to chemical reactions. Section 6, p. II-25, (compare also [P3]: Walther et al. (2013b)) describes such an advanced viscosity (and density) depending process modelling due to gelation of an injected solution into a porous medium. In the thermohaline application of section 7, p. II-33, determination of viscosity (and density) is not that simple and discussed in more detail.

2.3 Modelling and Visualization Tools

2.3.1 Modelling Tools

With the apparent impossibility of acquiring all needed parameters without any uncertainty, numerical modelling tools are inevitable for sensitivity studies or scenario simulations. Throughout the last decades, a large number of different numerical simulation tools that are capable of reproducing variable-density flow became available. Alongside the ability to solve the governing equations, these software "toolboxes" often additionally accommodate model setup, data and parameter management, automatic parameter calibration, or result visualization options. Some of those tools are freely available (occasionally supplied within an open-source license), others are sold commercially.

It has become increasingly common to build upon a modular based structure, sometimes already expressed by the naming e.g. as it is done by the well known groundwater modelling package MODFLOW (Harbaugh, 2005). Often used techniques for solving the partial differential equation systems are finite difference (FD), finite element (FE), finite volume (FV), or boundary element method. Table 2.1, p. I-12, gives a short overview on relevant software tools and some of their features (all cited URLs as of Monday 20th October, 2014). Such an overview cannot be complete, as many of the presented toolboxes continuously develop by adding and extending features.

In this work, OpenGeoSys was used for numerical modelling (Kolditz et al., 2012a). OpenGeoSys is a scientific open-source modelling software based on the Galerkin Finite Element Method, and is able to couple numerous THMC (thermal, hydraulic, mechanical, and chemical) processes in porous and fractured media ([A1]: Kalbacher et al. (2011)). Various applications of variable-density flow using Open-GeoSys have already been published (e.g. Park and Aral (2008); Böttcher et al. (2012)). Essential processes for density-driven flow are benchmarked in section 3, p. I-15; see also Kolditz et al. (2012b).

Additional simulation codes capable of density-dependent flow simulations, and not mentioned in table 2.1, p. I-12, are MITSU3D (Ibaraki, 1998), TOUGHRE-ACT (Xu et al., 1999), MIN3P (Mayer et al., 2001), PHT3D (Prommer et al., 2002), HYTEC (van der Lee et al., 2003), RetrasoCodeBright (Saaltink et al., 2005), CrunchFlow (Steefel, 2009), or UG (Musuuza et al., 2011a).

2.3.2 Visualization Tools

Proper visualization will help to evaluate results of numerical modelling. It is often the key to validate correct model setup, or understand process behaviour. This is especially important as model setups become increasingly complex, i.e. heterogeneous, and/or three-dimensional, as in the application presented in section 5, p. II-9. With the use of adequate visualization tools, vital information can be extracted from complex datasets and displayed in more convenient ways. In some occasions, employment of visualization techniques is yet unavoidable, for example to present three-dimensional data in two-dimensional environments. Thus, scientific results are easier to percept and can be transferred to an audience with less inside knowledge about the specific field of application.

In the following, the open-source visualization programme ParaView (PV, version 4.01, Henderson (2007), `http://www.paraview.org`) was used for data analysis and visualization. PV is based on the Visualization Toolkit (VTK, Schroeder et al. (2006)), and provides a toolbox for data processing in the form of various applicable filters, i.e. visualization algorithms (contouring, slicing, glyphing, etc.), which can also be combined in a "pipeline".

As nowadays increasingly detailed and larger scale setups consist of immense datasets, results from parallel simulations often, both, exceed bandwidth limitations to transfer output data to local computers, and demand strong computation capabilities for visualization. PV offers a client-server architecture to handle large datasets. A powerful cluster computer (server) manages data processing and generates a visualization, which is then sent to the user's local personal computer (client). For example, datasets of simulation output for the regional scale application described in section 5, p. II-9, are $\approx 150\,\mathrm{MB}$ per time step resulting in a total of $\approx 75\,\mathrm{GB}$ for the long-term simulation. Processed and transmitted visualization data from the server are $< 2\,\mathrm{MB}$ per figure. Section E.3, p. App-7, describes the connection procedure from the local client to the remote server for a parallel ParaView session.

Table 2.1: Toolboxes for density-dependent numerical modelling.

Name of Software	PDE Method	Supported Operating System	Latest Version	License	Comments
FEFLOW[1] Finite element subsurface flow system	FE	MS Windows, Linux	6.1 (2012)	commercial	"Public programming interface" to include custom user code or couple external software, parallelized simulation included
SUTRA[2] Saturated-Unsaturated Transport	FE	MS Windows	2.2 (2010)	open-source	One of the first available codes to solve density-dependent flow and transport
TOUGH[3] Transport of Unsaturated Groundwater and Heat	FD	MS Windows, Linux	2.1 (2012)	commercial/ open-source	Several variations for multiple application purposes (e.g. multiphase transport, fracture media)

Continued on next page

---

[1] Diersch (1981), http://www.feflow.info
[2] Voss (1984), http://water.usgs.gov/nrp/gwsoftware
[3] Oldenburg and Pruess (1995), http://esd.lbl.gov/research/projects/tough/

Table 2.1 – *Continued from previous page*

Name of Software	PDE Method	Supported Operating System	Latest Version	License	Comments
ROCKFLOW[4]	FE	MS Windows, Linux(?)	5.1 (2012)	open-source	Simulation of flow, mass and heat transfer and deformation in fractured porous rock
GeoSys[5]	FE	MS Windows, Linux	4.7	open-source	Predecessor of OpenGeoSys, discontinued
HGS[6] HydroGeoSphere	control-volume FE, FD	MS Windows	n.n.	commercial/closed-source	Simulation of flow, mass and heat transfer and deformation in fractured porous rock
d3f[7] distributed density driven flow	FV	Linux, Mac	n.n.	closed-source, scientific license	Based on UG, programmable interface, adaptive grid, multi-grid techniques, parallelized

Continued on next page

[4]Kolditz et al. (1998), http://esd.lbl.gov/research/projects/tough/
[5]Beinhorn et al. (2005)
[6]Graf and Therrien (2005); Brunner and Simmons (2012), http://www.aquanty.com
[7]Fein and Schneider (1999); Grillo et al. (2010), http://www.grs.de/content/transportmodellierung

Table 2.1 – *Continued from previous page*

Name of Software	PDE Method	Supported Operating System	Latest Version	License	Comments
MIKE SHE[8]	FD	MS Windows	2012	commercial	Coupling of whole water cycle including overland flow, reservoirs, unsaturated, saturated zone, groundwater flow.
SEAWAT[9]	FD	MS Windows	4 (2012)	open-source	Coupled MODFLOW and MT3DMS for density-dependent flow process, thus combinable with other MODFLOW related packages.
OGS[10] OPENGEOSYS	FE	MS Windows, Linux	5.5 (2013)	open-source	Modelling of flow in porous media and fractures; THM/C coupling including several third-party simulation codes, e.g. PhreeqC, Gems, Eclipse.

---

[8]Hughes and Liu (2008), http://www.dhi-wasy.de/Software/Grundwasser/MIKESHE.aspx
[9]Langevin and Guo (2006), http://water.usgs.gov/ogw/seawat/
[10]Kolditz et al. (2012a); Kolditz et al. (2012b), http://www.opengeosys.org/

Chapter 3

Benchmarks for OpenGeoSys

Identification, measurement and estimation of parameters are the keys for the conceptual and numerical representation of physical processes ([A2]: Kolditz et al. (2012b)). Yet, the general understanding of subsurface flow and transport processes, especially for non-linear applications like density-dependent, coupled flow and transport, is still rather low compared to other components of the hydrological cycle. One approach to close this gap of knowledge is to combine measurements of laboratory experiments and results from numerical simulations within so called benchmarks. This will help to identify possibly missing processes, provide vital parameterization data, as well as validate the numerical tool for further appliances.

In this chapter, a number of benchmarks will be presented, that evaluate the capability of OPENGEOSYS to resemble the important processes needed for general groundwater table and variable-density flow calculations. These include application of fixed or variable pressure head boundary conditions (DIRICHLET 1st-type), fixed flux BCs (NEUMANN 2nd-type), elevation of stationary and development of transient groundwater table, stationary and transient intrusion and push-back of saltwater, as well as formation and recovery of a freshwater lens. For some benchmarks, analytical solutions exist, others are validated against real-world, laboratory data from experimental setups.

3.1 Steady-state Unconfined Groundwater Table, Discharge Through Plain, and Source Term

Problem Description. This benchmark features the solution to three issues in one setup: i) groundwater flow under unconfined conditions, ii) determination of discharge through a defined, vertical, rectangular plain (i.e. "surface" in OPENGEO-SYS), and iii) definition of source term at a plain (surface) using the dimensions $[L^3 \cdot T^{-1}]$. The problems will be evaluated using the analytical solution for a free groundwater table with the DUPUIT-FORCHHEIMER assumptions (i), and the DARCY-Law (ii, iii).

Figure 3.1: Conceptional model, boundary conditions, gridding, plains for discharge calculations

Methods and Model Setup. To achieve an unconfined groundwater table, the groundwater flow equation (2.2) is used combined with an adopted approach described by Sugio and Desai (1987) (see section 2.1, p. I-7). The conceptional model is depicted in figure 3.1, p. I-16, relevant simulation parameters are listed in table 3.1, p. I-17.

The DUPUIT-FORCHHEIMER assumption is utilized to solve the elevation of the free groundwater table at several points along the flow direction x for the one-dimensional case between two given heads $h_{in} = h(x = 0)$ and $h_{out} = h(x = L)$ over the flow distance L using equations (3.2) and (3.3) (see David (1998)). The DARCY-Law (2.3) and the continuity equation (3.1) can be used to determine the discharge Q_{in} of the inflow boundary condition (as 2nd type for an inflow area $A = 100$ x $30\,m^2$) with the given head difference $\Delta h = h_{out} - h_{in} = -5\,m$ over $L = 100\,m$ to the outflow boundary condition h_{out} (as 1st type) in a homogeneous rectangular cuboid (dimensions 100 x 100 x 50 m^3). The discharge will be calculated for two rectangular, vertical plains in the middle of the domain: plain 1 ($\overline{AB}$) lies perpendicular to the flow direction, plain 2 is rotated around A connecting $\overline{AC}$. The discharge for both plains should equal the inflow boundary condition.

The continuity equation yields the discharge Q as

$$Q = A\,|\mathbf{v}| \tag{3.1}$$

where A is the area through which the discharge is routed, and $|\mathbf{v}|$ is the magnitude of velocity vector $\mathbf{v}$. Integration of the one-dimensional DARCY-Law in terms of hydraulic head (equations 2.3, p. I-7, 2.4, p. I-8)

$$\frac{\partial}{\partial x}\left(K_f \frac{\partial h}{\partial x}\right) = q \tag{3.2}$$

yields the stationary, analytical solution with the hydraulic head h at the location x

Table 3.1: Simulation parameters for unconfined groundwater surface

Parameter	Value
Discharge Q_{in} $\left(\text{m}^3 \cdot \text{s}^{-1}\right)$	$1.4715 \cdot 10^{-2}$
Dynamic viscosity μ $(\text{Pa} \cdot \text{s})$	$1 \cdot 10^{-3}$
Fluid density ρ^{f} $\left(\text{kg} \cdot \text{m}^{-3}\right)$	$1 \cdot 10^3$
Gravity constant g $\left(\text{m} \cdot \text{s}^{-2}\right)$	9.81
Hydraulic conductivity K_f $\left(\text{m} \cdot \text{s}^{-1}\right)$	$9.81 \cdot 10^{-5}$
Intrinsic permeability κ $\left(\text{m}^2\right)$	$1 \cdot 10^{-11}$
Model length L (m)	100
Inflow hydraulic head h_{in} (m)	30
Outflow hydraulic head h_{out} (m)	25
Initial water level h (m)	25
Residual reduction factor ζ_{res} $(-)$	$1 \cdot 10^{-4}$
Residual reduction pressure p_{res} (Pa)	5000

(without sources/sinks, i.e. $q = 0$) as

$$h(x) = \left[h_{\text{in}}^2 - \left(h_{\text{in}}^2 - h_{\text{out}}^2 \right) \frac{x}{L} \right]^{\frac{1}{2}} \tag{3.3}$$

where x is spatial variable, h_{in} is head at inflow boundary, h_{out} is head at outflow boundary.

Results. Figure 3.2, p. I-18, shows the analytical solution of the free groundwater table in comparison to the numerical simulation results. Additionally, table 3.2, p. I-17, shows the comparison of the calculated values after DARCY and the output of the water balance through the two vertical plains. All outcomes from OPEN-GEOSYS show very low deviations from the theoretical solutions. Accuracy of the solution depends on vertical grid resolution and the residual reduction variables of the Sugio approach ζ_{res} and p_{res}.

Table 3.2: Comparison of discharge through plains vs. calculations

	Darcy / BC 2$^{\text{nd}}$ type	Plain $\overline{\text{AB}}$	Plain $\overline{\text{AC}}$
Result $[\text{m}^3 \cdot \text{s}^{-1}]$	$1.4715 \cdot 10^{-2}$	$1.4715 \cdot 10^{-2}$	$1.4703 \cdot 10^{-2}$
Rel. difference [%]	$-$	$-6.3854 \cdot 10^{-4}$	$-8.3602 \cdot 10^{-2}$

3.2 Theis Transient Pumping Test for Unconfined Conditions

Problem Description. This benchmark compares the spatio-temporal water table development for a transient pumping situation against THEIS' analytical solution (Theis, 1935). Although the analytical solution is based on confined conditions, it

(a) 3D view of gridded domain, scaled velocity vectors, free groundwater table with $p = 0$, isolines of hydraulic head; green line depicts reference line for output in figure 3.2(b), p. I-18.

(b) Comparison of analytical solution vs. OPENGEO-SYS output along green reference line in figure 3.2(a), p. I-18.

Figure 3.2: 3D view and groundwater table comparison

is known to be still valid for small drawdown values. For larger drawdowns, the Neuman (1974) solution should be used.

Methods and Model Setup. The geometry and location of the boundary conditions are pictured in figure 3.3, p. I-19. OPENGEOSYS is used to solve the benchmark with the set of parameters given in table 3.3, p. I-19.

THEIS' equations for computing a drawdown in relation to space and time $s(r, t)$ are described as follows.

$$s(r, t) = \frac{Q}{4\pi T} W(u) \tag{3.4}$$

with s is drawdown, Q is pumping rate, $T = K_f d'$ is transmissivity as product of hydraulic conductivity K_f and saturated aquifer thickness d', and $W(u)$ is the so called "well function". The argument of $W(u)$ is obtain by solving

$$u = \frac{r_p^2 S}{4Tt} \tag{3.5}$$

with r_p is the radial distance from the pumping well, S is storage coefficient (for this unconfined case as specific yield S_y). The function $W(u)$ is defined by the exponential integral E_1

$$W(u) = \mathrm{E}_1(z) = \int_z^\infty \frac{e^{-x}}{x} dx \qquad |\mathrm{Arg}(z)| < \pi \tag{3.6}$$

which can be approximated by

$$\mathrm{E}_1(z) = -\gamma - \ln z + \sum_{k=1}^\infty \frac{(-1)^{k+1} z^k}{k\, k!} \qquad |\mathrm{Arg}(z)| < \pi \tag{3.7}$$
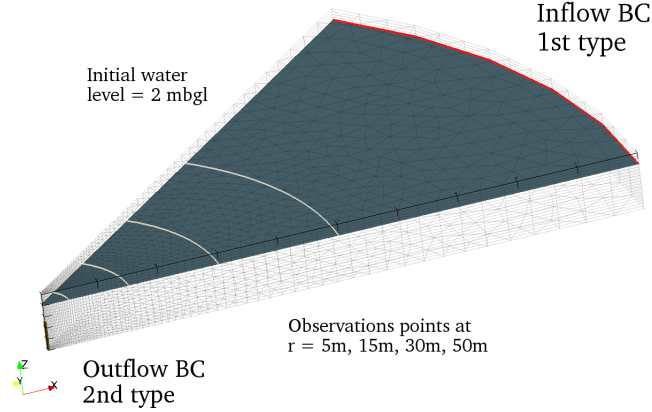
Figure 3.3: Conceptional model, boundary conditions, gridding, initial hydraulic head, location of observations for $s(t)$

with $\gamma \approx 0.57721$ as the EULER-MASCHERONI constant.

The homogeneous, isotropic model domain consists of a $1/8^{th}$ section of a cylinder with radius $r = 100$ m and height $d' = 10$ m around a central pumping well. At $r = 100$ m, a 1st type boundary condition is positioned at $z = -2$ m with a pressure of $p = 0$ Pa. To represent an incomplete well, at $r = 1$ m, a 2nd type boundary condition is positioned at 0 m $< z < 5$ m with a total abstraction of $1/8^{th}$ of the value used for the analytical solution, i.e. $Q_{\mathrm{model}} = 0.125 \cdot Q_{\mathrm{analyt}}$.

Table 3.3: Benchmark parameters for THEIS solution

Parameter	Value
Well abstraction analytical Q_{analyt} $\left(\mathrm{m} \cdot \mathrm{s}^{-3}\right)$	$2.315 \cdot 10^{-4}$
Well abstraction model Q_{model} $\left(\mathrm{m} \cdot \mathrm{s}^{-3}\right)$	$2.894 \cdot 10^{-5}$
Specific yield S_y $\left(\mathrm{m}^{-1}\right)$	0.2
Dynamic viscosity μ $(\mathrm{Pa} \cdot \mathrm{s})$	$1 \cdot 10^{-3}$
Fluid density ρ^{f} $\left(\mathrm{kg} \cdot \mathrm{m}^{-3}\right)$	$1 \cdot 10^{3}$
Gravity constant g $\left(\mathrm{m} \cdot \mathrm{s}^{-2}\right)$	9.81
Hydraulic conductivity K_f $\left(\mathrm{m} \cdot \mathrm{s}^{-1}\right)$	$1 \cdot 10^{-5}$
Intrinsic permeability κ $\left(\mathrm{m}^{2}\right)$	$1.0194 \cdot 10^{-12}$
Aquifer thickness d' (m)	10
Initial water level h (mbgl)	2
Transmissivity T $\left(\mathrm{m}^{2} \cdot \mathrm{s}^{-1}\right)$	$8 \cdot 10^{-5}$
Residual reduction factor ζ_{res} $(-)$	$1 \cdot 10^{-4}$
Residual reduction pressure p_{res} (Pa)	5000

Results. Numerical results are compared against the analytical solution i) for temporal development of the drawdown at several points with a specified radial distance

(a) Comparison of drawdown over time for different radii

(b) Scatter plot for different radii

(c) Comparison of drawdown over radius for different times

(d) Scatter plot for different times
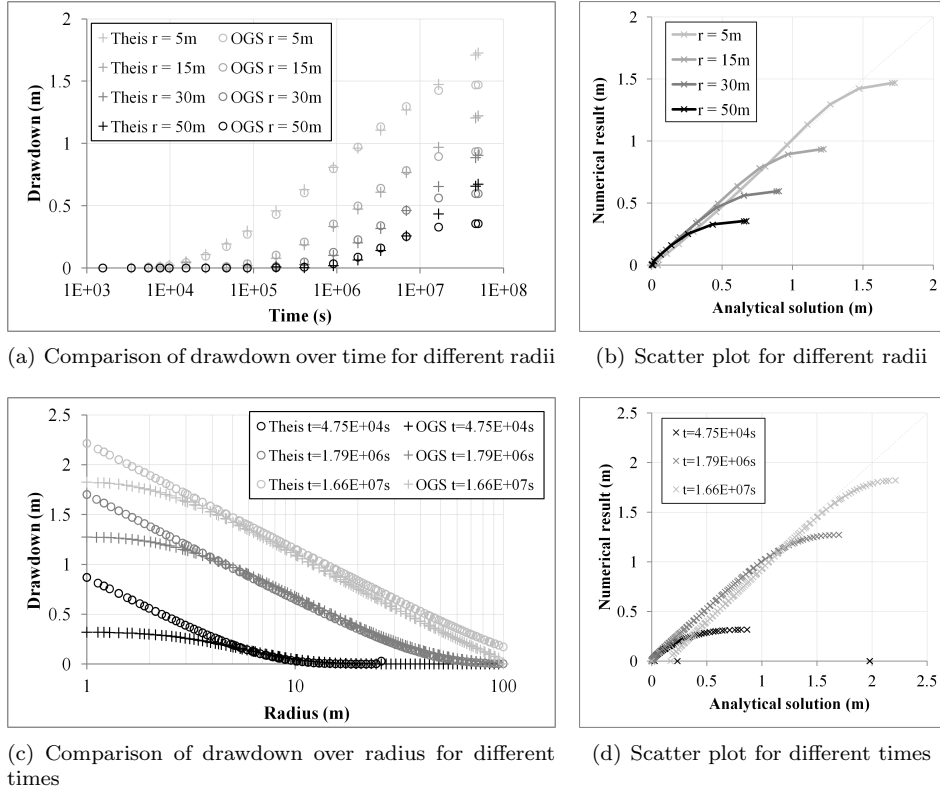
Figure 3.4: Comparison between numerical results and analytical solution of drawdown.

r_i from the pumping well, i.e. $s(r_i, t)$, and ii) for the spatial distribution of the drawdown at several simulation time steps t_i, i.e. $s(r, t_i)$. Figures 3.4(a), p. I-20, and 3.4(b), p. I-20, account for i), figures 3.4(c), p. I-20, and 3.4(d), p. I-20, for ii).

In general, the numerical results are in good accordance with the analytical solution. Deviations occur to the end of the simulation especially near the 1st-type constant pressure boundary condition, and in the beginning of the simulation within the very vicinity of the 2nd-type constant flux well boundary. The former is due to the assumption of an infinitely large groundwater body of the analytical solution which cannot be taken into account in the numerical model. The latter may be because of balance errors emerging from the Sugio approach (see [P2]: Walther et al. (2012b) or Sugio and Desai (1987)), too low grid resolution, or may signify the limitation of applying THEIS' equation for unconfined conditions.

3.3 Transient Saltwater Intrusion for Unconfined Conditions

Problem Description. This benchmark verifies the capabilities of OPENGEOSYS to model transient, variable-density groundwater flow and transport against a labo-
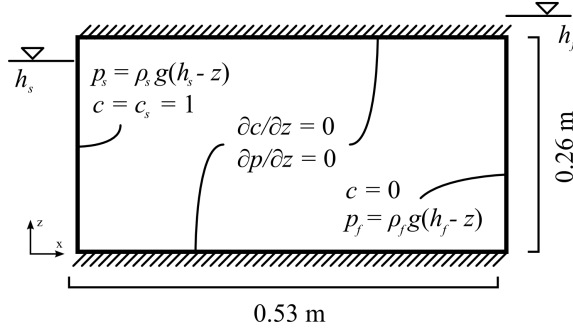
Figure 3.5: Model domain and boundary conditions after Goswami and Clement (2007) (altered, not to scale).

Table 3.4: Benchmark parameters for GOSWAMI-CLEMENT problem

Parameter	Value
Freshwater head h_f (m)	0.267
Saltwater head h_s (m)	0.255
Porosity φ $(-)$	0.385
Permeability κ $\left(\text{m}^2\right)$	$1.239 \cdot 10^{-9}$
Dynamic viscosity μ $(\text{Pa} \cdot \text{s})$	$1 \cdot 10^{-3}$
Freshwater density ρ_f^{f} $\left(\text{kg} \cdot \text{m}^{-3}\right)$	1000
Saltwater density ρ_s^{f} $\left(\text{kg} \cdot \text{m}^{-3}\right)$	1026
Saltwater-freshwater density relation γ_c $(-)$	0.026
Longit. / transv. dispersivity $\alpha_{l/t}$ (m)	$1 \cdot 10^{-3}$ / $1 \cdot 10^{-4}$
Diffusion coefficient D_m $\left(\text{m}^2 \cdot \text{s}^{-1}\right)$	0
Residual reduction factor ζ_{res} $(-)$	$1 \cdot 10^{-4}$
Residual reduction pressure p_{res} (Pa)	100

ratory setup and numerical SEAWAT simulation data (Langevin and Guo, 2006). Goswami and Clement (2007) show a saltwater intrusion experiment after Henry (1960), using a laboratory scale tank. The benchmark is an extension to the steady-state setup documented in [P2]: Walther et al. (2012b).

Methods and Model Setup. The GOSWAMI-CLEMENT problem features a horizontally intruding and withdrawing saltwater front in an initially present freshwater environment. The conceptual model is depicted in figure 3.5, p. I-21, important model parameters are listed in table 3.4, p. I-21.

The saltwater reservoir is situated on the left side of the tank. General flow points from right to left in the homogeneous, isotropic material. Dimensions of the experimental tank were 0.53 x 0.26 x 0.027 m^3 (length x height x width). A vertical x-z model domain was constructed using a grid resolution of uniform, rectangular

(a) Transient state TS1 (intrusion).

(b) Transient state TS2 (withdrawal).
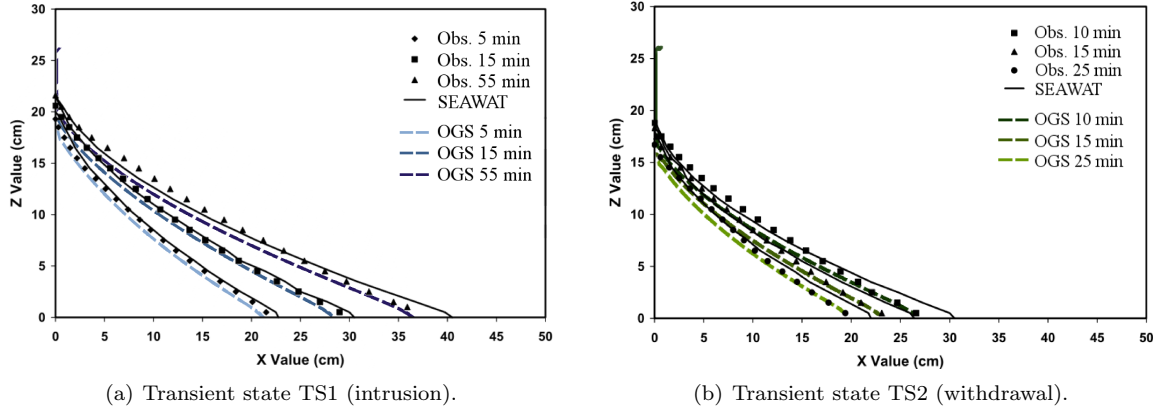
Figure 3.6: Concentration $c = 0.5$ isolines for GOSWAMI-CLEMENT's experimental data (point symbols), their SEAWAT simulation (black lines), and OPENGEOSYS results (coloured lines); after Goswami and Clement (2007) (altered).

quad-elements each $\Delta x = \Delta z = 5 \cdot 10^{-3}$ m in size. At top and bottom edges, BCs are 2nd-type no-flow for flow and transport. Applied to the vertical edges are 1st-type BCs as linear pressure gradients $p_i(z) = \rho_i^f g \left(h_i - z \right)$ for groundwater flow including the respective fluid densities $\rho_{f/s}^f$ as well as pressure heads $h_{f/s}$ of fresh or saltwater, respectively. Transient states TS1 (transition of steady-states SS1 to SS2) and TS2 (SS2 to SS3) for experiments and simulations are controlled by an immediate variation of the right-side freshwater pressure head. Constant concentration 1st-type BCs are $c = 0$ and $c = c_s = 1$ on the fresh and salt water side, respectively.

Longitudinal dispersivity was determined within the laboratory experiments to $\alpha_l = 10^{-3}$ m, transversal dispersivity was assumed to be $\alpha_t = 0.1 \cdot \alpha_l = 10^{-4}$ m. Following Sugio and Desai (1987), diffusion effects were neglected due to the primarily advection-dominated flow regime (compare [P2]: Walther et al. (2012b)).

Note: Goswami and Clement (2007) do not explicitly state a value for specific storativity, although the domain becomes confined for $x \gtrsim 0.25$ m. In this application, it is assumed that the response from the change of the right-side pressure head BC happens relatively fast on small scale and has only little impact on the saltwater wedge emerging from the left side.

Results. Figure 3.6, p. I-22, depicts the comparison of the transient simulations between the experiment and the numerical models. Both simulation tools, SEAWAT and OPENGEOSYS, resemble the measurements quite well in terms of temporal development, shape of the saltwater wedge, and intrusion length. Nevertheless, they also show deviations from the laboratory measurements. While SEAWAT overestimates intrusion length at the toe of the saltwater wedge, OPENGEOSYS generally yields a better prediction or slightly underestimates intrusion length. Near the left-side

BC, SEAWAT results are in better compliance with measurements, than OPENGEO-SYS outcome, which may be due to the circumstance that OPENGEOSYS does not feature a mass transport BC, sometimes referred to as "constrained BC", which switches automatically between fresh or saltwater depending on the flow direction, i.e. $c = c_s$ for flow into and $c = c_{water}$ (i.e. concentration of outflowing water) for flow out of the model domain. Although, the left side mass transport boundary condition is not ideal and still shows concentrations $c = 1$ (compare also figure 3.8, p. I-24), the influence on relevant model results is insignificant in comparison to parameter insecurity (e.g. value and distribution of hydraulic conductivity). Recent efforts to implement such a "constrained BC" into OPENGEOSYS show improving results in the close vicinity of the left side BC, yet still same results for the relevant model features (e.g. salt toe intrusion length, transient development).

3.4 Development and Recovery of a Freshwater Lens under Transient Conditions

Problem Description. This benchmark shows the capability of OPENGEOSYS to represent displacement of saline water due to an infiltration recharge process from top in a saturated, initially completely salinized domain. Experimental data from Stoeckl and Houben (2012) are used to validate temporal development and maximum penetration depth of the freshwater lens.

Methods and Model Setup. The geometry of the physical model of Stoeckl and Houben (2012) was a symmetrical trapezoid. The conceptual model includes the left side of the real-world setup, dividing the model at the symmetry line to reduce computational burden (see figure 3.7, p. I-24). Table 3.5, p. I-24, shows simulation parameters.

The experiment was two-folded: i) starting from an initial state of full salinization, a constant recharge q was applied on top of the domain until a steady state was reached at time t_1; ii) when the freshwater lens was fully evolved, recharge flux was stopped and the reduction of the lens was observed. The homogeneous, isotropic domain was set up using triangular elements with a mean edge length $\Delta l \approx 3 \cdot 10^{-3}$ m. At right and bottom sides, BCs are 2nd-type no-flow for flow and transport. On the top edge, a 2nd-type recharge rate was applied uniformly with $q(0 < t \leq t_1) = 1.3 \cdot 10^{-5} m \cdot s^{-1}$ and $q(t > t_1) = 0$. Mass transport BC on top was $c = 0$ for $0 < t \leq t_1$ and switched to no-flow for $t > t_1$. For the left, inclined edge, constant 1st-type linear pressure gradient $p(z)$ and concentration BC $c = c_s = 1$ were set.

Results. Figure 3.8, p. I-24, shows the steady state flow regime at t_1. A stable freshwater lens evolved with a mixing zone visible at the interface between the fresh and saltwater. During evolution of the lens, recharge applied on top forced saltwater

Table 3.5: Benchmark parameters for freshwater lens development

Parameter	Value
Saltwater head h_s (m)	0.0
Porosity φ $(-)$	0.39
Permeability κ $\left(\text{m}^2\right)$	$4.601 \cdot 10^{-10}$
Dynamic viscosity μ $(\text{Pa} \cdot \text{s})$	$1 \cdot 10^{-3}$
Specific storage S_s $(-)$	$1 \cdot 10^{-4}$
Freshwater density ρ_f^f $\left(\text{kg} \cdot \text{m}^{-3}\right)$	997
Saltwater density ρ_s^f $\left(\text{kg} \cdot \text{m}^{-3}\right)$	1021
Saltwater-freshwater density relation γ_c $(-)$	0.02407
Longit. / transv. dispersivity $\alpha_{l/t}$ (m)	$5 \cdot 10^{-3}$ / $5 \cdot 10^{-4}$
Diffusion coefficient D_m $\left(\text{m}^2 \cdot \text{s}^{-1}\right)$	$1 \cdot 10^{-9}$
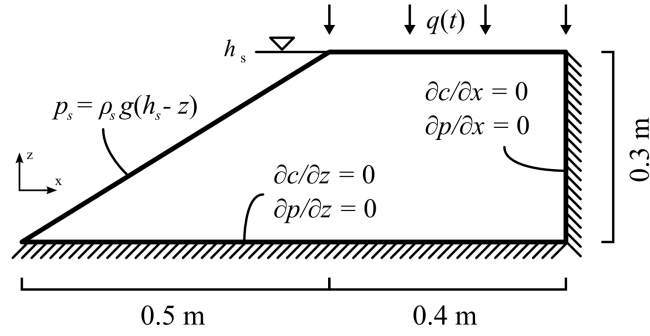
Figure 3.7: Model domain and boundary conditions after Stoeckl and Houben (2012) (not to scale).
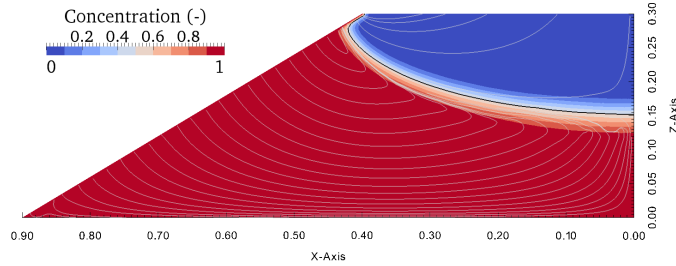
Figure 3.8: Concentration and flow paths for steady state of freshwater lens.
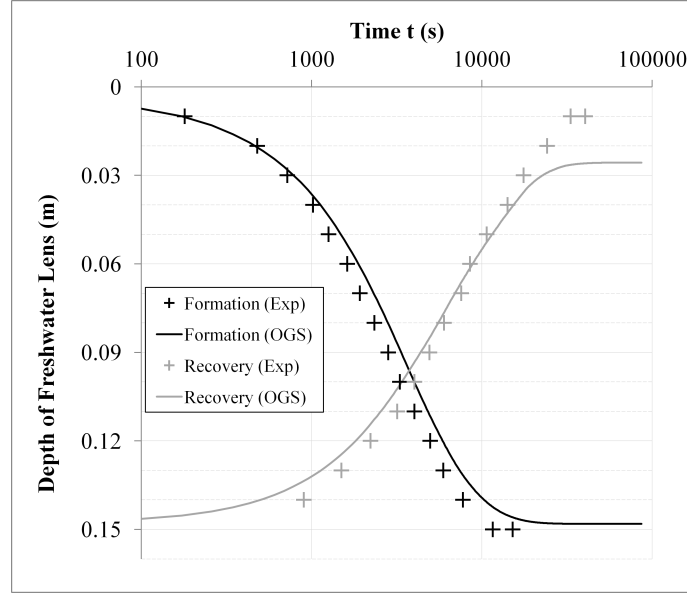
Figure 3.9: Depth of freshwater lens (isoline $c = 0.5$) at right edge of domain.

to retreat and flow out of the domain on the left boundary. Stream tracers show homogeneous flow paths with only small disturbance in the mixing zone.

On the right side, at the symmetrical line of the domain, the depth of the isoline of $c = 0.5$ (black line in figure 3.8, p. I-24) is observed over time for formation and recovery of the lens. The results are compared to experimental data in figure 3.9, p. I-25. Generally, numerical results from OpenGeoSys are in good accordance with laboratory observations. The temporal development of the formation and recovery, as well as total penetration depth of the freshwater lens are met with deviations in the range of $\leq 1\,\text{cm}$, which is likely below visual accuracy of laboratory observations. Small deviations only occur to the end of the recovery experiment, when differences between laboratory and numerical results slightly increase. Despite limited observation accuracy, deviations might also be due the interpolation technique used for data extraction in ParaView.

Part II

Applications

Part II Preface Note

In the preceding chapter 3, OPENGEOSYS could successfully be validated for the relevant density-dependent flow and transport processes including the associated coupling mechanisms. The following Part II with its chapters 4-7 presents a number of applications for the numerical modelling tool OPENGEOSYS, forming the central part of the thesis. The examples show a small part of the large variety of possible utilizations for a numerical toolbox like OPENGEOSYS on different scales, and stress the pertinence of continued development of the software to maintain the ability to answer important research questions for stake holders, consumers and scientists.

Firstly, the development of an extended inverse distance weighting method is documented. The tool can be used for the parameterization of a tilted, layered, heterogeneous virtual domain of any scale or application purpose. See [P1]: Walther et al. (2012a).

Secondly, a regional scale study for a heterogeneous, three-dimensional groundwater model is presented. The study region is situated in a coastal area with large pumping activity and, thus, prone to marine saltwater intrusion. Findings of the investigations can be used to decide on inevitable action plans for managing and securing the regional groundwater resources. See [P2]: Walther et al. (2012b) and [A6]: Walther et al. (2013a).

Thirdly, a novel approach to simulate viscosity change due to rapid gelation of an injected solution in porous media is shown. The modelling approach is successfully validated against small scale laboratory data. The novel simulation technique provides a basis to plan and evaluate future field scale remediation activities. See [P3]: Walther et al. (2013b).

Fourthly, a medium scale study of thermohaline convection within a double-diffusive Rayleigh regime is conducted. Results of the study reveal possible research questions that will be valuable for the characterization of a bilateral, thermohaline Rayleigh regime.

Chapter 4

Extended Inverse Distance Weighting Interpolation

For Tilted, Layered, Hydro-Geological Formations

[P1]: Walther et al. (2012a)

4.1   Motivation

Numerical modelling is common practice nowadays for various purposes, e.g. process understanding, scenario analysis, or system management and decision making. When implementing a realization of any real-world application in a numerical approach, every single discretization entity, i.e. point or element of a grid or mesh, needs to be parametrized in order to solve the governing equations at each of these entities. Parametrization is especially relevant for heterogeneous domains. Usually, interpolation is used to find the unknown parameter values from given information in the vicinity, e.g. measurements. Frequently used interpolation techniques are Kriging (Bargaoui and Chebbi, 2009), Inverse Distance Weighting (IDW, Lu and Wong (2008)), triangulation (Watson, 1982), or spline interpolation (Dubrule, 1984). Many of these techniques are utilized in two-dimensional algorithms. Only a small number of three-dimensional methods exist, mostly designed for specific tasks, e.g. fracture or fault meshing, requiring increased computational effort and user experience. Popular software tools are ArcGis (ESRI, 2011), Surfer (Golden Software, 2010), GMS (Aquaveo, 2011), Petrel (Schlumberger Limited, 2012), Hydro GeoAnalyst (Schlumberger Water Services, 2011), and recently Leapfrog Hydro (ARANZ Geo Limited, 2012).

For the challenge at hand, a three-dimensional domain had to be parametrized. The task included the development of a numerical model for a highly heterogeneous groundwater domain consisting of recent sedimentary deposits with tilted, layered structures of aeolian, marine, or fluviatile origin (see chapter 5, p. II-9). While

the individual layers are mostly homogeneous, significant features, e.g. tilting of layers, must not be omitted, as these will influence groundwater flow paths and mass transport (see equations (2.2), (2.3), or (2.5), chapter 2.1, p. I-7). As availability of interpolation tools was limited by either simply the inability of the tools to model the required structures or by funding circumstances, a simple method was developed based on IDW, extending the interpolation approach to represent the tilted, layered structures in a three-dimensional environment.

4.2 Extension of IDW Method

The basic principle of IDW when finding parameters for a mesh cell is to search for information within a given distance from the parametrization entity. If more than one information is found, individual search results are weighted with the inverse of the distance between the entity (i.e. grid point or mesh cell) and the point of given information. The parametrization value is defined as the sum of all weighted distances.

From hydro-geological interpretation of given borehole information, layering and tilting of the sediments is acquired, and used to "point" from one profile layer to another. The IDW method was extended by utilizing a coordinate transformation resulting in an additional vertical shift of the found information, thus altering the inverse distance weighting factor.

4.3 Artificial Test and Regional Scale Application

A synthetic example was used to test the developed method: figure 4.1, p. II-7, compares the given borehole information and interpreted hydro-geological layering (a) to the result of the IDW interpolation (b). The algorithm produces the expected structure, including layer thickness, characteristics, and extent. Minor shortcomings of interpolation results, that arise in areas with only few given information, hold common issues for interpolation algorithms, and are addressed in [P1]: Walther et al. (2012a).

Figure 4.2, p. II-8, shows the interpolation result for a regional scale application. The interpolation reveals two typical features of the aquifer system, which are independently documented by different literature (see BRGM (1992) or Macumber (1998)). Firstly, the system consists of mainly two aquifers: a higher permeable upper and a less permeable lower one. Secondly, in the middle of the domain, the upper aquifer reaches a large extent, known as the "Ma'awil trough", and reduces in thickness closer to the coast. Utilizing the "TESSIN-VISLab" at Helmholtz-Centre for Environmental Research UFZ, Leipzig (VISLAB, 2013), a virtual reality centre with a high-resolution video wall, stereoscopic projection, and an optical tracking system, the hydro-geological model could be intensively evaluated. At this occasion, geological experts from the Ministry of Water Resources and Regional Municipalities,
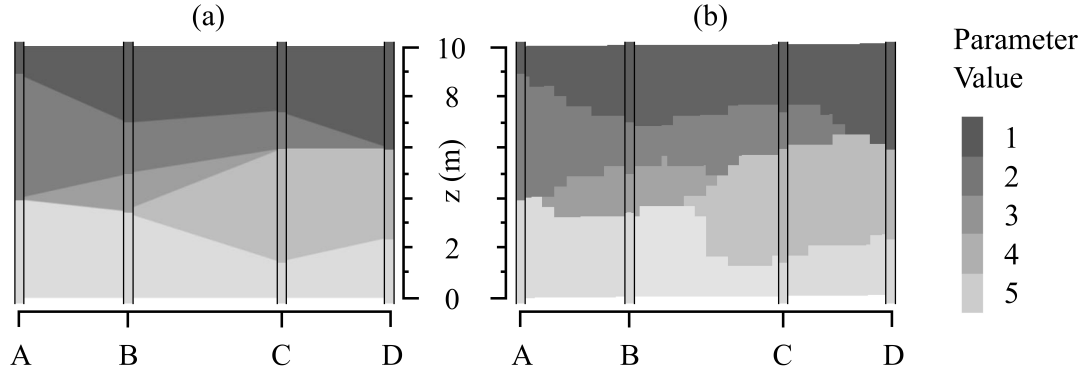
Figure 4.1: (a) Given hydro-geological interpretation of boreholes A-D with layers of parameter values 1-5; (b) Interpolation result of the extended IDW; altered from [P1]: Walther et al. (2012a), compare also for location of boreholes.

Muscat, Oman, helped to successfully validate the interpolation results.

4.4 Summary and Conclusions

An extended IDW method was developed to include hydro-geological information, i.e. tilted, layered structures, that is vital for groundwater flow and mass transport simulations, into conceptual models. The method could successfully be tested on a synthetic example and applied to a regional scale domain. Results of the latter were used in a saltwater intrusion modelling study (see chapter 5, p. II-9). The developed extension may also be used for arbitrary purposes of virtual or real-world applications of any scale, that demand the unique features of the algorithm (see also scenario simulation in section 6.3.2, p. II-28).
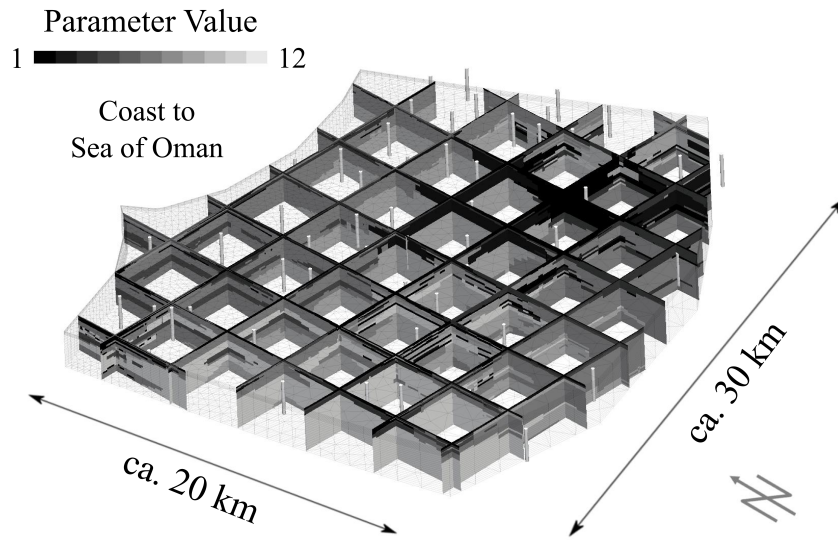
Figure 4.2: Interpolation result of twelve distinct material groups from ca. 50 boreholes for a 3D regional scale real-world domain; higher parameter values mean lower permeability; vertically five times exaggerated; altered from [P1]: Walther et al. (2012a).

Chapter 5

Modelling Transient Saltwater Intrusion

In an Agriculturally Used, Coastal Area

[**P2**]: **Walther et al. (2012b)**

[**A6**]: **Walther et al. (2013a)**

5.1   Background and Motivation

Funded by the German Ministry of Education and Research (BMBF, Bundesministerium für Bildung und Forschung), the project International WaterResearchAlliance Saxony (IWAS) approached various challenges related to water availability and quality in different parts of the world (Kalbus et al., 2011). As part of the IWAS-Oman sub-project, a groundwater study had to be carried out to investigate several aspects of the groundwater regime and to delineate possible future scenarios in an agriculturally used area at the "Al-Batinah" coast in northern Oman.

In the study area (see figure 5.1, p. II-10), highly productive soils, that evolved from fine-grained, silty Wadi deposits, sustained a large amount of agriculture since hundreds of years (BRGM, 1992). Source for irrigation was groundwater from hand-dug wells until the beginning of the 1970s. The system balanced itself in a natural equilibrium between mountainous recharge (reaching the coastal area mainly as subsurface groundwater flow), well extraction rates, and the relatively stable sea level. Abstraction depth and amount was limited already by the hand-dug well type. If salinity of the extracted groundwater increased, and cultivated crops reached their level of salt tolerance, farmers could not increase agricultural activities furthermore, thus, restraining irrigation and abstraction. However, when upcoming industrialization offered access to advanced groundwater exploitation technology, extensive construction of drilled borehole wells began. With tremendously raising water ab-
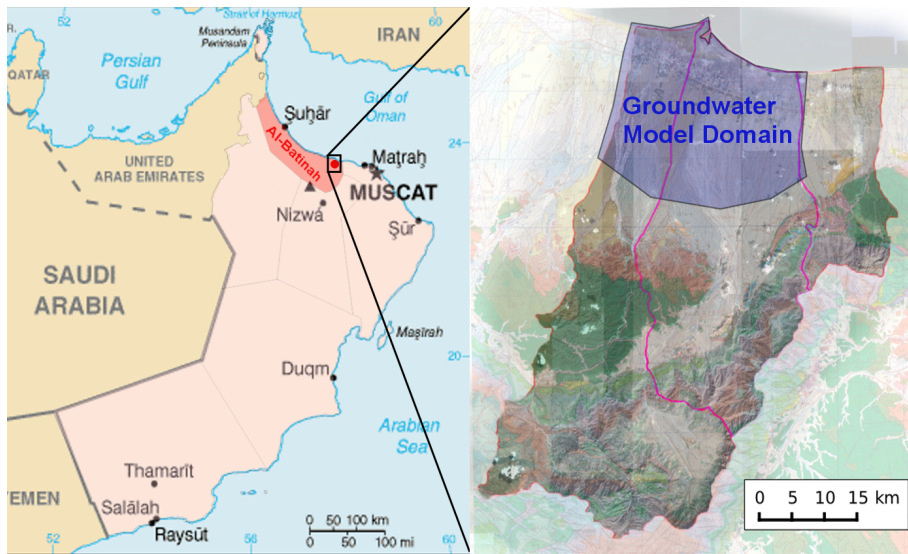
Figure 5.1: Location of groundwater model domain; altered from [P2]: Walther et al. (2012b)

straction rates, groundwater levels started to decline until the beginning of the 21st century up to 10 m even near the coast. As a result, the hydraulic potential is now decreasing from the sea onshore, and marine saltwater began to intrude into the freshwater aquifer, disturbing the prior balanced system. Limited groundwater availability, as a quantitative constraint, and escalating salinity levels, as a qualitative one, demanded for management plans of the uncontrolled, and scarcely supervised abstraction system.

Within the framework of an integrated water resources management (IWRM), the Assessment, Prognoses, Planning and Management tool (APPM, Grundmann et al. (2012)) was developed assessing multiple aspects of the regional water cycle. In addition to satisfying current agricultural irrigation demands, the entire (ground-)water usage should be optimized for long-term stability. Groundwater abstraction should be diminished by utilizing improved irrigation techniques (surface or subsurface drip irrigation instead of sprinkler systems), deficit irrigation could augment water efficiency of different crops (Kloss et al., 2011), and chip-based, programmable control systems, trained by surrogate models (artificial neural networks), might optimize irrigation schedules ([A3]: Schmitz et al. (2010), [A4]: Brettschneider et al. (2010), Schütze et al. (2012)). On the other hand, amount and origin of mountainous groundwater recharge ([A5]: Gerner et al. (2011), Gerner et al. (2012)), as well as Wadi flow and recharge dams contribution (Philipp et al., 2010) was evaluated.

In addition to the afore mentioned optimization measurements, a common management goal of the APPM was to halt or even push back saline intrusion. Therefore, numerical groundwater flow and mass transport simulations should be utilized to assess recent and future development of the highly heterogeneous aquifer system, in-

cluding impact of decreased abstraction rates (e.g. through optimized irrigation techniques) on the saline interface. Quantification of the aquifer's remediation potential might help identifying strategies to reduce salinization in future water management. Also, inter-comparison of mountainous groundwater recharge and estimates of prior unknown abstraction rates should contribute to the IWRM.

5.2 Methods and Model Setup

A three-dimensional, density-dependent, numerical model of the study area's aquifer was set up using the scientific open-source tool OpenGeoSys (2.3.1, p. I-10). OpenGeoSys is based on the Galerkin-FEM method and, in this application, uses an approach of Sugio and Desai (1987) to resemble the unconfined groundwater level (see sections 2.1, p. I-7, and 3, p. I-15). Level-1-Oberbeck-Boussinesq approximations and a linear relation between (relative) concentration and density are applied (see section 2.2, p. I-9).

The regional scale model domain included an approximately 20 km long stretch of the Al-Batinah's coast reaching about 30 km inland (see figure 5.1, p. II-10) with a maximum thickness of up to 450 m. The numerical model consisted of $\approx 350'000$ nodes and $\approx 700'000$ elements, distributed over 25 layers. Four boundary conditions were applied (compare figure 5.2, p. II-12): upstream, subsurface inflow from mountainous recharge (2nd type); spatially distributed pumping abstraction near the coast (2nd type); sea water level and marine salinity concentration at the coast (both 1st type). Philipp and Grundmann (2013) could show, that recharge contribution of dams and Wadi channels is significantly smaller than mean annual mountainous inflow. Therefore, only the latter is included in the groundwater model. Not mentioned model boundaries were defined as 2nd type "no-flow". More detailed explanations on the used boundary conditions (e.g. pumping abstraction) and simulation parameters are given in [P2]: Walther et al. (2012b), section 4.

The extended IDW algorithm (see chapter 4, p. II-5) was used to parametrize the highly heterogeneous hydro-geological model. A video of viewing the hydro-geological domain is attached in the digital appendix (see E.1, p. App-3). Based on few groundwater level observations, the Parameter Estimation Tool (PEST, Gallagher and Doherty (2007); Sun et al. (2011)) helped to calibrate the twelve distinguishable aquifer material groups, which where identified from various geological investigations within the area, as well as upstream recharge, and abstraction rates for a pre-development steady state (i.e. time before 1974). Based on the steady state, a manual calibration was carried out for a transient period (i.e. 1974-2005). Subsequently, long-term scenario simulations were conducted under the assumption of a best-case scenario, i.e. cease of groundwater abstraction after the year 2005.

To evaluate results for the long-term scenario simulation and the capability of the groundwater system to return to a near-natural state, a qualitative value, remediation potential of the upper aquifer Φ, was defined from salinity half-life after pump stop
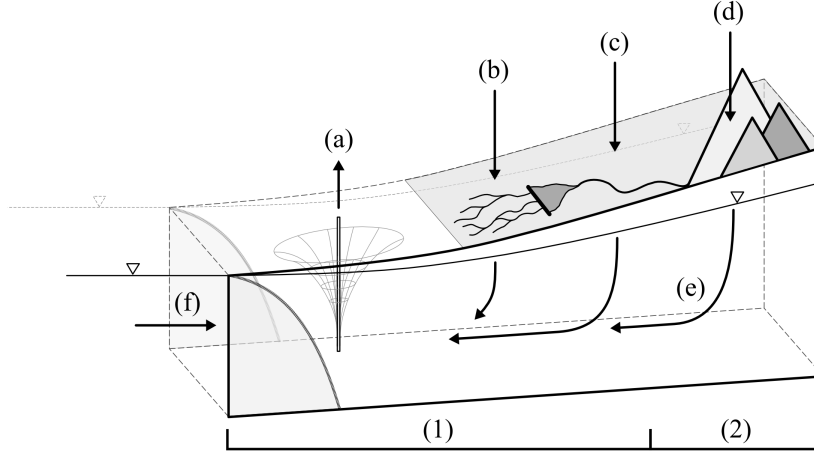
Figure 5.2: Conceptual model, boundary conditions: (a) pumping abstraction, (b)-(d) infiltration from precipitation, or surface flow (e) effective subsurface groundwater recharge, (f) sea level and saltwater concentration; (1) symbolizes the groundwater model domain, (2) the mountainous recharge area.

through equation (5.1).

$$\Phi = 1 - c_{\text{rel}} \cdot \frac{\lambda^c}{\max\left(\lambda^c\right)} \tag{5.1}$$

with c_{rel} is relative concentration of salinity $10\,\text{m}$ below groundwater level in 2005, λ^c is half-life of c_{rel}, and $\max\left(\lambda^c\right)$ is maximum of λ^c. The qualitative value Φ had to be multiplied with c_{rel} to avoid overestimations for cells with initially already low salinity.

5.3 Simulation Results and Discussion

5.3.1 Pre-development Steady State

Setup and results of the numerical simulations for the steady state in year 1974 are documented in detail in [P2]: Walther et al. (2012b); results are shortly summarized in the following. After benchmarking the approach of Sugio and Desai (1987) using experimental data from Goswami and Clement (2007), the heterogeneous model could be calibrated successfully resulting in a biased correlation coefficient for simulated and observed groundwater levels of > 0.9 (compare figure 5 and table 4 in [P2]: Walther et al. (2012b)). Calibration results revealed expected permeability values for the twelve distinct hydro-geological materials (compare table 5.1, p. II-13). Also, subsurface inflow from upstream and near-coastal pumping abstraction rates yielded ranges that were estimated independently by other research (Stanger, 1987;

Table 5.1: Parameters of material groups obtained from PEST calibration.

MatGroup	Hydrogeol. description	Permeability (m^2)	eff. Porosity	% of Elements
1	gravel	$1.033 \cdot 10^{-10}$	0.25	4.9
2	sandy gravel	$1.674 \cdot 10^{-11}$	0.22	6.7
3	sand	$1.864 \cdot 10^{-11}$	0.15	10.7
4	medium sand	$5.849 \cdot 10^{-12}$	0.20	0.9
5	silty gravel	$2.949 \cdot 10^{-13}$	0.18	8.0
6	gravelly silt/clay	$7.392 \cdot 10^{-12}$	0.22	5.3
7	silty/clayey sand	$2.187 \cdot 10^{-13}$	0.20	1.9
8	sandy silt/clay	$3.212 \cdot 10^{-14}$	0.18	2.5
9	silt, mud, marl[1]	$8.663 \cdot 10^{-11}$	0.25	38.8
10	cemented gravel	$1.070 \cdot 10^{-13}$	0.18	1.2
11	clayey calcrete, limestone	$4.580 \cdot 10^{-17}$	0.02	19.0
12	sandstone, siltstone	$6.245 \cdot 10^{-17}$	0.02	0.2

Al-Shoukri, 2008; Gerner et al., 2012), i.e. mean, annual upstream inflow from mountainous recharge $Q_{\text{in}} \approx 70 \cdot 10^6 \, \text{m}^3 \cdot \text{a}^{-1}$, and total groundwater abstraction rate through pumping activity $Q_{\text{out}} \approx 40 \cdot 10^6 \, \text{m}^3 \cdot \text{a}^{-1}$. The numbers indicate, that the groundwater balance is still positive for the pre-development state, retaining saltwater intrusion near the coast.

5.3.2 Transient Simulation

For transient simulations, the initial state of process parameters is of high importance. Figure 5.3, p. II-14, shows a scatter plot of an ensemble of possible initial states using different parameter combinations. Changes to the parameters (K as permeability field, Q_in as recharge inflow, Q_out as total pumping abstraction) were based on the calibrated steady state parameter set and attained by multiplication of the mentioned factors with the respective parameters. All plotted realizations show only small deviations from the optimal fit (i.e. black main diagonal). The figure shows, that even minor changes can lead to equivalent sufficiently good results.

As observation data (e.g. groundwater levels, salinity profiles) and hydro-geological information was very limited, the "correct" parameter combination could only be restricted to a certain range through manual calibration. Limits of the deviations from the mean parameter values deducted from other research or given information helped to restrain parameter variations. Although not showing the best correlation for the steady state, deviations of transient groundwater level results could be minimized by using the parameter combination factors K=5, Q_in=1, Q_out=2.5 for the initial state. Prior steady state calibration results (i.e. factor 1) might still be valid; the results presented here are based on the limited and often doubtful available transient data (see discussion at end of paragraph).

---

[1]high permeability of material group 9 presumingly due to karstic character
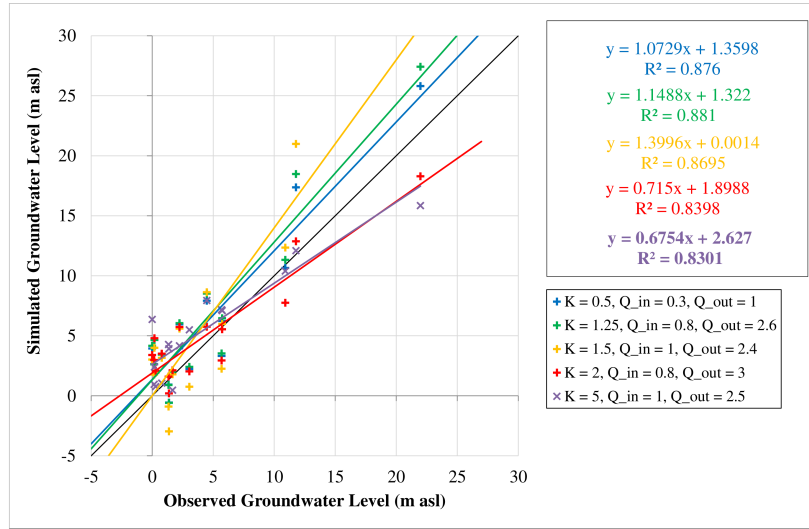
Figure 5.3: Different possible initial states in year 1974 for transient simulation; fitted linear regression functions with concurrent correlation coefficients; changes of parameters applied by multiplication to permeability field (K), recharge inflow (Q_in), total pumping abstraction (Q_out).

In order to assess statistical spread of the results based on variations of input parameters (also in terms of measurement insecurity), one might utilize PEST in a Monte-Carlo-like approach (Murthy, 2004) to find a large number of possible parameter combinations, choosing the found parameters as the basis for several transient runs. However, as model run times are relatively long, such an approach would require large computation times: steady state PEST result was found within $\approx 5\,\mathrm{d}$ runtime on a parallel cluster computer; a statistically well founded data base might need ≥ 50 results; additionally, model runtime for transient simulations was $\approx 2\,\mathrm{d}$; total model runtime would easily exceed $1\,\mathrm{a}$ (excluding statistical analysis).

Figure 5.4, p. II-15, shows the deviations of the simulated from the observed groundwater levels over time with subtraction of initial deviation for the chosen parameter set. If the system behaviour is resembled correctly in the model, the result would be a horizontal line covering the x-axis. For the calibration, the mean value of the difference is nearly horizontal, thus, the general trend of simulated groundwater levels is in concordance with the observed ones. Larger divergences (higher standard deviations) occur to the end of simulation time when the assumption of equal distribution of pumping rates throughout the available pump location data might not be sufficient any more. Some individual observations also reveal too low or high groundwater levels; with upcoming industrialization, dug wells (with generally similar abstraction rates) are partially replaced by drilled boreholes with pumps of higher variation of abstraction potentials, yet this information is not explicitly available (e.g. from census data). Periodic oscillations of the groundwater levels,
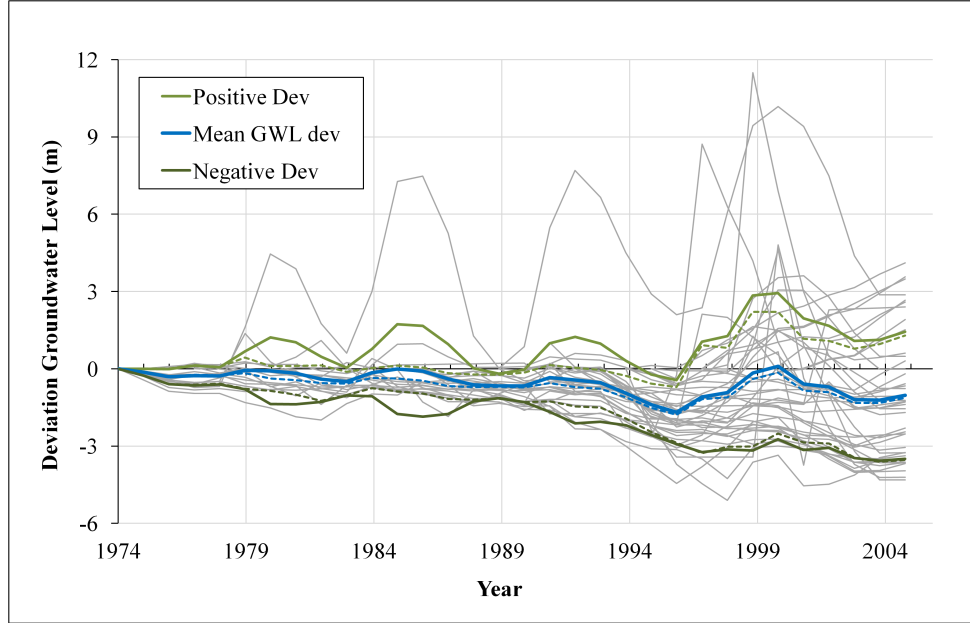
Figure 5.4: Difference of observed and simulated groundwater levels with subtracted initial deviation; blue lines are mean value, green lines standard deviation from mean; solid lines with, dashed lines without oscillating observation well "JT-11".

as observed by one of the monitoring wells that is situated near to the mountainous recharge region ("JT-11"), are probably due to medium-term precipitation cycles and their respective influence on groundwater recharge; this currently cannot be taken into account with the model as (again) underlying data for process parametrization or validation is not available. Neglecting this specific observation yields a much smaller standard deviation from the mean value especially for the first half of the simulation time (see dashed lines in Figure 5.4, p. II-15).

Figure 5.5, p. II-16, shows a scatter plot for observed vs. simulated groundwater levels over a simulation time of 31 years. Initial state for 1974 (red dots in figure) could be calibrated with high correlation. Until the end of the transient simulation (blue dots), and within calibration time (grey dots), observation wells with low groundwater levels (i.e. near coast) are met with only little deviation. However, simulated groundwater levels with higher values (i.e. further inland) generally show too high values and no significant drawdown. The reason might once more be the BC for pumping activity: as no detailed information on abstraction rates is available, the BC was derived from over 5000 known locations of pumps using an areal density filter assuming constant abstraction for every single pump (compare [P2]: Walther et al. (2012b)). This assumption excludes areas with low density of pumps (like upstream) and thus might lead to the "missing" drawdown.

Groundwater fluxes of upstream recharge and saline intrusion were observed in
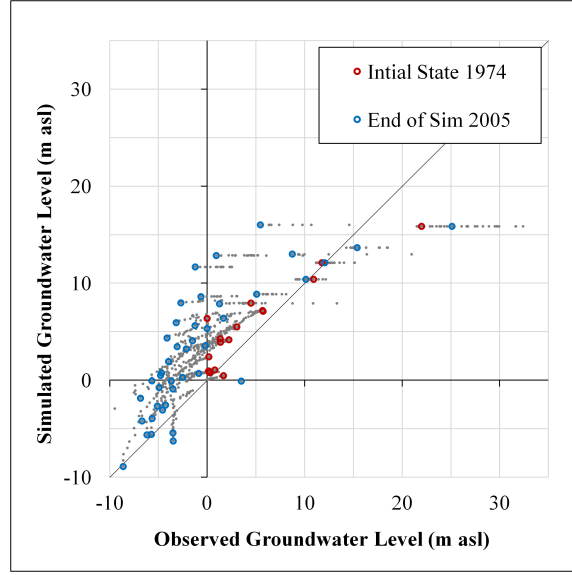
Figure 5.5: Scatter plot observed vs. simulated groundwater levels, red dots additionally indicate initial state for transient simulation (i.e. 1974), blue dots show final state (i.e. 2005).

the simulation. Fluxes were evaluated as the net water flow through vertical planes which are placed with a displacement of $1\,\mathrm{km}$ parallel to the respective boundaries. Figure 5.6, p. II-17, plots the temporal development of groundwater fluxes, abstraction rates, as well as aquifer storage for transient simulation time. Inflow from upstream recharge remains constant over time; however, as pumping rates increase, aquifer storage decreases, and saltwater intrusion raises. Although total estimated storage volume is very large, relatively small storage changes unbalance the groundwater regime leading to the apparent problems. Marine saltwater intrusion in 2005 is estimated as $118 \cdot 10^6\,\mathrm{m}^3/\mathrm{a}$, and total abstraction rate as $183 \cdot 10^6\,\mathrm{m}^3/\mathrm{a}$.

5.3.3 Saline Intrusion

Figure 5.7, p. II-18, shows simulated groundwater levels, flow direction and magnitude, as well as saline intrusion of year 2005. Simulation results of saline intrusion (see also figure 5.8, p. II-20, a, b) show similar heterogeneous patterns of salinity along the coast as reported by various measurements (see MAF (2012) and appendix figures in E.2, p. App-5). In the digital appendix (see E.1, p. App-3), a video shows the intrusion state of 1985 and streamtracer flow paths. The heterogeneous outline of saline intrusion is depending on the local hydrogeology, the subsequent spatially highly variable flow regime, and locally distributed pumping activities. Mean intrusion length and the general trend of saltwater intrusion also show similar values as published data (2-4 km in 1975 to 5-7 km in 2005). Deviations from observations may be due to several reasons: structure and parameters of the hydrogeology, as
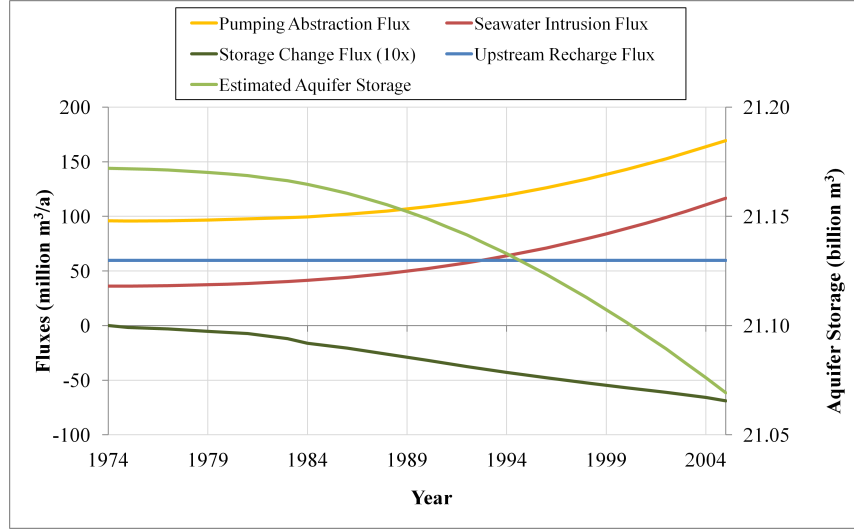
Figure 5.6: Water fluxes and estimated aquifer storage in model area within transient simulation period; NB: storage change flux plotted with 10 times exaggeration.

well as abstraction rates of groundwater pumps are not exactly known; spatially and temporally limited recharge events in Wadi channels, which are not included in the simulation, might influence short-term groundwater levels and salinity, thus, might affect a measurement at one point in space and time; published maps of salinity show doubtful salinization development, e.g. the reduction of salinity in a "sabkha" (a salt desert) at northern coastal stretch between 1995-2010 (compare figure E.2.4, p. App-6).

5.3.4 Scenario Simulation

For evaluation of the aquifer's remediation potential, a "best-case" scenario simulation was defined with the assumption that all groundwater pumping activity would be ceased immediately after the year 2005. The scenario simulation time was 470 years starting in year 2005. Figure 5.8, p. II-20, presents several time steps for saline intrusion, drawdown and flow paths (via stream tracers), starting with the initial state 1974, throughout the calibration period to 2005, and until 100 years after pump stop, i.e. 2105. The pre-development state 1974 (figure 5.8a) shows only little abstraction near the coast. The plotted recharge plumes, originating in the southern mountainous areas, mostly reach the sea. As fresh water discharges into the sea, the saline intrusion interface is retained near the coast. In the year 2005 (figure 5.8b), all recharge plumes are captured completely by groundwater pumping activities. Due to huge agricultural water demand, apparent high extraction rates lead to immense drawdown and accordingly excessive saltwater intrusion of up to 3 km. After 100 years (figure 5.8c), mountainous recharge plumes partly reach the

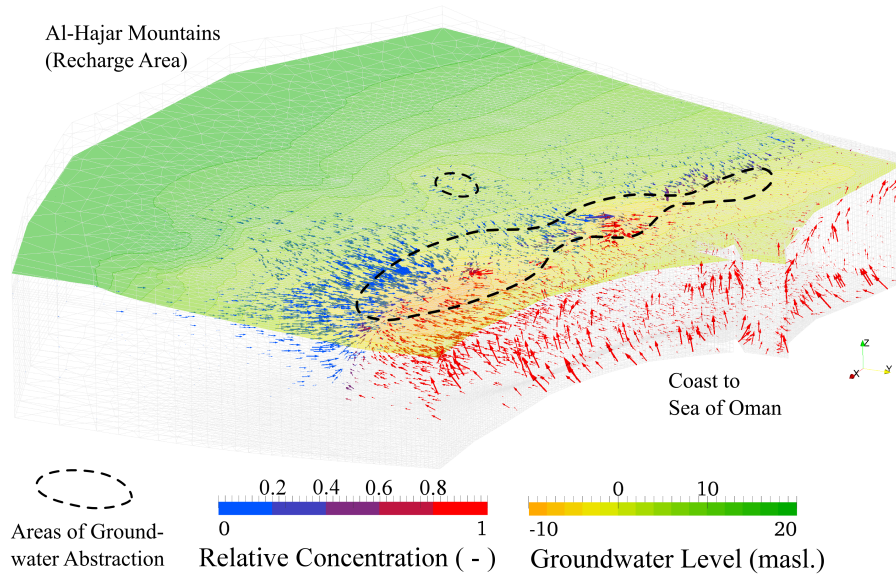Figure 5.7:   Groundwater model domain, final state of transient simulation (year 2005); ground-water levels, scaled velocity vectors with relative concentration; dashed lines symbolize major areas of groundwater abstraction; from [A6]: Walther et al. (2013a).

sea again and slowly refill the aquifer storage. Yet, groundwater levels and salinity did not return to their former values in the 1970s.

Groundwater fluxes for 2005-2475 are plotted in figure 5.9, p. II-21. A complete pumping stop results in slowly replenishing aquifer storage, as both, marine saltwater intrusion and upstream groundwater recharge aid to recover decreased groundwater levels. Eventually, intrusion flux becomes lower than recharge flux and even changes direction, i.e. freshwater flows out of the domain leaking into the sea.

Figure 5.10, p. II-21, plots salinity against groundwater drawdown for the years 1974-2070, with each arrow symbolizing one year. The general system behaviour shows increasing drawdown (due to pumping activity), and thus, growing salinity values. As soon as pumping stops (year 2005), groundwater levels begin to recover (i.e. drawdown reduces). Yet, salinity values mostly still increase revealing a hysteresis: although groundwater abstraction is ceased after 2005, the hydraulic gradient will still point onshore, i.e. from the sea into the direction of the pumps' location. Hence, simulated saline concentrations continue to increase. It can be observed, that even with only small drawdown, high salinization is possible (e.g. "JT-69"), however, maximum drawdown is simulated to reach up to $12\,\text{m}$ within 30 years of pumping activity. Recovery times of groundwater levels are supposedly $> 100\,\text{a}$ and even longer for salinity concentrations. Additionally, even when drawdown reaches zero (i.e. initial state value), salinity is mostly higher than in the beginning of the simulation (1974).

Figure 5.11, p. II-22, shows heterogeneous patterns of Φ along the coast. The eastern study area shows isolines of Φ relatively parallel to coast line with slight deviations close to the coast. In the western area, relatively high potential areas (due to highly permeable porous media) with steep gradients to low potential areas (low permeabilities) can be identified. The region south of the coastal bay with low potential results from very low permeable media which might pose a reason for the development of the sabkha. Yellow areas symbolize regions that do not reach $0.5 \cdot c_{\text{rel}}$ within 470 years of simulation; near-coastal areas are probably showing the undisturbed situation of marine salinity intrusion (i.e. no groundwater abstraction), areas further inland are due to low permeable hydro-geological units.

5.4 Summary, Conclusion and Outlook

In the IWRM-frame of the APPM, a regional groundwater model could successfully be set up using the numerical simulation tool OPENGEOSYS. The extended IDW method was applied to parametrize a hydro-geological model ([P1]: Walther et al. (2012a)). For a steady state, PEST could be used to calibrate a pre-development state, including a heterogeneous aquifer parameter field (permeability), as well as a priori unknown model boundary conditions, i.e. mean upstream inflow, distributed pumping abstraction ([P2]: Walther et al. (2012b)). Furthermore, the latter could be used to cross-validate results from independent research groups estimating moun-

(a) Year 1974

(b) Year 2005

(c) Year 2105

Figure 5.8: Time series of salinity (at 10 m below groundwater level), groundwater levels (isolines), stream tracer, and selected observation wells, from [A6]: Walther et al. (2013a).
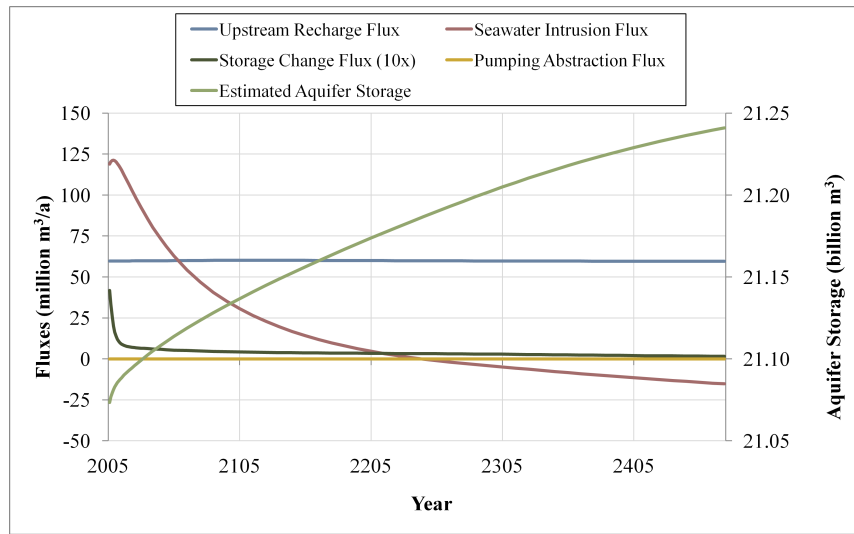
Figure 5.9: Water fluxes and estimated aquifer storage in model area within scenario simulation period; NB: storage change flux plotted with 10 times exaggeration.
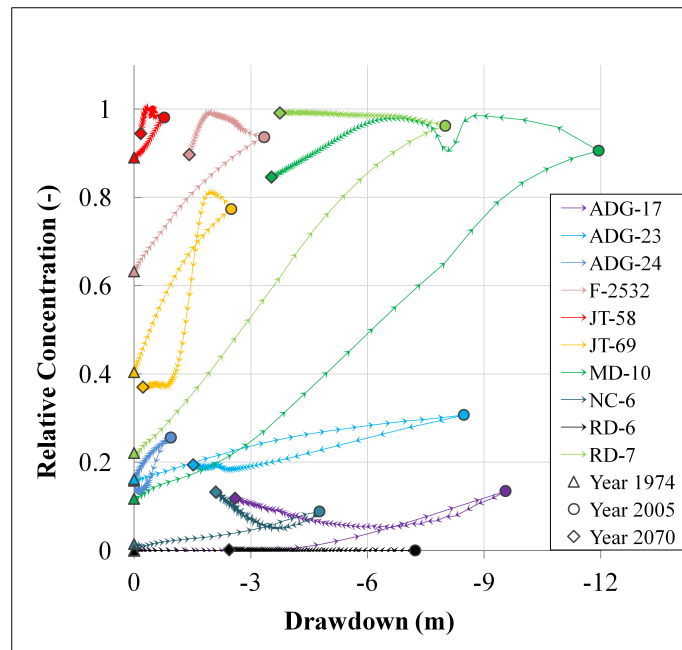
Figure 5.10: Salinity vs. drawdown over time, scenario simulation for ca. 100 years, start pumping 1974, stop pumping after 2005, from [A6]: Walther et al. (2013a).
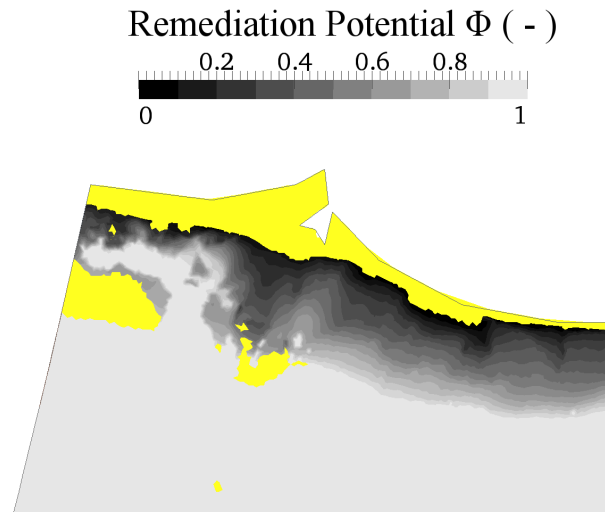
Figure 5.11: Salinity remediation potential Φ of coastal area $10\,\text{m}$ below groundwater level ($0 =$ low potential, $1 =$ high potential), based on salinity half-life after pump stop; yellow areas do not reach half initial concentration within 470 years, from [A6]: Walther et al. (2013a).

tainous recharge as calibration results yielded values within the independently estimated bandwidths. Afterwards, a transient state calibration yielded relatively good concordance between observed and simulated groundwater level and saline intrusion development, both, in spatial and temporal distribution. Budget calculations indicate high marine saltwater intrusion rates as a result from high pumping rates. A subsequent long-term scenario simulation showed, that the estimated time scale of the system to return to a natural state is supposedly $> 100\,\text{a}$. Scientific visualization could be utilized to validate the hydro-geological setup and transient simulation results in detail ([A6]: Walther et al. (2013a)).

Yet, the study area's aquifer offers remediation potential. Concluding from the current simulation results, while keeping in mind the parameter insecurity bandwidth, the apparent advice for water management in the study area is to immediately decrease pumping activity and start further measurement campaigns to determine aquifer parameters, and long-term groundwater level and salinity observations. Also, additional measurements to increase groundwater recharge or limit saltwater intrusion might aid in remediating the aquifer, e.g. positive or negative hydraulic barriers (see also Werner et al. (2013)).

This study showed on several occasions, that profound knowledge about the key parameters is vital in order to restrain and narrow the bandwidth of possible simulation results. With the given data and in the current setup, the reliability of the model's results is approximated to lie within one order of magnitude. Gaining information about the shape of aquifer (thickness, layering), e.g. near the coast, where

most pumping activity is occurring, will potentially increase model prediction quality. Water metering for the multitude of the widely scattered groundwater abstractions could be supported by "crowd sourcing" (Lowry and Fienen, 2013) and will help to gather information on pumping rates and locations. In future, with less parameter insecurity, existing model setups could be improved and numerical simulations be used to deduct detailed management actions, e.g. to find safe locations for new built abstraction wells by using maps similar to 5.11, p. II-22. Alternatively, surrogate models can be utilized in combination with optimization algorithms to determine future pumping field locations and groundwater abstraction rates managing the aquifer system on a trans-catchment scale, additionally aiding remediation in retaining saline intrusion at an acceptable level while satisfying irrigation water demand. Finally, similar to Leidel et al. (2011), intensified application of various options of capacity development or socio-economic measurements, which have already partly been incorporated, will help to set IWRM management plans into action.

Chapter 6

Gelation of a Dense Fluid

Due to Rapid Change of Viscosity

[P3]: Walther et al. (2013b)

6.1   Motivation

Remediating contaminated subsurface water bodies has become one of the elementary tasks in groundwater management. As a consequence of wide-spread usage of various, often hazardous chemicals, or due to anthropogenic activities influencing natural equilibrium systems and subsequent regime changes, many approaches were developed to restore usability of contaminated aquifers. Excavating the contaminant source might only be suitable when source spreading is spatially limited; otherwise, often on-site (in-situ) techniques are used. Among the popular in-situ approaches are "funnel and gate" (in combination with e.g. stabilization or oxidation measurements), various air or liquid stripping techniques, pump&treat, (enhanced) natural attenuation, and numerous variations of the named (Wiedemeier et al., 1999; Khan et al., 2004; Bhandari, 2007). All of these have the common intention to minimize human and material resources expenses. If a contaminant plume could be diminished (or even removed) by injecting an appropriate remediating fluid only once and without further effort, operating costs of on-site machinery could be reduced significantly. However, the injected fluid, which would render the contaminant harmless, e.g. through oxidation, or immobilization, must not be carried away by groundwater flow and needs to stay right within the pollutant plume.

To fulfil this requirement, Solpuker et al. (2012) could utilize a dense fluid's behaviour to form a gel after a given time due to a rapid change in viscosity. The concept is to inject the fluid into fractures or boreholes, let it sink to the desired horizon (e.g. until a natural or artificial barrier), and have it become a gel that will remain at the location. By diffusion, the gel will then release appropriate remediation chemicals into the plume. The used injection fluid consists of silicate solutions; initial

density, viscosity, and time until gelation can be influenced through the solution's composition.

In most applications, numerical models are used to predict contaminant fate or respective remediation measurements. Strong gradients or rapid changes of fluid or material properties, however, pose huge challenges on the stability of numerical simulation codes. Due to the lack of availability, a novel method was developed to simulate the fate of the gelling fluid. Simulations showed good numerical stability even with the emerging strong gradients and fast change of viscosity at the boundaries of the gelling area. In addition, laboratory small scale tank experiments could be used to validate the approach, and the principle behaviour and components of the gelation process.

6.2 Methods and Model Setup

The basic approach comprises the following procedure: next to the groundwater flow equation (2.2, p. I-7), two mass transport equations (2.5, p. I-8) are solved with the respective concentration c_i ($i = 1, 2$). While concentration c_1 is coupled to fluid density $\rho^f(c_1)$, an auxilliary concentration c_2 is not influencing $\rho^f(c_1)$, i.e. $\gamma_{c_1} > 0$ and $\gamma_{c_2} = 0$ in equation (2.10, p. I-9). However, c_2 is prone to a 1st-order decay following equations (6.1) and (6.2). The key feature of the method is the relative difference between the two concentrations, which can be used to deduct temporal information of the solute. From this relative difference, equations (6.3) and (6.4) are used to calculate the viscosity increase (i.e. gelation) by the first factor d from (6.5). The second term e in equation (6.4) was introduced in order to represent the phenomenon, that a too much diluted solute does not become gel (see equation (6.6)). The approach was implemented in OPENGEOSYS.

$$\frac{\partial c_2}{\partial t} = -\lambda \cdot c_2 \tag{6.1}$$

with λ is decay coefficient, that is defined by the time until gelation t_{gel} through

$$\lambda = -\frac{\ln 0.5}{t_{\text{gel}}} \tag{6.2}$$

$$\mu = f \cdot \mu_0^{ac_1} \tag{6.3}$$

where μ_0 is initial viscosity, a is a factor describing the result of viscosity change due to concentration c_1, and $f > 1$ is the factor for viscosity increase due to gelation.

$$f = 1 + d \cdot e \tag{6.4}$$

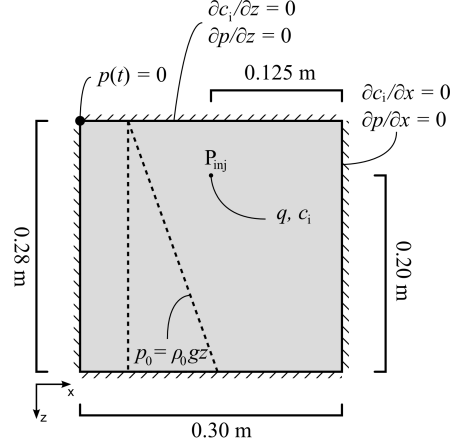$$d = (\beta_{\max} - 1) (2c_{\text{rel}})^{\beta_s} \tag{6.5}$$

Figure 6.1: Conceptual model, initial and boundary conditions; altered, from [P3]: Walther et al. (2013b).

with $\beta_{\max} \geq 1$ is maximum viscosity increase, $c_{\mathrm{rel}} = \frac{c_1 - c_2}{c_1}$ relative difference between the two concentrations, and $\beta_s \geq 1$ is a parameter defining the gelation speed.

$$e = \left(\frac{c_1}{c_{1,\mu_{\max}}} \right)^{\psi} \tag{6.6}$$

with $c_{1,\mu_{\max}} \leq 1$ is the concentration of solute 1 when the maximum viscosity increase should be reached, and $\psi \geq 1$ is a factor altering the viscosity increase depending on the present concentration c_1. Variation and influence of parameters d and e are presented in [P3]: Walther et al. (2013b), figures 2 & 3.

The conceptual model for the numerical simulations and the boundary conditions are shown in figure 6.1, p. II-27. At time $0 < t < t_{\mathrm{inj}}$, concentrations c_1 and c_2 are injected at point P_{inj} with a given flow rate q; for $t > t_{\mathrm{inj}}$, internal BC's at P_{inj} are changed to have no given pressure or flow rate. "No-flow" 2nd-type BC's are defined on all edges of the fully saturated, vertical x-z-domain, except for the top left corner, were a 1st-type constant pressure boundary is defined. Decay coefficient λ, which influences the time until gelation, could be estimated by visual observations during the laboratory experiments. The whole simulation parameter set is presented in [P3]: Walther et al. (2013b), tables 1-3.

U. Solpuker and F.W. Schwartz, cooperating researchers at the School of Earth Sciences, The Ohio State University, Columbus, Ohio, USA, conducted three laboratory experiments, each with different solute concentrations, thus, different gelation times. Solutes were coloured with Rhodamine WT. Time series of the experimental observations were processed with a visual technique following McNeil et al. (2006), accentuating isolines of relative light density, which are comparable to relative concentrations.

6.3 Results and Conclusions

6.3.1 Method Validation

Experimental results are pictured in figure 6.2, p. II-29; numerical simulation output is shown in figure 6.3, p. II-30. Comparing experimental and numerical results, the following observations can be made. The first solute (a) gelates very quickly ($t_{\mathrm{gel}} \approx 5 \, \mathrm{min}$), forming a blob near the location of injection; below a certain threshold of concentration, the diluted solute does not gelate but continues to descend. The second solute (b) starts to sink, too, but gelates on the way to the bottom ($t_{\mathrm{gel}} \approx 15 \, \mathrm{min}$) forming a coniform shape of gel. The third solute (c) completely sinks to the bottom of the tank, where it gelates as the latest of the three experiments ($t_{\mathrm{gel}} \approx 23 \, \mathrm{min}$).

The numerical simulations reproduce the observations from the laboratory experiments very well. While the precise determination of essential process parameters might be very difficult (e.g. β_s, or β_{max}), key features of the density-dependent gelation process could successfully be modelled. Citing [P3]: Walther et al. (2013b), these are namely:

- density-dependent movement of the solute (including arrival of the solute at the bottom of the domain),

- viscosity change after a given residence time,

- continued movement of non-gelated solute due to too low concentration,

- persistence of solute in gelated area due to high viscosity, and

- fingering as a result of slight heterogeneity of hydraulic conductivity.

Also, the series of simulations could be solved using only one set of parameters. Future validation and application success of the presented method will strongly depend on reducing the broad bandwidth of possible parameter combinations.

6.3.2 Summary and Outlook

A novel approach to simulate rapid gelation of an injected solute in porous media was developed. The method could be validated against laboratory data. Considering the empirical nature of the current implementation of the viscosity change, applying the technique on a field scale will require i) to determine the injection solute's parameters in the laboratory to a higher certainty, and ii) profound knowledge of field parameters, especially the permeability and (effective) porosity distribution. If both conditions are met, a gelating fluid could be injected into an aquifer to sink until it reaches a confining layer and form a gel exactly after it passes through a hole leaching into a second, assumingly contaminated aquifer. Then it may release a chemical to remediate the pollutant plume. Figure 6.4, p. II-31, shows the conceptual setup and
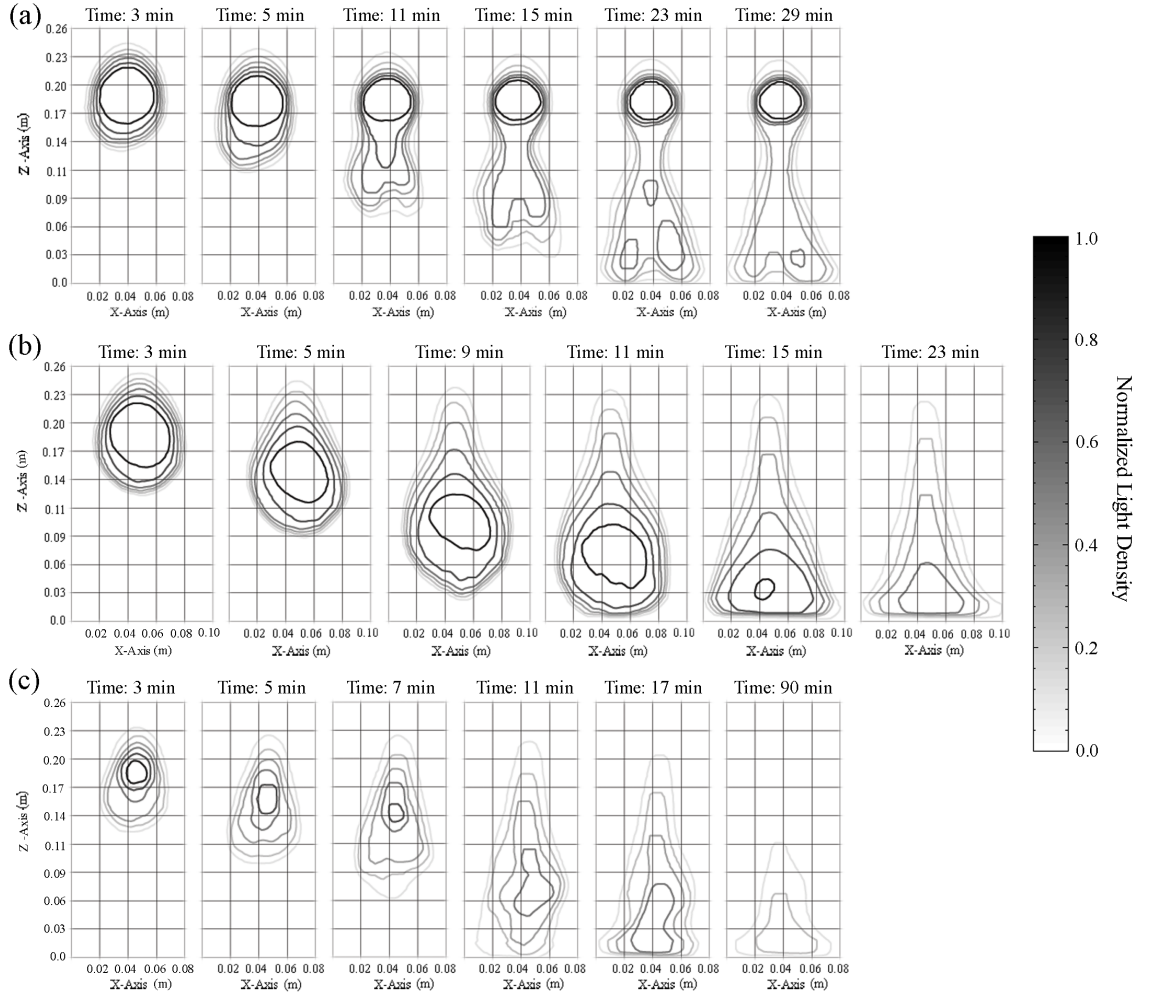
Figure 6.2: Temporal evolution of the gelation of silicate solutions. The first, second and third experiments are shown in (a), (b) and (c), respectively; from [P3]: Walther et al. (2013b).
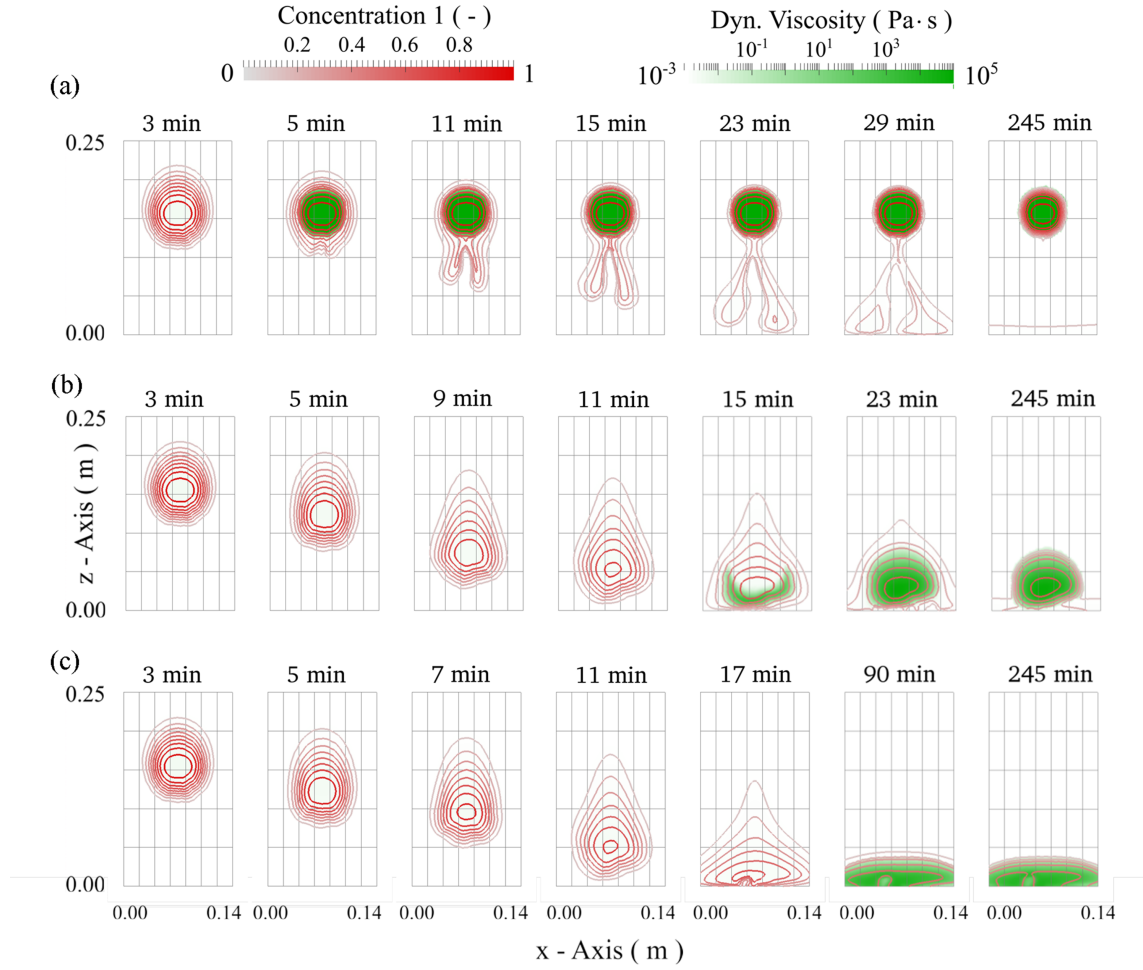
Figure 6.3: Results of numerical simulation for experimental setups 1 (a), 2 (b), and 3 (c); isolines are concentration 1 c_1, shading is viscosity μ; from [P3]: Walther et al. (2013b).

right BC
q_i = const
$q_{top} > q_{bottom}$
$c = 0$

$P_{inj}(0, 0.8)$

Aquifer 1

left BC
$\partial c/\partial x = 0$
$\partial p/\partial z = g\rho_0$

GW Flow
Direction

Perforated
Aquiclude

Aquifer 2
(contaminated)

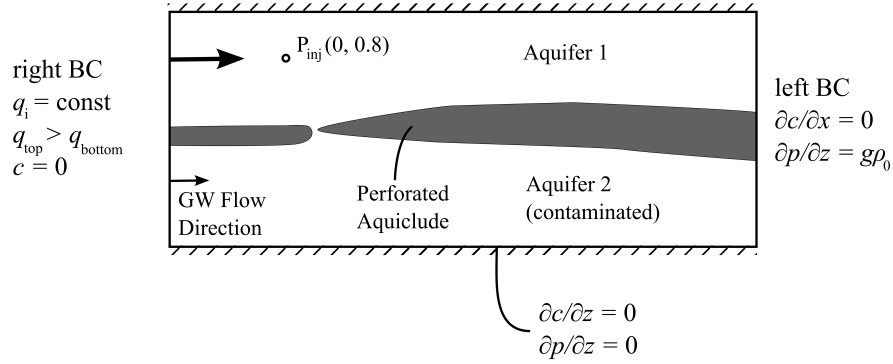$\partial c/\partial z = 0$
$\partial p/\partial z = 0$

Figure 6.4: Conceptual model and boundary conditions for gelation scenario simulation.

figure 6.5, p. II-32, simulation results of a time series for such a possible scenario. The extended IDW (see 4, p. II-5) was used to produce the synthetic, layered, hydrogeological structure. A video of the simulation output is attached as supplementary material to the digital version of the thesis (see E.1, p. App-3).

In fact, the presented approach is not mutually bound to a variation of dynamic viscosity, but could be extended to be used in combination with changes of any fluid or material parameters, e.g. porosity, density. Also, an additional mass transport equation could be solved, where this concentration c_3, which has the same BCs as c_1 and c_2, might diffuse out of the gel and react with a groundwater contamination solute c_4. Further chemical reactions could be defined between c_3 and c_4 representing a remediation procedure.

(a) Time 60s.

(b) Time 1200s.

(c) Time 2400s.

(d) Time 3600s.

(e) Time 4800s.

(f) Time 6000s.

(g) Time 7200s.
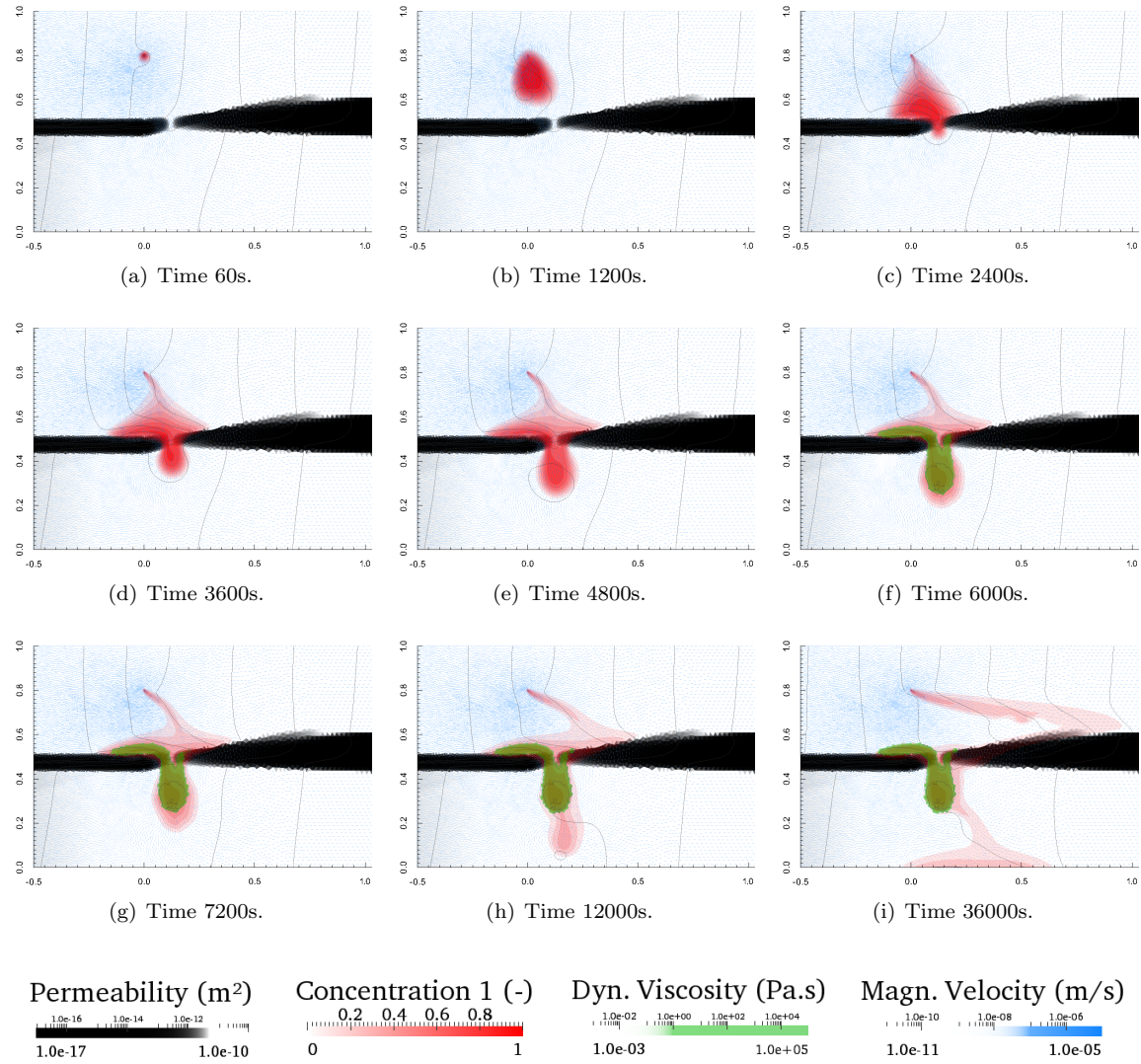
(h) Time 12000s.

(i) Time 36000s.

Figure 6.5: Scenario simulation for emplacement of gelating solute into heterogeneous two-story aquifer; grey isolines show hydraulic head; see also attached video in digital appendix (see E.1, p. App-3).

Chapter 7

Delineating Double-Diffusive Rayleigh Regimes

In a Thermohaline Diffusive-Convective Setting

Preceding note: this chapter contains some figures which, due to the nature of the investigated setups, show many small details. As the printed version of the thesis may not show all details, the reader may consult the digital version, which provides high-resolution images of all figures.

7.1   Background and Motivation

In groundwater management, aquifer systems normally show only little variation in temperature, standard conditions are assumed at $\approx 10\,°C$. The probably most important parameter in groundwater applications, (saturated) hydraulic conductivity K_f, is prescribed as a lumped parameter to express the material's and fluid's resistance to a gradient induced flow, combining soil's permeability κ, water's density ρ^f, and dynamic viscosity μ at $10\,°C$ (see equation (2.4))[1]. When temperature, however, is not constant, e.g. when the geothermal gradient becomes relevant due to large aquifer layer thickness, or due to strongly varying external atmospheric boundary conditions, density and viscosity have to be considered as functions of temperature. In contrast to prior investigations, where fluid density ρ^f only depended on concentration c, in the following thermohaline application, density will additionally vary with temperature as $\rho^f(c, \Theta)$. Examples of such two-folded density-dependent systems can be found in deep sea circulation (Rahmstorf, 1996), porous media with high salinity, as in a "Sabkha" (Yechieli and Wood, 2002), or in the atmospheric boundary layer (Young, 1988; Oke, 1992).

---

[1]For the sake of completeness: gravitational acceleration g is an additional lumped parameter, though probably the most exact one of the listed.

Numerous numbers were derived to characterize such density-driven (here: thermohaline) systems, e.g. Prandtl, Nusselt, Lewis, Sherwood, Taylor, or Froude number. In this investigation, the Rayleigh number Ra is utilized to define the stability of a thermohaline regime (equation (7.1)). Ra expresses the relation between convective and diffusive transport, i.e. high Ra symbolizes a convective, low Ra a diffusive regime.

$$\text{Ra}_\Psi = \frac{\rho^{\text{f}} g \kappa}{\mu} \cdot \frac{\gamma_\Psi L \Delta\Psi}{D_{m,\Psi}} \tag{7.1}$$

with Ψ as an arbitrary system variable, g as gravity constant, γ_Ψ as expansion coefficient due to change of Ψ, L as length of the system, $\Delta\Psi$ as difference of boundary conditions, and $D_{m,\Psi}$ as molecular diffusivity of Ψ. In a thermohaline system, two Rayleigh numbers can be defined, both, for heat and mass transport, Ra_Θ and Ra_S, respectively (subscript S for mass transport and not c, as Ra_c was defined as critical Rayleigh number by Nield and Bejan (1999)).

Nield and Bejan (1999) chose the Rayleigh number to perform a linear stability analysis with perturbations of the relevant flow and transport equations and found two boundaries segregating diffusive and convective regimes (see section 7.2). Others used these principle investigations for further categorization of thermohaline systems applying advanced theoretical, mathematical approaches, e.g. Tagare et al. (2007); Ma and Wang (2010); Chen et al. (2011); Babu et al. (2012). Also, numerical simulations can be found to delineate regimes, or even to use thermohaline setups as possible benchmarks, e.g. Oltean et al. (2008); Musuuza et al. (2011b); Musuuza et al. (2012), or Ataie-Ashtiani and Aghayi (2006).

To fill the gap between theory (i.e. standardized, and mostly highly simplified formulations to keep the problem solvable) and real-world applications (e.g. heterogeneous, thus mostly relatively unknown parametrization), Graf and Therrien (2009) and Graf et al. (2009) applied findings of Nield and Bejan (1999) by running numerical simulations with the scientific simulation code HydroGeoSphere (Brunner and Simmons, 2012) on a vertical, homogeneous plain. Typically, when boundary condition gradients induce a Rayleigh-Bernard convection, the self-organizing system evolves a number of cells, as already described in the "long heater" experiment by Elder (Diersch and Kolditz, 1996). Graf et al. (2009) found several regime behaviours, namely diffusive, stable-convective, periodically oscillating, and chaotic systems.

Being able to predict a system's principle trend of behaviour a priori by simply analysing BCs and system properties, and while not having to prepare and run a numerical model, a fast response to accidents with potentially hazardous contaminants could help to diminish possible harm of environment. For example, if transport of a spilled chemical is rather dominated by a convective, than a diffusive process, fingering might occur, resulting in very fast movement of the contaminant into deeper aquifer horizons. For further demarcation of the double-diffusive Ra_Θ-Ra_S regimes, more detailed investigations were carried out using OpenGeoSys.

This chapter presents a work in progress, showing simulation output and a short discussion. Final conclusions will not be stated. Yet, an outlook combines the current results and shortcomings of the simulations for possible future investigations.

7.2 Methods and Model Setup

Equations 7.2 and 7.3 are postulated as the two possible boundaries between diffusive and convective regimes (see (Nield and Bejan, 1999, equations 9.15, 9.16)).

$$J^2 - \phi\omega^2 = (\text{Ra}_\Theta + \text{Ra}_S)\,\alpha^2 \tag{7.2}$$

$$\omega\left[J^2\,(1+\phi) - (\phi\text{Ra}_\Theta + \text{Ra}_S)\,\alpha^2\right] = 0 \tag{7.3}$$

with $J = j^2\pi^2 + \alpha^2$, and $j = 1, 2, 3, ...$, arising from perturbation analysis, $\pi = 3.1415...$ as Ludolph's number, α as an overall horizontal wavenumber, $\phi = \text{Le} \cdot \varphi/\sigma$, and φ as porosity, $\sigma = (\rho C_p)^\text{s} / (\rho C_p)^\text{f}$ as heat capacity ratio, and C_p^i as solid or fluid isobaric heat capacities, and $\text{Le} = \alpha^\text{s}/D_m^\text{f}$ as the Lewis number, and $\alpha^\text{s} = \lambda^\text{s}/(\rho C_p)^\text{f}$ as thermal diffusivity, and λ^s as thermal conductivity of the solid, $D_m^\text{eff} = \varphi D_m$ as effective molecular diffusion coefficient, and finally ω as oscillation frequency.

Furthermore, when finding the minimum of (Nield and Bejan, 1999, equation 6.29) with respect to α:

$$\text{Ra} = \frac{(j^2\pi^2 + \alpha^2)^2}{\alpha^2} \tag{7.4}$$

one can find $\alpha^2 = j^2\pi^2$, thus

$$J = 2j^2\pi^2 \tag{7.5}$$

or $\text{Ra}_\text{min} = 4j^2\pi^2$. Using 7.5, equations (7.2) and (7.3) can be rewritten as

$$\text{Ra}_\Theta + \text{Ra}_S = 4j^2\pi^2 - \frac{\phi\omega^2}{j^2\pi^2} \tag{7.6}$$

which simplifies for the case of "no oscillation", i.e. $\omega = 0$ to:

$$\text{Ra}_\Theta + \text{Ra}_S = 4j^2\pi^2 \tag{7.7}$$

and

$$\phi\text{Ra}_\Theta + \text{Ra}_S = (1 + \phi)\,4j^2\pi^2 \tag{7.8}$$

In the following, we varied j; the resulting boundaries from 7.7 and 7.8 are plotted in figure 7.2, p. II-37, in the first quadrant Q1 with $\omega = 0$ (obs.: double-logarithmic plot, Rayleigh numbers as multiples of π^2). In the figure, condition C1b (equation 7.7) conceals C1 (equation 7.6), which yields the same values for $\omega = 0$.

The conceptual model is shown in figure 7.1, p. II-37. Process and system parameters are listed in table 7.1. The setup consists of a vertical, homogeneous x-z-domain.

For mass and heat transport processes, BCs are given on horizontal edges as constant 1st-type and on vertical edges 2nd-type "no-flow". For fluid flow, all boundaries are "no-flow". Initial conditions are hydrostatic pressure distribution and given linear gradient between applied mass and heat transport BCs. To minimize influence on system behaviour of the limited numerical accuracy, a disturbance of 10 % from the linear gradient was initially introduced at P_{dist}. Pressure dependency on density, as well as influence of temperature, concentration, or pressure on viscosity are significantly lower in comparison and, thus, in this application omitted.

Investigations were carried out for quadrant Q1 and Q4; in Q1, mass and heat BCs have an opposite gradient; in Q4, BC gradients are both positive in upward direction. The first simulations (in Q1) were accomplished using a 1:1 scale with an edge length of 100 m; afterwards, domain scale was changed to 1:10 (H:W) with a width W of 1000 m (for Q1 and Q4). Grid resolution of 1:1 was $\Delta x = \Delta z = 0.25$ m, and had to be reduced to $\Delta x = \Delta z = 1$ m for 1:10 because of computational limitations. Time discretization was automatically determined based on the error of relative global norm of the processes. The simulations were run in a parallel computing environment.

Rayleigh numbers had to be calculated as approximation, as Ra is depending on fluid density ρ^f, which is a function of temperature Θ and concentration c. As both, Θ and c, are defined through a gradient between bottom and top boundaries, density will vary throughout the domain, hence, does $\mathrm{Ra}\big(\rho^f(\Theta, c)\big)$. The relation between top and bottom densities after equation (2.10) or Rayleigh numbers for different combinations of thermal and haline gradients is plotted in figure 7.3, p. II-37. The figure shows, that for the given setup, thermal gradients have a larger influence on the differences between top and bottom densities, than haline gradients. For a linear density-relationship, as used in this case, taking the mean of the two Ra_i might be sufficient. Yet, for higher order, non-linear relationships, considering integration of Ra over the vertical coordinate z from z=0 to z=H (i.e. $\int_0^H \mathrm{Ra}\, dz$), where $\int \rho\, dz$ is the relevant part, might help to find a correction factor for Ra.

7.3 Results

7.3.1 Quadrant Q1, Scale 1:1

Figure 7.4, p. II-40, shows exemplary formations of steady states for Q1 at scale 1:1 as results of OpenGeoSys simulations. Four regimes can be recognized in this setup: diffusive (non-convective), stationary convective with one roll, with two rolls, and non-stationary chaotic regimes. Figure 7.5, p. II-41, plots several combinations of Ra and visualizes the individually observed regimes. In the digital appendix, an exemplary video of a chaotic regime is attached (see E.1, p. App-3).

Increasing Rayleigh numbers indicate, that regimes become more and more advective, i.e. magnitude of velocity increases, and more convection rolls develop until
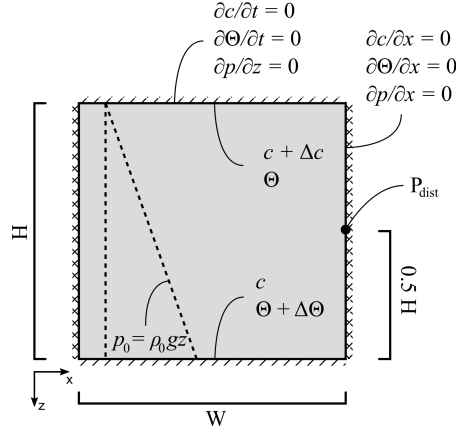
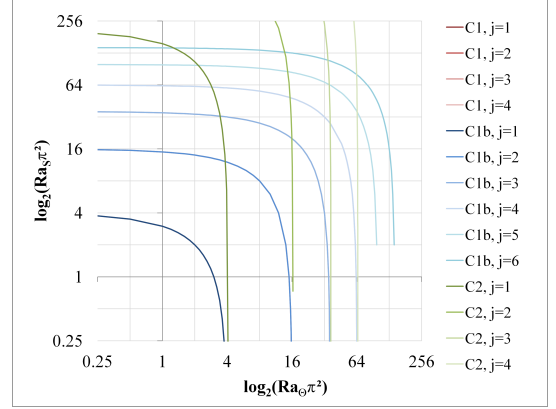Figure 7.1: Conceptual model setup for thermo-haline simulations.

Figure 7.2: Boundaries postulated by Nield and Bejan (1999) with varying j, $\omega = 0$, and parameters from table 7.1, p. II-38; C1 from 7.6, and C1b from 7.7, and C2 from 7.8.
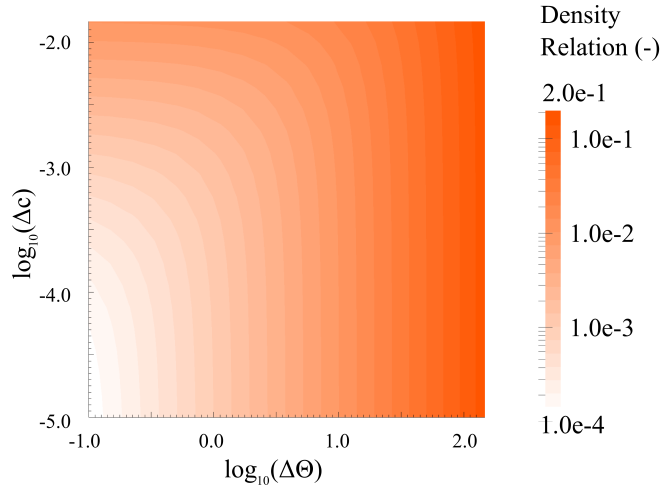

Figure 7.3: Relation between top and bottom densities or Rayleigh numbers for the given setup with parameters from table 7.1, p. II-38.

Table 7.1: Parameters used in thermohaline simulations

Parameter	Value
Density solid ρ^{s} $\left(\mathrm{kg}\cdot\mathrm{m}^{-3}\right)$	2650
Heat capacity solid C_p^{s} $\left(\mathrm{J}\cdot\mathrm{kg}^{-1}\cdot\mathrm{K}^{-1}\right)$	800
Thermal conductivity solid λ^{s} $\left(\mathrm{W}\cdot\mathrm{m}^{-1}\cdot\mathrm{K}^{-1}\right)$	1.5
Initial density fluid ρ_0^{f} $\left(\mathrm{kg}\cdot\mathrm{m}^{-3}\right)$	1000
Heat capacity fluid C_p^{f} $\left(\mathrm{J}\cdot\mathrm{kg}^{-1}\cdot\mathrm{K}^{-1}\right)$	4184
Thermal conductivity fluid λ^{f} $\left(\mathrm{W}\cdot\mathrm{m}^{-1}\cdot\mathrm{K}^{-1}\right)$	0.5
Dynamic viscosity μ $(\mathrm{Pa}\cdot\mathrm{s})$	0.0011
Permeability κ $\left(\mathrm{m}^2\right)$	$2.7\cdot 10^{-12}$
Molecular diffusion coefficient D_m $\left(\mathrm{m}^2\cdot\mathrm{s}^{-1}\right)$	$1\cdot 10^{-8}$
Porosity φ $(-)$	0.3
Haline expansion coefficient γ_c $(-)$	0.7
Thermal expansion coefficient γ_Θ $\left(\mathrm{K}^{-1}\right)$	-0.001

the regime falls into chaotic behaviour. Such chaotic regimes could be identified easily, as observations at $\mathrm{P_{dist}}$ yielded fluctuations of all process parameters, that were neither converging to a specific value, nor showed repetitive signatures. The individual regimes can clearly be separated from each other; the boundary between diffusive and 1-roll-convective regime follows equation (7.7) with $j = 1$ ("C1b, j=1") as predicted by Nield and Bejan (1999). The next boundary, the transition between one and two rolls, seems to be defined by "C2, j=2", probably also by "C1b, j=3". Finally, the boundary to the chaotic regime, might be separated by "C1b, j=6". Additional simulations might be necessary to distinguish the regimes in more detail, especially when one Ra becomes a multiple > 8 of the other Ra. Simulations in the chaotic regime were only successful with spatial resolution $\Delta x, z \leq 0.25\,\mathrm{m}$; with lower grid refinement, simulations would not converge showing values for the primary variables out of the bandwidth given through the BCs. Exemplary shown simulation results of HYDROGEOSPHERE lie within the same regimes as identified by OPENGEOSYS.

Figure 7.6, p. II-41, presents three detailed views within Q1. In 7.6 (a) and (b) the accuracy of the predicted boundaries can be estimated to lie within $\approx 0.25\pi^2 \cdot \mathrm{Ra}_i$. Figure 7.6 (c) reveals non-steady development with increasing Ra_i, i.e. stationary two-roll-regimes are followed by one-roll-regimes, which can be interpreted as the numerical accuracy of the chosen setup in OPENGEOSYS ($\approx 1.4 \cdot 10^{-4}\pi^2 \cdot \mathrm{Ra}_i$). Simulation results in (c) may vary between different operating systems (Windows, Linux, Mac etc.), their respective distributions (e.g. Ubuntu vs. Redhead), release versions (e.g. Windows XP vs. Windows 7), or system architecture (nowadays 32bit vs. 64bit).

From the observation, that increasing Ra_i yielded larger diameters of developing rolls, it was deducted, that BCs might have significant influence on the simulation results, forcing the convection cells into either one or two rolls. A setup with the

scale 1:10 was created to reveal possible additional patterns, i.e. not exclusively 10 or 20 rolls.

7.3.2 Quadrant Q1, Scale 1:10

Exemplary for Q1 scale 1:10, figure 7.7, p. II-42, shows the steady state of one combination of Rayleigh numbers, where a total of twelve rolls evolved. The individual convection cells appear to be equally sized and of symmetric shape (comparing two adjacent rolls). The simulation converged quickly after all convection rolls had formed.

Figure 7.8, p. II-42, exemplary plots the diameter of the sixth evolving convection cell for different Ra over time. With increasing Ra_i ("Ra_i" in the figure), the size of the rolls decrease due to a higher number of evolving rolls. Also, when Ra_i increase, the time until the sixth roll develops a stable diameter is larger.

Combinations of Ra_i are pictured in figure 7.9, p. II-42. In general, when Rayleigh numbers increase, the number of convection cells in the domain increases, too. Again, the diffusive regime is bounded by "C1b, j=1". The former segregation between one and two rolls in 1:1 (i.e. "C2, j=2") is surrounded by regimes of 14 or 15 rolls, which would support the assumption that BCs are limiting the free development, and convection cells cannot evolve partly (e.g. 1.4 cells), but as a discrete number. The maximum number of rolls found was 19. Due to the decrease of the spatial resolution to $\Delta x, z = 1\,\mathrm{m}$, the simulations' stability was limited especially for higher Ra. Chaotic behaviour could not be observed, but is suspected for higher Ra.

An attached video (see E.1, p. App-3) shows the development of a stable regime with several rolls. When all convection cells have evolved, all cells change in size, equilibrating their spacial demand. It is suspected, that this behaviour is again due to the BCs; in the beginning, the cells form freely with a diameter specific to the Ra; when the last cell is forming, it will have less free space, thus, firstly assemble with a smaller diameter; when fully developed, the observed shifting happens, and all cells acquire the same diameter. Similarly, when the last cell will have more space to evolve, all cells will afterwards increase in diameter. Hence, it is assumed, that in an infinite horizontal domain, with changing Ra, the change of the diameter of the cells will be continuous, and not discrete, as currently observed.

7.3.3 Quadrant Q4, Scale 1:10

In quadrant Q4, when $Ra_\Theta > 0$ and $Ra_S < 0$, an additional regime can be identified, next to stable diffusive and convective regimes. Observing temperature and relative concentration at the point P_{dist}, as plotted in figure 7.10, p. II-43, a steady, oscillatory behaviour is revealed. Peaks can be identified in all observed variables. A pattern in the variation of the peak magnitude could not be detected; increasing spatial discretization might diminish this variation, and if not, application of a Fourier transformation may be used to find multiple overlaying frequencies. Al-
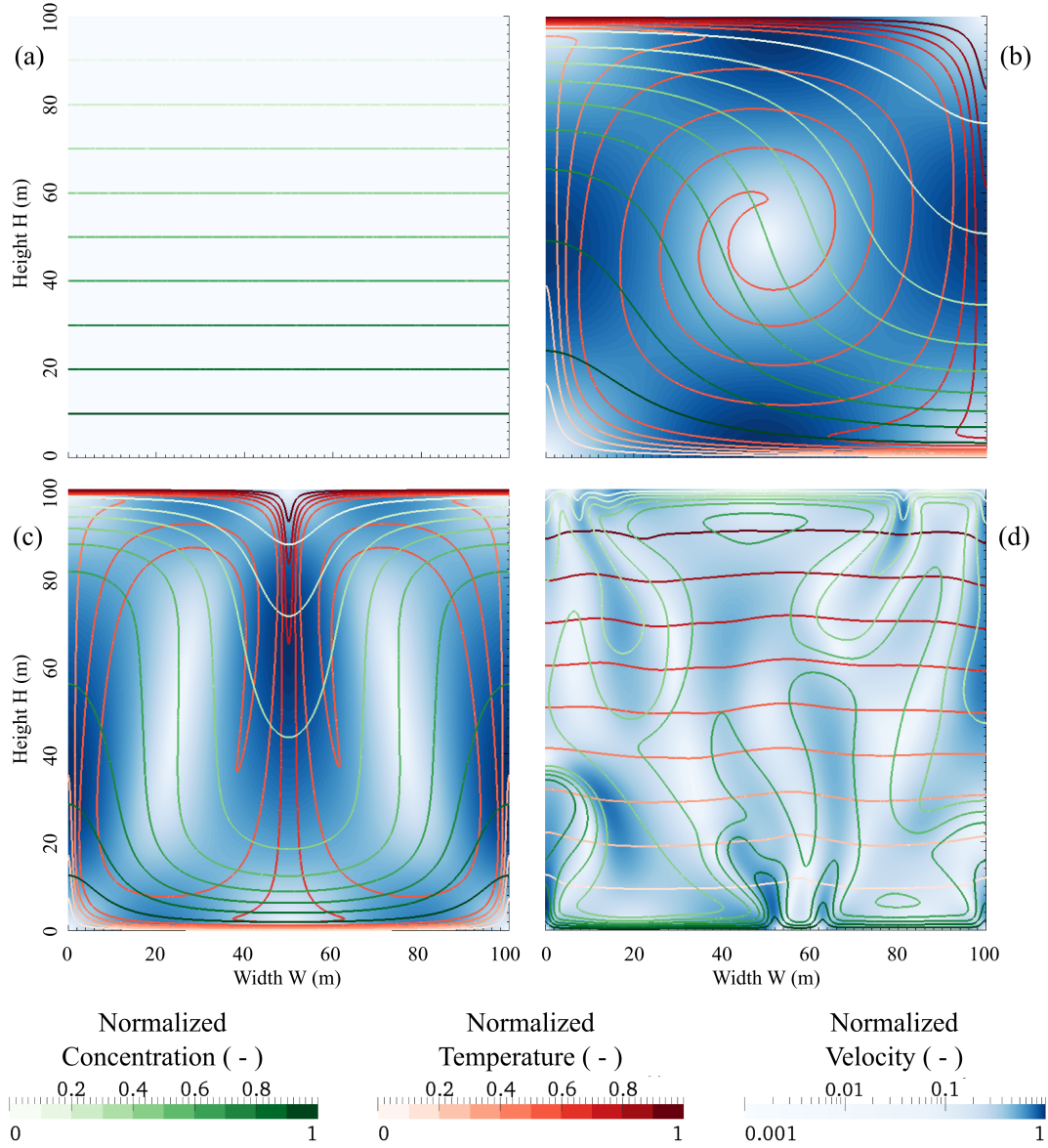
Figure 7.4: Examples of identified states for simulation results in Q1, scale 1:1; (a) diffusive: $Ra_\Theta = 1\pi^2$, $Ra_S = 1\pi^2$, (b) stable single convection: $Ra_\Theta = 6\pi^2$, $Ra_S = 3\pi^2$, (c) stable double convection: $Ra_\Theta = 16\pi^2$, $Ra_S = 32\pi^2$, (d) chaotic: $Ra_\Theta = 256\pi^2$, $Ra_S = 128\pi^2$.
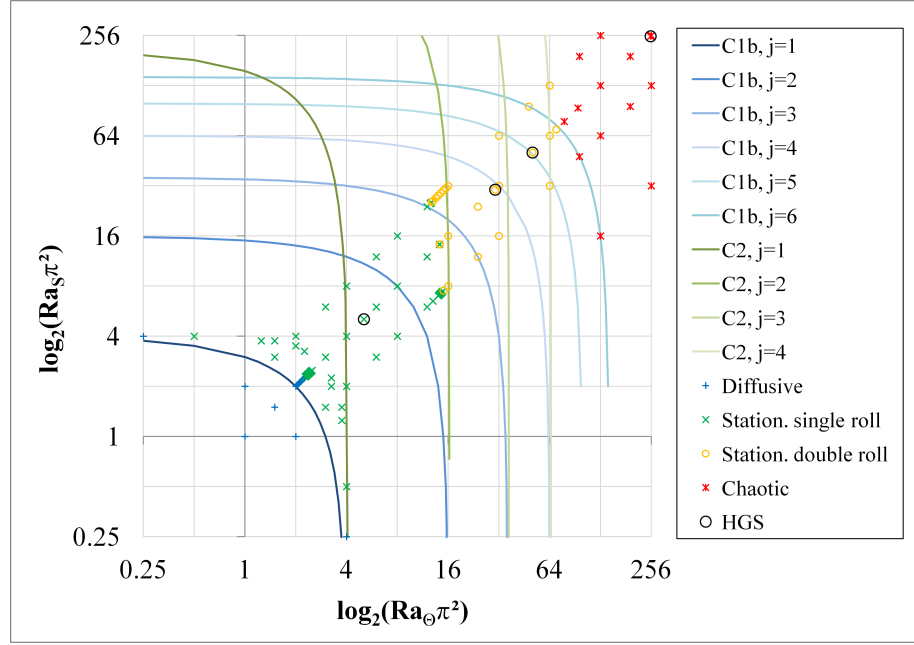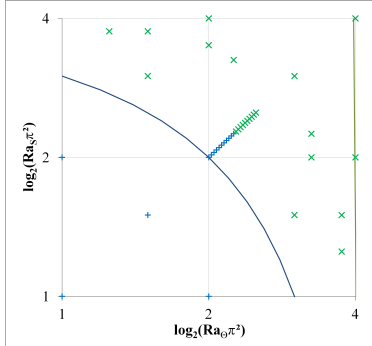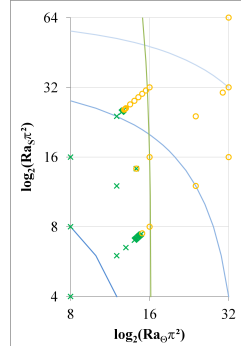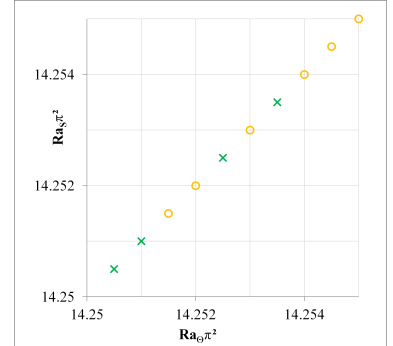
Figure 7.5: Identified states for simulation results in Q1, scale 1:1, in double-diffusive Rayleigh regime.

(a) Boundary between diffusive and stationary single roll.

(b) Boundary between stationary single and double roll.

(c) Detailed view of boundary between stationary single and double roll.

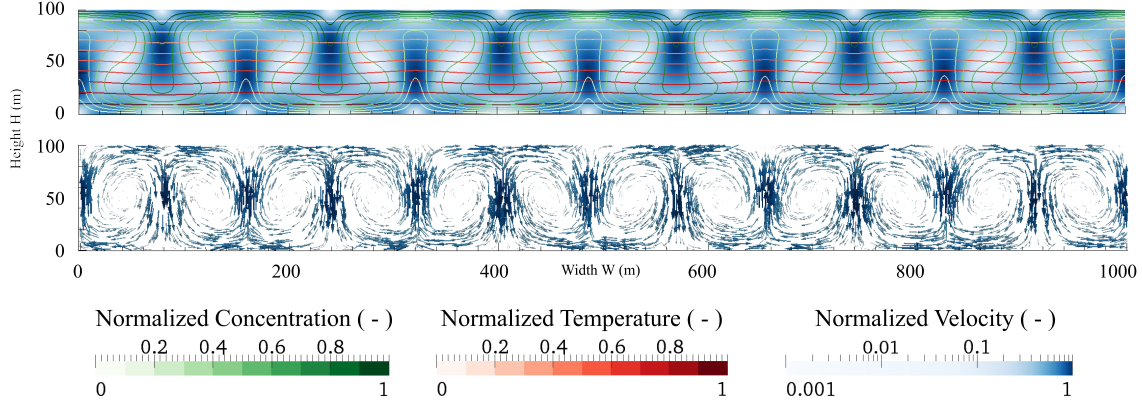Figure 7.6: Details of figure 7.5, p. II-41; legends as in figure 7.5, p. II-41.

Figure 7.7: Simulation results for Q1, scale 1:10; exemplary output of steady state for $\mathrm{Ra}_\Theta = 3\pi^2$, $\mathrm{Ra}_S = 3\pi^2$.
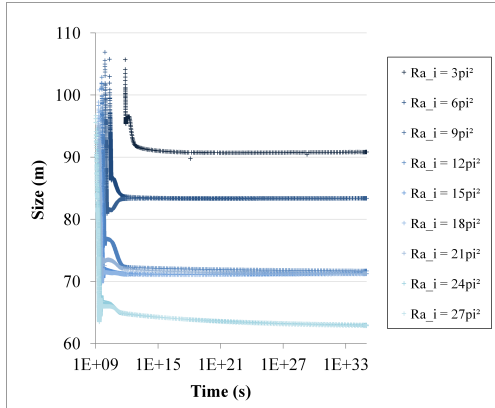
Figure 7.8: Development of diameter for sixth roll for selected Ra combinations in Q1, scale 1:10.
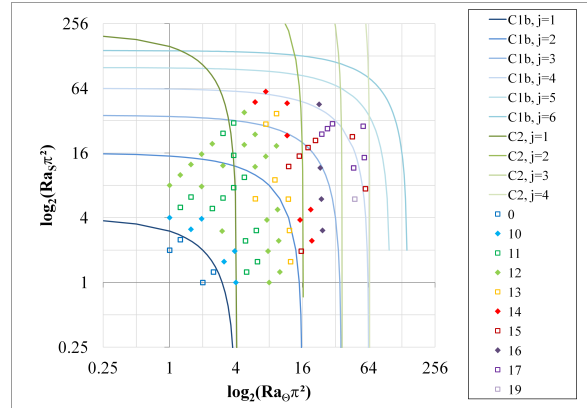

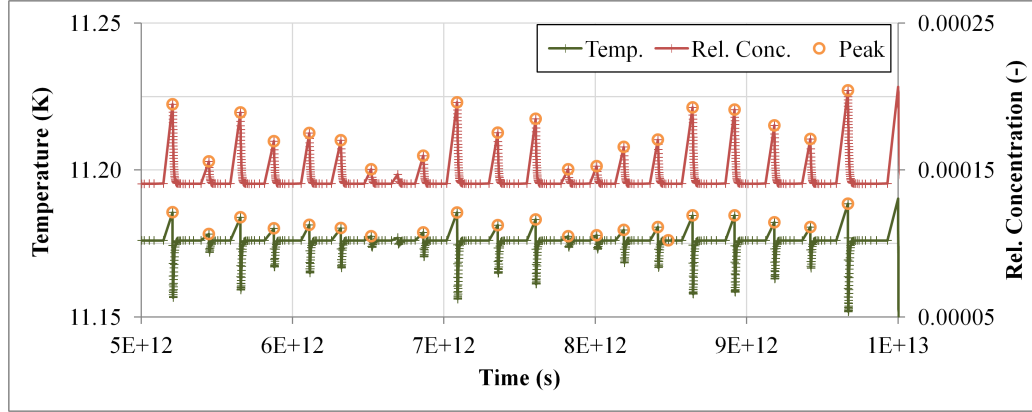Figure 7.9: Number of rolls in Q1, scale 1:10, in double-diffusive Rayleigh regime.

Figure 7.10: Exemplary output for temperature and relative concentration of simulation in Q4, scale 1:10, at P_{dist}.

though the utilized procedure for peak identification does not capture every local maximum/minimum (missing e.g. at time $t \approx 6.6 \cdot 10^{12}$ s), the period T' between the peaks appears to be similar for all observed variables. The location of the oscillatory regime is plotted in figure 7.12, p. II-44, together with several boundaries; "C2, j=1" seems to separate oscillatory and convective regimes. Calculating a mean value for T' for the individual Ra_i (figure 7.11, p. II-44), yields a general trend: when Ra_S increases, periods become larger, until the system falls into a diffusive state. As values for the period T' are relatively large, frequency ω of the first boundary will be very small, thus, conditions C1 (equation (7.6)) and C1b (equation (7.7)) will yield nearly the same values. If Ra_Θ increases, a convective behaviour might develop as a result of stronger driving gradients from BCs. In the digital appendix, an exemplary video of a stable oscillatory regime is attached (see E.1, p. App-3).

A general explanation for the oscillations might be as follows: when a fluid "package" is situated at the bottom of the domain, its density will be low and the package will start to rise. On the way upwards, closing to the upper BCs, its concentration and temperature will be reduced due to mass and heat dispersion and diffusion to the surrounding porous media and fluid. However, both dynamic dispersion processes are not equally strong, as the package might also lose heat to the solid material through thermal conduction. Thus, in some Ra combinations, the density increase due to temperature decrease will have a stronger influence than the density loss due to a lower concentration, which will force the package to sink down again. Reaching the bottom, temperature and concentration will increase again, hence, density decrease (for the exemplary stronger relation of temperature to density), making the package to rise again, and creating the oscillatory behaviour. Similar observations can be made in atmospheric boundary layers (e.g. adiabatic processes, Oke (1992)).
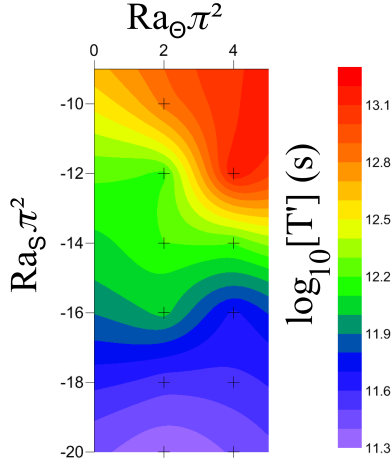
Figure 7.11: Contour plot of logarithmic, mean oscillation period T' in Q4, (see dashed area in figure 7.12, p. II-44).
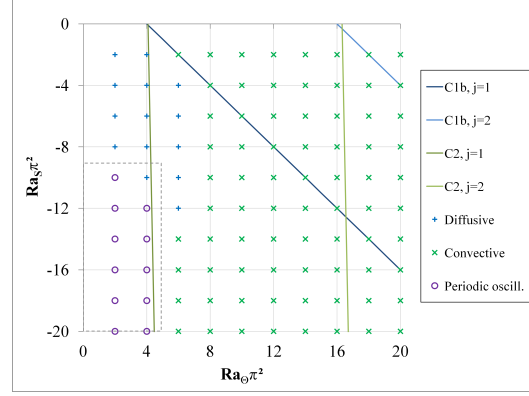
Figure 7.12: States of simulation results in Q4, scale 1:10, in double-diffusive Rayleigh regime.

7.4 Preliminary Conclusions and Outlook

Through variation of haline and thermal Rayleigh numbers, several regimes could be identified for both, a 1:1 and a 1:10 scale setup. Following Nield and Bejan (1999), some regime boundaries could be demarcated. Also, numerical computation accuracy could be estimated.

Generally, boundary conditions pose a significant influence on the developing system. Yet, it may be possible to mimic the correct BC for a free roll development to some extent: although one cannot foretell the value of the primary variables at the vertical domain edges when flow direction points into the domain, a free outflow for transport processes, following flow pointing out of the domain, might help to obtain better results. On the other hand, when only one half of the BC is depicted correctly (i.e. outflow), the regime might become unstable, as the inflow BC remains inadequately defined.

Rayleigh numbers depend on the density (and viscosity, which was considered as a constant value in this investigation) of the fluid, thus, cannot be determined exactly for a given setup. A correction factor might be introduced to attain more "correct" realizations of the individual Ra_i domains. Future variation of Ra might also be attained by changing transport parameters, e.g. permeability, fluid or solid heat capacity. It is unknown, whether the same Rayleigh numbers, acquired by variations of the parameter set, lead to the same regimes.

Gresho and Lee (1981) already emphasized: "Don't suppress the wiggles - They're telling you something!". Therefore, to find the convergence grid, it is believed, that more precise results may be acquired by increasing grid resolution to $\Delta x, z \leq 0.25\,\mathrm{m}$,

similar as for the first simulations. When using finer grids for the 1:10 scale, up to 25 rolls in a steady state convective regime, or even chaotic regimes may be found. Also, observed patterns of different roll numbers might become clearer, and less disarranged (figure 7.9, p. II-42). Presumingly, a 1:100 scale setup might reveal an even finer "regime resolution" with a minimum of 100 rolls up to 250 rolls. Even oscillatory behaviour in Q4 could be delimited more precisely. Currently, defining a boundary to a chaotic regime is rather speculative. Evaluating the results in Q1, one might deduct, that the chaotic regime evolves as soon as convection cell horizontal diameter (width) becomes smaller than 1/2.5 times vertical diameter (height).

From personal correspondence with D. Nield, the following can be added: it is yet unclear, whether the boundary between one and two-roll convective states in the 1:1 setup and for stable convections with about 15 rolls in the 1:10 setup in Q1, is related to "C2, j=2". The same applies for additional boundaries where j > 2. Further investigation on both, analytical and numerical side, is needed to characterize such double-diffusive regimes in more detail.

Part III

Summary and Conclusions

Chapter 8

Important Achievements

This thesis combines several process and application studies for variable-density flow and mass/heat transport on different scales, including the relevant, adjacent developments for model setup and process reproduction (i.e. benchmarking). Most essential achievements are listed comprehensively in the following.

1. Several numerical benchmarks for groundwater flow and variable-density mass transport were developed for the numerical modelling software OpenGeoSys. Benchmarks include a steady-state and transient groundwater table, saline intrusion and withdrawal, as well as groundwater recharge in an initially salinized aquifer. Model verification was achieved against analytical and experimental data and provides the basis for further model applications.

2. An inverse distance weighting interpolation method (IDW) was extended for general usage of interpolating three-dimensional, tilted, layered structures from given borehole data and (hydro-geological) structural interpretation.

3. The extended IDW was verified on a synthetic example. A regional scale heterogeneous conceptual subsurface model was set up in combination with the extended IDW interpolation for a real-world groundwater usage study.

4. A regional scale model, comprising a coastal aquifer system used as freshwater source for extensive agricultural irrigation, was calibrated. Results for groundwater levels, aquifer material parameter, and boundary conditions for a pre--development steady state were obtained with the aid of the parameter optimization algorithm PEST using free parameter boundaries. Calibration results show high agreement with measurements. Considering the situation of limited data availability, acceptable results could be acquired for a manual transient state calibration of the groundwater table and mass transport of saline intrusion.

5. Calibration results of the regional scale modelling for material properties (permeability), boundary inflow (mountainous recharge) and outflow (pumping ab-

straction) show similar values when cross-referencing to independent research groups' results. Deviations reveal weaknesses of the current setup and several possibilities for improvements of the model input data (e.g. through measurements).

6. Long-term scenario simulations yield an approximate time scale for the future development of the saltwater intrusion of the regional scale model. Scenario simulation results were utilized to estimate the study areas' relative remediation potential.

7. A novel method for numerical simulation of gelation due to rapid viscosity change of the fluid in porous media was developed. Model verification was provided by reproducing results from small-scale laboratory experiments for three differently gelling solutes.

8. The layout of a possible remediation application scenario of a gelling solute in a heterogeneous aquifer setup was documented; the subsurface structure was constructed by utilizing the extended IDW method.

9. A numerical modelling application of a thermohaline double-diffusive theory on medium scale domain was presented. Several convection schemes could be demarcated, namely, diffusive, steady-state convective, chaotic, and stable oscillatory. Probable relations to theoretically derived boundaries were shown. Possible future areas of scientific interest were identified.

10. Scientific visualization methods of different degrees of complexity were utilized to validate model setups and simulation output. Visualization was proven to be a vital component for information and result presentation.

Chapter 9

Conclusions and Outlook

The presented investigations underline the importance of density-driven flow in various fields of interest, may these be applications of small to regional scale domain models, real-world challenges, research of novel methods of remediation, or theoretical investigations on stability behaviour. Additionally to the conclusions already mentioned in the corresponding chapters, an overall review of the studies shows the following strengths of numerical modelling and general weaknesses as possibilities for improvement and challenges of future research.

Numerical models are currently the only way to assess management alternatives for aquifer systems on larger scales. With a sufficient data base for validation, numerical modelling can be used as a tool to delineate possible futures for groundwater system on various scales. The open-source project OPENGEOSYS provided a valuable platform to adapt the modelling tool to specific tasks and to present results to a broad community. With a properly handled code versioning, the open-source philosophy gave the opportunity for many individuals to develop and implement new ideas and required necessities to work on a common goal. While trying to push the boundaries of possible modelling, still a number of issues has to be addressed in order to improve modelling capabilities, robustness of results and general conclusion quality.

Parameter insecurity: the provided aquifer material parameters and boundary conditions comprised fuzziness, i.e. high bandwidths for permeability, porosity, dispersion coefficients. Similarly, source terms of model inflow, and outflow could only be derived from estimations or cross-referenced from other research estimation. Hence, numerical studies of real-world applications with large, time demanding computational tasks will need to assess ways to handle parameter insecurities, which will most likely not be diminishable in near future, other than through multiple simulation runs. Concepts from "fuzzy logic" (Ayvaz et al., 2007; Banerjee et al., 2011; Gerner et al., 2012) or "surrogate models" (Schmitz et al., 2010) might aid in reducing model runtimes.

Numerical dispersion: although it was not the main focus of the presented studies,

it is generally difficult to determine the influence of the usually undesirable artificially generated dispersion. It may be suspected, that in the regional application (chapter 5, p. II-9), numerical dispersion is present, but may be of minor importance in comparison to the apparent issue of parameter insecurity. The effect of numerical dispersion on the modelling of a gelating solute (chapter 6, p. II-25) might be relatively weak, as velocities (i.e. advection) are small close to the high-viscous area. Due to the fact, that the thermohaline studies (chapter 7, p. II-33) comprised an enormous sensible behaviour in regime stability when altering the setup only very little, the amount of numerical dispersion might be extremely hard to quantify or even omit. In general, grid conversion studies could provide information on the strength of numerical dispersion, e.g. by adjusting the spatial resolution and acknowledging the Peclét number. However, sufficient (hydro-geological) parametrization data, as well as computational capabilities have to be provided in order to satisfy the finer grid resolution. There was and still is an undeniable demand for further research on the issue of numerical dispersion (Diersch, 1981; Frind, 1982b; Reilly and Goodman, 1987; Simmons and Narayan, 1997; Diersch and Kolditz, 2002; Graf and Degener, 2011).

Parameter diversity, and significance: numerous parameters were needed to describe processes (e.g. viscosity change due to gelation, chapter 6, p. II-25). With increasing number of parameters, it becomes harder to find a global optimum of a target function, and more parameter combinations are possible to achieve a sufficiently good calibration. The determination of empirical parameters in laboratory experiments for the use in numerical modelling without proper interpretation of the variable's meaning is complicated. As a general issue, additional difficulties may be encountered when upscaling experimental data. Therefore, relating the empirical nature of a parameter to a determinable process value will be required in future. "Transfer functions", similarly to the concept of pedotransfer functions (Tietje and Tapkenhinrichs, 1993), may provide a solution to describe the parameter-process-relations.

Multi-dimensionality of parameter sets: the combination of the previous issues yields a multi-dimensional field for parameter optimization. Sensitivity of the parameters may likely vary depending on the position in the optimization field. These circumstances might limit applicability of numerical simulations in real-world challenges. Yet, besides small-scale experimental setups, alternatives for e.g. scenario simulations on medium and larger scales do not exist. Decreasing the insecurity for any of the parameters will heavily contribute to narrowing down a "correct" parameter set. Field measurement campaigns (pumping or infiltration tests, drilling log analysis, etc.) or the development of transfer functions relating laboratory analysis to empirical parameters might aid in the process of decreasing uncertainty.

In summary, the various presented studies demonstrate, that the relevant methods for simulating variable-density flow are well developed, potent computing capabilities are available, yet, the lack of data seems a limitation. Employing novel techniques for

the simulation of subsurface flow processes might only be important for very specific tasks. Although this may lead to the conclusion to file this field of modelling as an engineering task, the afore mentioned issues pose not only relevant, but moreover demanding scientific challenges in current and future applications.

Bibliography

Al-Shoukri, S. S. M. Mathematical Modeling of Groundwater Flow in Wadi Ma'awil Catchment, Barka in Sultanate of Oman. Master's thesis, Arabian Gulf University, Bahrain, 2008.

Aquaveo. GMS - Groundwater Modeling Software, 2011. URL `http://www.aquaveo.com/`.

ARANZ Geo Limited. Leapfrog Hydro, 2012. URL `http://www.leapfrog3d.com/`.

Ataie-Ashtiani, B. and Aghayi, M. A note on benchmarking of numerical models for density dependent flow in porous media. *Advances in Water Resources*, 29(12): 1918–1923, Dec. 2006. ISSN 03091708. doi: 10.1016/j.advwatres.2006.01.009.

Ayvaz, M. T., Karahan, H., and Aral, M. M. Aquifer parameter and zone structure estimation using kernel-based fuzzy c-means clustering and genetic algorithm. *Journal of Hydrology*, 343(3-4):240–253, Sept. 2007. ISSN 00221694. doi: 10.1016/j.jhydrol.2007.06.018.

Babu, A., Ravi, R., and Tagare, S. Double diffusive Rotating convection In a sparsely packed Porous Medium. *ipcsit.com*, 33(Fdtt):110–117, 2012.

Banerjee, P., Singh, V., Chatttopadhyay, K., Chandra, P., and Singh, B. Artificial neural network model as a potential alternative for groundwater salinity forecasting. *Journal of Hydrology*, 398(3-4):212–220, Feb. 2011. ISSN 00221694. doi: 10.1016/j.jhydrol.2010.12.016.

Bargaoui, Z. K. and Chebbi, A. Comparison of two kriging interpolation methods applied to spatiotemporal rainfall. *Journal of Hydrology*, 365(1-2):56–73, Feb. 2009. ISSN 00221694. doi: 10.1016/j.jhydrol.2008.11.025.

Bear, J. *Dynamics of fluids in porous media*. Courier Dover Publications, New York, 1972. ISBN 04866567561, 97804866567551.

Bear, J. *Hydraulics of groundwater*. McGraw-Hill series in water resources and environmental engineering. McGraw-Hill International Book Co., 1979. ISBN 9780070041707.

Bear, J. *Seawater Intrusion in Coastal Aquifers Concepts, Methods and Practices*. Theory and Applications of Transport in Porous Media. Springer, 1999. ISBN 9780792355731.

Beinhorn, M., Dietrich, P., and Kolditz, O. 3-D numerical evaluation of density effects on tracer tests. *Journal of Contaminant Hydrology*, 81(1-4):89–105, Dec. 2005. ISSN 0169-7722. doi: 10.1016/j.jconhyd.2005.08.001.

Bhandari, A. *Remediation technologies for soils and groundwater*. American Society of Civil Engineers, 2007. ISBN 9780784408940.

Böttcher, N. *Thermodynamics of porous media: non-linear flow processes*. PhD thesis, Technische Universität Dresden, 2013.

Böttcher, N., Singh, A., Kolditz, O., and Liedl, R. Non-isothermal, compressible gas flow for the simulation of an enhanced gas recovery application. *Journal of Computational and Applied Mathematics*, 236(18):4933–4943, Dec. 2012. ISSN 03770427. doi: 10.1016/j.cam.2011.11.013.

Boussinesq, J. Recherches théoriques sur l'écoulement des nappes d'eau infiltrées dans le sol et sur le débit des sources. *J. Math. Pure. Appl. 5me. Ser.*, 10:5–78, 1904.

Brettschneider, M., Grundmann, J., Schütze, N., and Walther, M. Development of Surrogate Models for reproduction of complex numerical simulation models and application in a water resource management system. In *The New Zealand Hydrological Society Annual Conference (NZHS Conference)*, Dunedin, New Zealand, 2010.

BRGM. Study of A New Organization of Irrigation in Barka-Rumais Area: Data Analysis and Modelling Report. Technical Report 33, BRGM L'ENTREPRISE AU SERVICE DE LA TERRE, 1992.

Brunner, P. and Simmons, C. T. HydroGeoSphere: A Fully Integrated, Physically Based Hydrological Model. *Ground Water*, 50(2):170–176, Mar. 2012. ISSN 0017467X. doi: 10.1111/j.1745-6584.2011.00882.x.

Chen, X., Wang, S., Tao, J., and Tan, W. Stability analysis of thermosolutal convection in a horizontal porous layer using a thermal non-equilibrium model. *International Journal of Heat and Fluid Flow*, 32(1):78–87, Feb. 2011. ISSN 0142727X. doi: 10.1016/j.ijheatfluidflow.2010.06.003.

David, I. *Grundwasserhydraulik : Strömungs- und Transportvorgänge*. Vieweg, Braunschweig, Wiesbaden, 1998. ISBN 9783528077136.

Diersch, H. Finite element modelling of recirculating density-driven saltwater intrusion processes in groundwater. *Advances in Water Resources*, 11(1):25–43, 1988.

Diersch, H. and Kolditz, O. On finite-element analysis of spatio-temporal buoyancy-driven convection processes in porous media. *IAHS Publications-Series*, (237): 407–415, 1996.

Diersch, H.-J. Primitive Variable Finite Element Solutions of Free Convection Flows in Porous Media. *ZAMM - Journal of Applied Mathematics and Mechanics / Zeitschrift für Angewandte Mathematik und Mechanik*, 61(7):325–337, 1981. ISSN 1521-4001. doi: 10.1002/zamm.19810610707.

Diersch, H.-J. and Kolditz, O. Variable-density flow and transport in porous media: approaches and challenges. *Advances in Water Resources*, 25(8-12):899–944, Aug. 2002. ISSN 03091708. doi: 10.1016/S0309-1708(02)00063-5.

Dubrule, O. Comparing splines and kriging. *Computers & Geosciences*, 10(2-3): 327–338, 1984. ISSN 00983004. doi: 10.1016/0098-3004(84)90030-X.

Elder, J. W. Numerical experiments with free convection in a vertical slot. *Journal of Fluid Mechanics*, 24(04):823, Mar. 1965. ISSN 0022-1120. doi: 10.1017/S0022112066001022.

Elder, J. W. Transient convection in a porous medium. *Journal of Fluid Mechanics*, pages 609–623, 1967.

ESRI. ArcGIS Desktop: Release 10., 2011. URL `http://www.esri.com/`.

Farouki, O. T. Thermal properties of soils. Technical Report 1, U.S. Army Cold Regions Research and Engineering Laboratory Hanover, 1981.

Fein, E. and Schneider, A. d3f - Ein Programmpaket zur Modellierung von Dichteströmungen. Technical report, Gesellschaft für Anlagen- und Reaktorsicherheit (GRS) mbH, 1999.

Francke, H. and Thorade, M. Density and viscosity of brine: An overview from a process engineers perspective. *Chemie der Erde - Geochemistry*, 70:23–32, Aug. 2010. ISSN 00092819. doi: 10.1016/j.chemer.2010.05.015.

Frind, E. Simulation of long-term transient density-dependent transport in groundwater. *Advances in Water Resources*, 5(2):73–88, 1982a.

Frind, E. Seawater intrusion in continuous coastal aquifer-aquitard systems. *Advances in Water Resources*, 5:89–97, 1982b.

Gallagher, M. and Doherty, J. Parameter estimation and uncertainty analysis for a watershed model. *Environmental Modelling & Software*, 22(7):1000–1020, July 2007. ISSN 13648152. doi: 10.1016/j.envsoft.2006.06.007.

Gerner, A., Grundmann, J., Walther, M., and Schmitz, G. H. Groundwater recharge as a crucial aspect in water resources development for the Barka region. In *International Conference on Drought Management Strategies in Arid and Semi-Arid Regions*, Muscat, The Sultanate of Oman, 2011.

Gerner, A., Schütze, N., and Schmitz, G. H. Portrayal of fuzzy recharge areas for water balance modelling - a case study in northern Oman. *Advances in Geosciences*, 31:1–7, June 2012. ISSN 1680-7359. doi: 10.5194/adgeo-31-1-2012.

Glover, R. E. The pattern of fresh-water flow in a coastal aquifer. *Journal of Geophysical Research*, 64(4):457–459, 1959. ISSN 2156-2202. doi: 10.1029/JZ064i004p00457.

Golden Software. Surfer 9, 2010. URL `http://www.goldensoftware.com/`.

Goswami, R. R. and Clement, T. P. Laboratory-scale investigation of saltwater intrusion dynamics. *Water Resources Research*, 43(4):1–11, Apr. 2007. ISSN 0043-1397. doi: 10.1029/2006WR005151.

Graf, T. and Degener, L. Grid convergence of variable-density flow simulations in discretely-fractured porous media. *Advances in Water Resources*, 34(6):760–769, June 2011. ISSN 03091708. doi: 10.1016/j.advwatres.2011.04.002.

Graf, T. and Therrien, R. Variable-density groundwater flow and solute transport in porous media containing nonuniform discrete fractures. *Advances in Water Resources*, 28(12):1351–1367, Dec. 2005. ISSN 03091708. doi: 10.1016/j.advwatres.2005.04.011.

Graf, T. and Therrien, R. Stable-unstable flow of geothermal fluids in fractured rock. *Geofluids*, 9(2):138–152, May 2009. ISSN 14688115. doi: 10.1111/j.1468-8123.2008.00233.x.

Graf, T., Diersch, H.-J. G., and Simmons, C. T. On the Existence of Oscillatory - Convective Thermohaline Flow in Sedimentary Basins Work Area. In *AGU*, Toronto, 2009.

Gresho, P. and Lee, R. Don't suppress the wiggles - They're telling you something! *Computers & Fluids*, 9(2):223–253, 1981.

Grillo, A., Logashenko, D., Stichel, S., and Wittum, G. Simulation of density-driven flow in fractured porous media. *Advances in Water Resources*, 33(12):1494–1507, Dec. 2010. ISSN 03091708. doi: 10.1016/j.advwatres.2010.08.004.

Grundmann, J., Schütze, N., Schmitz, G., and Al-Shaqsi, S. Towards an integrated arid zone water management using simulation-based optimisation. *Environmental Earth Sciences*, pages 1381–1394, 2012. doi: 10.1007/s12665-011-1253-z.

Harbaugh, A. MODFLOW-2005, the US Geological Survey modular ground-water model: The ground-water flow process. In *Book 6. Modeling techniques*, chapter 16, page variously. U.S. Geological Survey Techniques and Methods 6-A16, 2005. URL `http://132.248.182.189/cursos/hidrogeologia/Software/MODFLOW/TM6A16.pdf`.

Henderson, A. *ParaView Guide, A Parallel Visualization Application*. Kitware Inc., 2007.

Henry, H. R. *Salt intrusion into coastal aquifers*. PhD thesis, Columbia University, New York, USA, 1960.

Hughes, J. D. and Liu, J. MIKE SHE: Software for Integrated Surface Water/Ground Water Modeling. *Ground Water*, 46(6):797–802, Nov. 2008. ISSN 0017467X. doi: 10.1111/j.1745-6584.2008.00500.x.

Ibaraki, M. A robust and efficient numerical model for analyses of density-dependent flow in porous media. *Journal of Contaminant Hydrology*, 34(3):235–246, Oct. 1998. ISSN 01697722. doi: 10.1016/S0169-7722(98)00092-8.

Kalbacher, T., Delfs, J.-O., Shao, H., Wang, W., Walther, M., Samaniego, L., Schneider, C., Kumar, R., Musolff, A., Centler, F., Sun, F., Hildebrandt, A., Liedl, R., Borchardt, D., Krebs, P., and Kolditz, O. The IWAS-ToolBox: Software coupling for an integrated water resources management. *Environmental Earth Sciences*, 65(5):1367–1380, Aug. 2011. ISSN 1866-6280. doi: 10.1007/s12665-011-1270-y.

Kalbus, E., Kalbacher, T., Kolditz, O., Krüger, E., Seegert, J., Röstel, G., Teutsch, G., Borchardt, D., and Krebs, P. Integrated Water Resources Management under different hydrological, climatic and socio-economic conditions. *Environmental Earth Sciences*, 65(5):1363–1366, Sept. 2011. ISSN 1866-6280. doi: 10.1007/s12665-011-1330-3.

Kestin, J., Khalifa, H. E., and Correia, R. J. Tables of the Dynamic and Kinematic Viscosity of Aqueous NaCl Solutions in the Temperature Range 20-150 C and the Pressure Range 0.1-35 MPa. *Journal of physical and chemical reference data*, 1981. doi: dx.doi.org/10.1063/1.555641.

Khan, F., Husain, T., and Hejazi, R. An overview and analysis of site remediation technologies. *Journal of Environmental Management*, 71(2):95–122, June 2004. ISSN 0301-4797. doi: 10.1016/j.jenvman.2004.02.003.

Kloss, S., Pushpalatha, R., Kamoyo, K. J., and Schütze, N. Evaluation of Crop Models for Simulating and Optimizing Deficit Irrigation Systems in Arid and Semi-arid Countries Under Climate Variability. *Water Resources Management*, 26(4):997–1014, Sept. 2011. ISSN 0920-4741. doi: 10.1007/s11269-011-9906-y.

Kolditz, O. *Computational Methods in Environmental Fluid Mechanics*. Engineering Online Library. Springer, 2002. ISBN 9783540428954.

Kolditz, O., Ratke, R., Diersch, H.-J. G., and Zielke, W. Coupled groundwater flow and transport: 1. Verification of variable density flow and transport models. *Advances in Water Resources*, 21(1):27–46, Feb. 1998. ISSN 03091708. doi: 10.1016/S0309-1708(96)00034-6.

Kolditz, O., Bauer, S., Bilke, L., Böttcher, N., Delfs, J. O., Fischer, T., Görke, U. J., Kalbacher, T., Kosakowski, G., McDermott, C. I., Park, C. H., Radu, F., Rink, K., Shao, H. B., Sun, F., Sun, Y. Y., Singh, a. K., Taron, J., Walther, M., Wang, W., Watanabe, N., Wu, Y., Xie, M., Xu, W., and Zehner, B. OpenGeoSys: an open-source initiative for numerical simulation of thermo-hydro-mechanical/chemical (THM/C) processes in porous media. *Environmental Earth Sciences*, 67(2):589–599, Feb. 2012a. ISSN 1866-6280. doi: 10.1007/s12665-012-1546-x.

Kolditz, O., Görke, U.-J., Shao, H., and Wang, W. *Thermo-Hydro-Mechanical-Chemical Processes in Porous Media: Benchmarks and Examples*. Lecture notes in computational science and engineering. Springer, 2012b. ISBN 3642271766.

Krueger, E. H. and Teutsch, G. International viewpoint and news. *Environmental Earth Sciences*, Mar. 2013. ISSN 1866-6280. doi: 10.1007/s12665-013-2280-8.

Langevin, C. D. and Guo, W. MODFLOW/MT3DMS-based simulation of variable-density ground water flow and transport. *Ground Water*, 44(3):339–51, 2006. ISSN 0017-467X. doi: 10.1111/j.1745-6584.2005.00156.x.

Leidel, M., Niemann, S., and Hagemann, N. Capacity development as a key factor for integrated water resources management (IWRM): improving water management in the Western Bug River Basin, Ukraine. *Environmental Earth Sciences*, 65(5): 1415–1426, Sept. 2011. ISSN 1866-6280. doi: 10.1007/s12665-011-1223-5.

Lowry, C. S. and Fienen, M. N. CrowdHydrology: crowdsourcing hydrologic data and engaging citizen scientists. *Ground Water*, 51(1):151–156, 2013. ISSN 1745-6584. doi: 10.1111/j.1745-6584.2012.00956.x.

Lu, G. Y. and Wong, D. W. An adaptive inverse-distance weighting spatial interpolation technique. *Computers & Geosciences*, 34(9):1044–1055, Sept. 2008. ISSN 00983004. doi: 10.1016/j.cageo.2007.07.010.

Ma, T. and Wang, S. Dynamic transition theory for thermohaline circulation. *Physica D: Nonlinear Phenomena*, 239(3-4):167–189, Feb. 2010. ISSN 01672789. doi: 10.1016/j.physd.2009.10.014.

Macumber, P. G. *The Cable Tool Program and Groundwater Flow in the Eastern Batinah Alluvial Aquifer*. Ministry of Water Resources, Muscat, Oman, 1998.

MAF. OMAN SALINITY STRATEGY (OSS) Oman Salinity Strategy. Technical report, Ministry Of Agriculture And Fisheries (MAF), Sultanate Of Oman International Center For Biosaline Agriculture (ICBA) Dubai, UAE, 2012.

Mayer, K. U., Blowes, D. W., and Frind, E. O. Reactive transport modeling of an in situ reactive barrier for the treatment of hexavalent chromium and trichloroethylene in groundwater. *Water Resources Research*, 37(12):3091–3103, 2001. ISSN 1944-7973. doi: 10.1029/2001WR000234.

McNeil, J., Oldenborger, G., and Schincariol, R. Quantitative imaging of contaminant distributions in heterogeneous porous media laboratory experiments. *Journal of Contaminant Hydrology*, 84(1-2):36–54, Mar. 2006. ISSN 0169-7722. doi: 10.1016/j.jconhyd.2005.12.005.

Murthy, K. *Monte Carlo methods in statistical physics*. Universities Press, 2004.

Musuuza, J. L., Radu, F. A., and Attinger, S. The effect of dispersion on the stability of density-driven flows in saturated homogeneous porous media. *Advances in Water Resources*, 34(3):417–432, Mar. 2011a. ISSN 03091708. doi: 10.1016/j.advwatres.2010.11.008.

Musuuza, J. L., Radu, F. a., and Attinger, S. The stability of density-driven flows in saturated heterogeneous porous media. *Advances in Water Resources*, 34(11): 1464–1482, Nov. 2011b. ISSN 03091708. doi: 10.1016/j.advwatres.2011.07.005.

Musuuza, J. L., Radu, F. a., and Attinger, S. Predicting predominant thermal convection in thermohaline flows in saturated porous media. *Advances in Water Resources*, 49:23–36, Dec. 2012. ISSN 03091708. doi: 10.1016/j.advwatres.2012.07.020.

Neuman, S. P. Effect of partial penetration on flow in unconfined aquifers considering delayed gravity response. *Water Resources Research*, 10(2):303–312, 1974. ISSN 1944-7973. doi: 10.1029/WR010i002p00303.

Nield, D. and Bejan, A. *Convection in Porous Media*. Springer, 1999. ISBN 0387984437.

Oke, T. *Boundary layer climates*. Halsted press book. Methuen & Company, 1992. ISBN 9780416705300.

Oki, T. and Kanae, S. Global hydrological cycles and world water resources. *Science (New York, N.Y.)*, 313(5790):1068–72, Aug. 2006. ISSN 1095-9203. doi: 10.1126/science.1128845.

Oldenburg, C. M. and Pruess, K. Dispersive Transport Dynamics in a Strongly Coupled Groundwater-Brine Flow System. *Water Resources Research*, 31(2):289–302, 1995. ISSN 1944-7973. doi: 10.1029/94WR02272.

Oltean, C., Golfier, F., and Buès, M. Experimental and numerical study of the validity of Hele-Shaw cell as analogue model for variable-density flow in homogeneous porous media. *Advances in Water Resources*, 31(1):82–95, Jan. 2008. ISSN 03091708. doi: 10.1016/j.advwatres.2007.06.007.

Ozbek, H., Fair, I., and Phillips, S. Viscosity Of Aqueous Sodium Chloride Solutions From 0 - 150C. In *American Chemical Society 29th Southeast Regional Meeting*, Tampa, FL, USA, 1977. Lawrence Berkeley Laboratory, University of California. URL http://www.escholarship.org/uc/item/3jp6n2bf.

Park, C. H. *Saltwater intrusion in coastal aquifers*. PhD thesis, Georgia Institute of Technology, Nov. 2004.

Park, C.-H. and Aral, M. Saltwater intrusion hydrodynamics in a tidal aquifer. *Journal of Hydrologic Engineering*, 13(September):863, 2008.

Philipp, A. and Grundmann, J. An Integrated Modeling System for Flash Flood Routing in Ephemeral Rivers under the Influence of Groundwater Recharge Dams. *Journal of Hydraulic Engineering*, 2013. doi: 10.1061/(ASCE)HY.1943-7900. 0000766.

Philipp, A., Schmitz, G., and Liedl, R. Analytical Model of Surge Flow in Non-Prismatic Permeable Channels and Its Application in Arid Regions. 2010. URL http://link.aip.org/link/?JHEND8/136/290/1.

Prommer, H., Barry, D., and Davis, G. Modelling of physical and reactive processes during biodegradation of a hydrocarbon plume under transient groundwater flow conditions. *Journal of Contaminant Hydrology*, 59(1-2):113–31, Nov. 2002. ISSN 0169-7722.

Rahmstorf, S. On the freshwater forcing and transport of the Atlantic thermohaline circulation. *Climate Dynamics*, 12(12):799–811, Nov. 1996. ISSN 0930-7575. doi: 10.1007/s003820050144.

Reilly, T. and Goodman, A. Analysis of saltwater upconing beneath a pumping well. *Journal of Hydrology*, 89:169–204, 1987.

Saaltink, M. W., Ayora, C., and Olivella, S. User's guide for RetrasoCodeBright (RCB). Technical report, 2005.

Schlumberger Limited. Petrel, 2012. URL http://www.slb.com.

Schlumberger Water Services. Hydro GeoAnalyst, 2011. URL http://www.swstechnology.com/.

Schmitz, G. H., Al-Hattaly, S., Grundmann, J., Schütze, N., and Walther, M. An Integrated Assessment, Prognoses, Planning and Management Tool (APPM) for a Most Efficient and Sustainable Arid Zone Water Management. In *9th Gulf Water*

Conference: Water Sustainability in the GCC Countries, page 986, Muscat, The Sultanate of Oman, 2010.

Schroeder, W., Martin, K., and Lorensen, B. *The Visualization Toolkit: An Object-oriented Approach to 3D Graphics.* Kitware, 2006. ISBN 9781930934191.

Schütze, N., Kloss, S., Lennartz, F., and Bakri, A. A. Optimal planning and operation of irrigation systems under water resource constraints in Oman considering climatic uncertainty. *Environmental Earth*, pages 1511–1521, 2012. doi: 10.1007/s12665-011-1135-4.

Simmons, C. T. and Narayan, K. a. Mixed convection processes below a saline disposal basin. *Journal of Hydrology*, 194(1-4):263–285, July 1997. ISSN 00221694. doi: 10.1016/S0022-1694(96)03204-0.

Solpuker, U., Hawkins, J., Schincariol, R., Ibaraki, M., and Schwartz, F. W. Harnessing the complex behavior of ultra-dense and viscous treatment fluids as a strategy for aquifer remediation. In *Models - Repositories of Knowledge*, Leipzig, 2012.

Stanger, G. *The Hydrogeology of the Oman Mountains.* PhD thesis, 1987.

Steefel, C. I. Software for Modeling Multicomponent Reactive Flow and Transport, User's Manual. Technical report, Lawrence Berkeley National Laboratory, Berkeley, CA, 2009.

Stoeckl, L. and Houben, G. Flow dynamics and age stratification of freshwater lenses: Experiments and modeling. *Journal of Hydrology*, 458-459:9–15, Aug. 2012. ISSN 00221694. doi: 10.1016/j.jhydrol.2012.05.070.

Sugio, S. and Desai, C. S. Residual flow procedure for sea water intrusion in unconfined aquifers. *International Journal for Numerical Methods in Engineering*, 24(8): 1439–1450, Aug. 1987. ISSN 1097-0207. doi: 10.1002/nme.1620240803.

Sun, F., Shao, H., Kalbacher, T., Wang, W., Yang, Z., Huang, Z., and Kolditz, O. Groundwater drawdown at Nankou site of Beijing Plain: model development and calibration. *Environmental Earth Sciences*, 64(5):1323–1333, Feb. 2011. ISSN 1866-6280. doi: 10.1007/s12665-011-0957-4.

Tagare, S., Ramana Murthy, M., and Rameshwar, Y. Nonlinear thermohaline convection in rotating fluids. *International Journal of Heat and Mass Transfer*, 50 (15-16):3122–3140, July 2007. ISSN 00179310. doi: 10.1016/j.ijheatmasstransfer. 2006.11.037.

Theis, C. The relation between the lowering of the piezometric surface and the rate and duration of discharge of a well using groundwater storage. *Trans. Amer. Geophys. Union*, 16:513–514, 1935.

Tietje, O. and Tapkenhinrichs, M. Evaluation of pedo-transfer functions. *Soil Science Society of America Journal*, 57(4):1088–1095, 1993.

van der Lee, J., De Windt, L., Lagneau, V., and Goblet, P. Module-oriented modeling of reactive transport with HYTEC. *Computers & Geosciences*, 29(3):265–275, Apr. 2003. ISSN 00983004. doi: 10.1016/S0098-3004(03)00004-9.

VISLAB. Visualization Center - Helmholtz-Zentrum für Umweltforschung UFZ, 2013. URL `http://www.ufz.de/index.php?en=14171`.

Voss, C. I. A finite-element simulation model for saturated-unsaturated, fluid-density-dependent ground-water flow with energy transport or chemically-reactive single-species solute transport. Technical report, U.S. Geological Survey Water Resources Investigations Report 84-4369, Tyndall, 1984.

Walther, M., Böttcher, N., and Liedl, R. A 3D interpolation algorithm for layered tilted geological formations using an adapted inverse distance weighting approach. In *ModelCare2011, Models - Repositories of Knowledge*, pages 119–126, Leipzig, 2012a. IAHS Publ. 355 (2012) ISBN 978-1-907161-34-6, 374.

Walther, M., Delfs, J.-O., Grundmann, J., Kolditz, O., and Liedl, R. Saltwater intrusion modeling: Verification and application to an agricultural coastal arid region in Oman. *Journal of Computational and Applied Mathematics*, 236(18): 4798–4809, Dec. 2012b. ISSN 03770427. doi: 10.1016/j.cam.2012.02.008.

Walther, M., Bilke, L., Delfs, J.-O., Graf, T., Grundmann, J., Kolditz, O., and Liedl, R. Visualizing Saline Intrusion in a Three-Dimensional, Heterogeneous, Coastal Aquifer. In *Workshop on Visualisation in Environmental Sciences (EnvirVis)*, Leipzig, 2013a.

Walther, M., Solpuker, U., Böttcher, N., Kolditz, O., Liedl, R., and Schwartz, F. W. Description and Verification of a Novel Flow and Transport Model for Silicate-Gel Emplacement. *Journal of Contaminant Hydrology*, 157:1–10, Nov. 2013b. ISSN 01697722. doi: 10.1016/j.jconhyd.2013.10.007.

Watson, D. ACORD: Automatic contouring of raw data. *Computers and Geosciences*, 8(I):97–101, 1982.

Werner, A. D., Bakker, M., Post, V. E., Vandenbohede, A., Lu, C., Ataie-Ashtiani, B., Simmons, C. T., and Barry, D. Seawater intrusion processes, investigation and management: Recent advances and future challenges. *Advances in Water Resources*, 51:3–26, Jan. 2013. ISSN 03091708. doi: 10.1016/j.advwatres.2012.03. 004.

Wiedemeier, T., Rifai, H., Newell, C., and Wilson, J. *Natural attenuation of fuels and chlorinated solvents in the subsurface*. Environmental engineering. Wiley, 1999. ISBN 9780471197492.

Xu, T., Pruess, K., and Brimhall, G. An improved equilibrium-kinetics speciation algorithm for redox reactions in variably saturated subsurface flow systems. *Computers & Geosciences*, 25(6):655–666, 1999. ISSN 0098-3004. doi: 10.1016/S0098-3004(99)00005-9.

Yechieli, Y. and Wood, W. W. Hydrogeologic processes in saline systems: playas, sabkhas, and saline lakes. *Earth-Science Reviews*, 58(3-4):343–365, Oct. 2002. ISSN 00128252. doi: 10.1016/S0012-8252(02)00067-3.

Young, G. S. Convection in the atmospheric boundary layer. *Earth-Science Reviews*, 25(3):179–198, Sept. 1988. ISSN 00128252. doi: 10.1016/0012-8252(88)90020-7.

Publications

Peer-reviewed Relevant First-Author Publications

[P1] Walther, M., Böttcher, N., and Liedl, R. A 3D interpolation algorithm for layered tilted geological formations using an adapted inverse distance weighting approach. In *ModelCare2011, Models - Repositories of Knowledge*, pages 119–126, Leipzig, 2012a. IAHS Publ. 355 (2012) ISBN 978-1-907161-34-6, 374

[P2] Walther, M., Delfs, J.-O., Grundmann, J., Kolditz, O., and Liedl, R. Saltwater intrusion modeling: Verification and application to an agricultural coastal arid region in Oman. *Journal of Computational and Applied Mathematics*, 236(18): 4798–4809, Dec. 2012b. ISSN 03770427. doi: 10.1016/j.cam.2012.02.008

[P3] Walther, M., Solpuker, U., Böttcher, N., Kolditz, O., Liedl, R., and Schwartz, F. W. Description and Verification of a Novel Flow and Transport Model for Silicate-Gel Emplacement. *Journal of Contaminant Hydrology*, 157:1–10, Nov. 2013b. ISSN 01697722. doi: 10.1016/j.jconhyd.2013.10.007

Additional Relevant Publications

[A1] Kalbacher, T., Delfs, J.-O., Shao, H., Wang, W., Walther, M., Samaniego, L., Schneider, C., Kumar, R., Musolff, A., Centler, F., Sun, F., Hildebrandt, A., Liedl, R., Borchardt, D., Krebs, P., and Kolditz, O. The IWAS-ToolBox: Software coupling for an integrated water resources management. *Environmental Earth Sciences*, 65(5):1367–1380, Aug. 2011. ISSN 1866-6280. doi: 10.1007/s12665-011-1270-y

[A2] Kolditz, O., Görke, U.-J., Shao, H., and Wang, W. *Thermo-Hydro-Mechanical-Chemical Processes in Porous Media: Benchmarks and Examples*. Lecture notes in computational science and engineering. Springer, 2012b. ISBN 3642271766

[A3] Schmitz, G. H., Al-Hattaly, S., Grundmann, J., Schütze, N., and Walther, M. An Integrated Assessment, Prognoses, Planning and Management Tool (APPM)

for a Most Efficient and Sustainable Arid Zone Water Management. In *9th Gulf Water Conference: Water Sustainability in the GCC Countries*, page 986, Muscat, The Sultanate of Oman, 2010

[A4] Brettschneider, M., Grundmann, J., Schütze, N., and Walther, M. Development of Surrogate Models for reproduction of complex numerical simulation models and application in a water resource management system. In *The New Zealand Hydrological Society Annual Conference (NZHS Conference)*, Dunedin, New Zealand, 2010

[A5] Gerner, A., Grundmann, J., Walther, M., and Schmitz, G. H. Groundwater recharge as a crucial aspect in water resources development for the Barka region. In *International Conference on Drought Management Strategies in Arid and Semi-Arid Regions*, Muscat, The Sultanate of Oman, 2011

[A6] Walther, M., Bilke, L., Delfs, J.-O., Graf, T., Grundmann, J., Kolditz, O., and Liedl, R. Visualizing Saline Intrusion in a Three-Dimensional, Heterogeneous, Coastal Aquifer. In *Workshop on Visualisation in Environmental Sciences (EnvirVis)*, Leipzig, 2013a

Acknowledgements

Appendix

Supplementary Material

E.1 Structure of Appendix

The following provides a list of attached, supplementary material. The appendix is split into hard copy content, attached afterwards, and soft copy content on a digital medium (see table E.1.1).

Hard copy content includes the following sections:

Soft copy content is listed in table E.1.1, p. App-4, and includes a number of supplementary movies. To view the supplied videos, either "Microsoft Windows Media Player", or "VLC Player" is suggested. The first is automatically installed with a standard Microsoft Windows installation; the latter can be obtained via this link (choose correct version depending on operating system): `http://www.videolan.org/vlc/`. A short problem description is given in the beginning of each video, the user may pause the video any time to examine details.

Table E.1.1: Structure of digital appendix.

Relative path	File Name	Description
.\	PhD_Thesis_MWalther.pdf	This document in the pdf-format, including clickable references and navigation links.
.\Videos\	OMAN_Hydrogeology.mp4	Video of heterogeneous hydrogeological structure for regional scale groundwater model, see chapter 5, p. II-9.
.\Videos\	OMAN_Streamtracer.mp4	Video of streamtracer paths for regional scale groundwater model in 1985, see chapter 5, p. II-9.
.\Videos\	VISC_het_scenario.mp4	Video of a heterogeneous scenario simulation described in section 6.3.2, p. II-28.
.\Videos\	TH_Q1_1-1_chaotic.mp4	Video of a thermohaline double-diffusive chaotic regime, see section 7.3.1, p. II-36.
.\Videos\	TH_Q1_1-10_stable.mp4	Video of a thermohaline double-diffusive stable regime, see section 7.3.2, p. II-39.
.\Videos\	TH_Q4_1-10_oscillatory.mp4	Video of a thermohaline double-diffusive stable oscillatory regime, see section 7.3.3, p. II-39.

E.2 Maps of Salinization in Groundwater Modelling Area
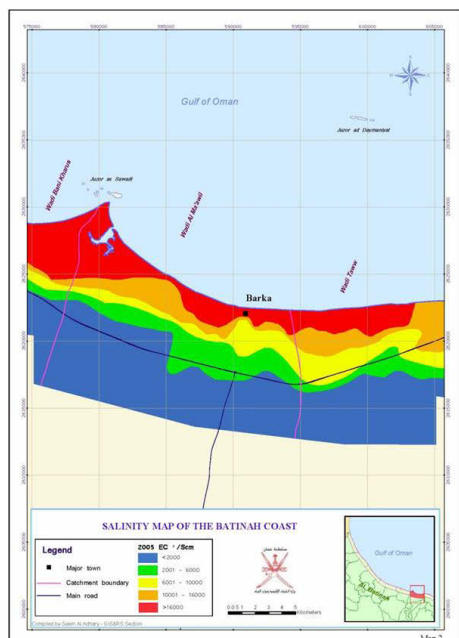
Figure E.2.1: Interpolation of saline intrusion measurements, year 2005, supplied by MRMWR.
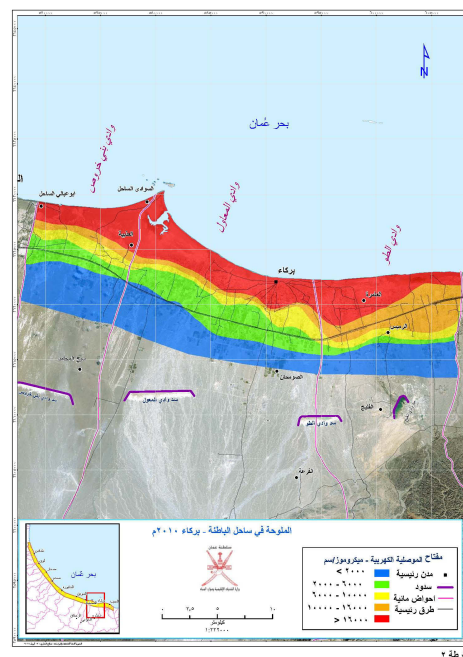
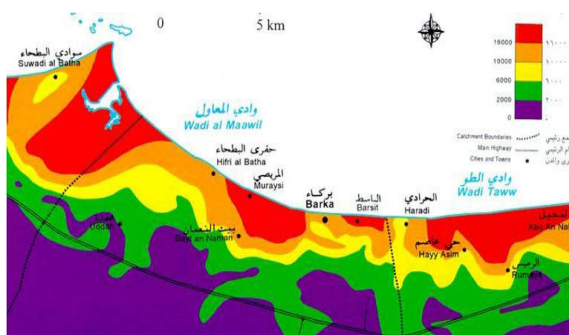Figure E.2.2: Interpolation of saline intrusion measurements, year 2012, supplied by MRMWR.

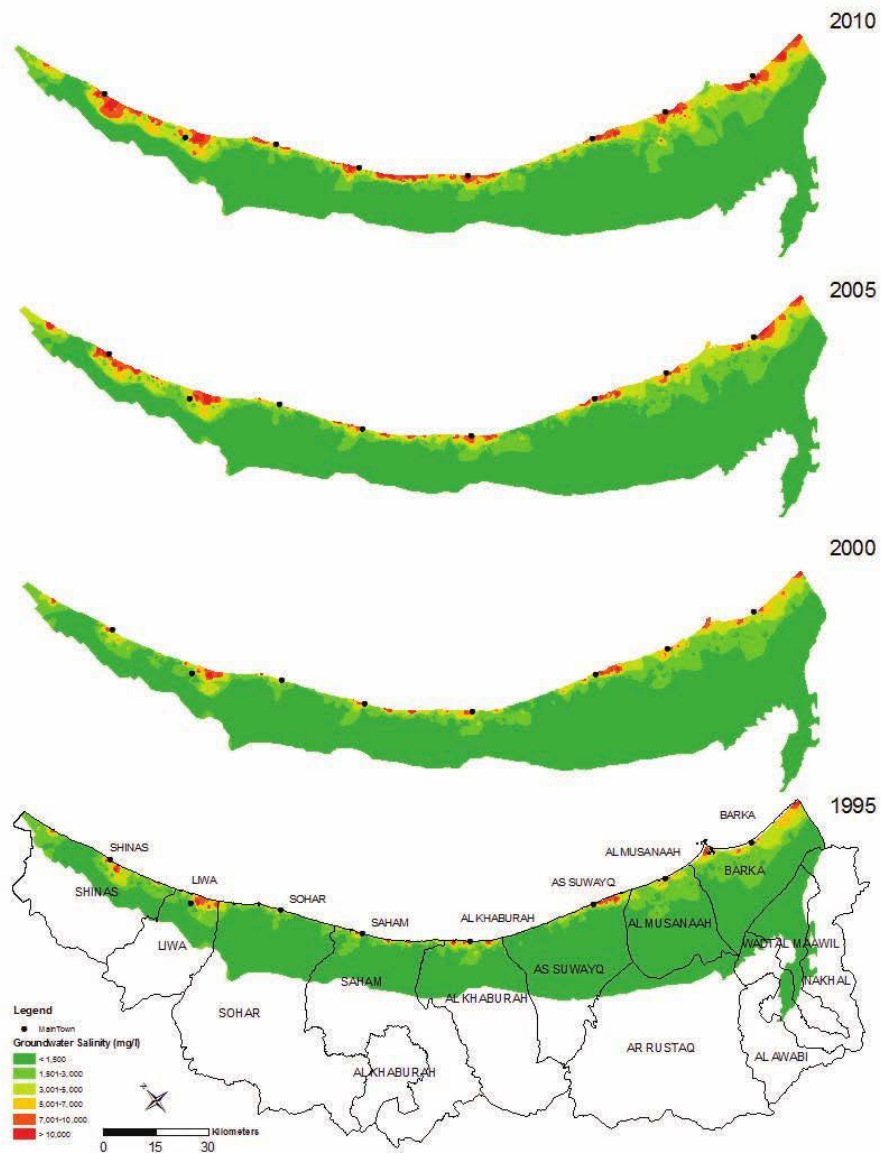Figure E.2.3: Interpolation of saline intrusion measurements, presumingly year 2000, supplied by MRMWR.

Figure E.2.4: Interpolation of saline intrusion measurements, years 1995-2010, (MAF, 2012, p. 44, figure 27).

E.3   ParaView Client-Server Connection

Modern, powerful computing environments, that can be connect to by the world-wide-web, are forced to restrict access due to countless threats from the open internet environment. Remote access to internal services (e.g. parallel cluster computing) is granted by offering "gateways". In order to start and connect to a PV server process from a local, cluster-external personal computer, port forwarding and reversing procedures via a remote gateway were needed, as both networks, client and server side, limited internal access (e.g. secured by firewall). Basically, the following steps are taken all emerging from the local client computer: 1) establish connection with port forwarding to remote cluster from local computer via gateway, thus enabling direct access to cluster, i.e. all further traffic is routed over gateway; 2) create connection with port reversing from cluster to local computer via prior established port forwarding connection, thus offering cluster access to local client; 3) submit parallel job script to start PV server on cluster via port forward connection; 4) send job information, i.e. execution status and cluster node id, from remote to local computer via port reverse connection; 5) start local PV client and connect to remote cluster node via port forwarding.

Publications

Title A 3D interpolation algorithm for layered tilted geological formations using an adapted inverse distance weighting approach.

Authors Walther, M., Böttcher, N., Liedl, R.

Abstract We present an algorithm for the 3D interpolation of layered tilted hydro-geological structures from point data. The method uses profile information and interpretations of the geological layering to interpolate discrete or continuous values in a meshed grid consisting of arbitrary element types. The user has the opportunity to tweak several options of the algorithm depending on the given application's circumstances (e.g. data availability and reliability) and additional soft information of the geology. The interpolation algorithm is implemented in Qt and can be used as a pre-processing tool for mesh-based numerical methods (i.e. finite difference method, finite element method, finite volume method).

Title Saltwater intrusion modeling: Verification and application to an agricultural coastal arid region in Oman

Authors Walther, M., Delfs, J.-O., Grundmann, J., Kolditz, O., Liedl, R.

Abstract This paper deals with numerical modeling of density-dependent flow of saltwater intrusion in coastal groundwater systems. We present the implementation of an approach to solve a moving boundary problem for a dynamic water table within an invariant finite element mesh. The model is successfully validated against laboratory experiment data for an unconfined, density-dependent benchmark. The validated software is applied to a regional-scale study area and sufficiently calibrated for a steady state of pre-development conditions. Transient mass transport scenario simulations show good concordance with salinity measurements satisfyingly supporting the model setup.

Keywords Saltwater intrusion; Density-dependent; Three-dimensional numerical simulation; OpenGeoSys; Al-Batinah; IWAS-Oman

Title Description and Verification of a Novel Flow and Transport Model for Silicate-Gel Emplacement

Authors Walther, M., Solpuker, U., Böttcher, N., Kolditz, O., Liedl, R., Schwartz, F. W.

Abstract We present a novel approach for the numerical simulation of the gelation of silicate solutions under density-dependent flow conditions. The method utilizes an auxiliary, not density-dependent solute that is subject to a linear decay function to provide temporal information that is used to describe the viscosity change of the fluid. By comparing the modeling results to experimental data, we are able to simulate the behavior and the gelation process of the injected solute for three different compositions, including long-term stability of the gelated area, and non-gelation of low concentrations due to hydro-dynamic dispersion. This approach can also be used for other types of solutes with this gelling property and is useful in a variety of applications in geological, civil and environmental engineering.

Title Visualizing Saline Intrusion in a Three-Dimensional, Heterogeneous, Coastal Aquifer.

Authors Walther, M., Bilke, L., Delfs, J.-O., Graf, T., Grundmann, J., Kolditz, O., Liedl, R.

Abstract We visualize remediation scenarios for a coastal aquifer in Oman, where the natural fresh-saltwater interface is negatively affected by groundwater pumping for irrigation. The 3D aquifer is characterized by strong heterogeneities ranging from local to regional scale, which impose visual challenges in the interpretation of large data amounts. This paper addresses the visualization workflow, which helped to ensure correct model setup and successful calibration of a transient model run. The modelling and visualization exercise identified sensitive areas for salinization along the coast and assessed the impact of remediation measures on the groundwater reservoir in space and time. Proper visualization helped to interpret and illustrate the complex results adequately, and to transfer scientific information to stakeholders.